秋田県立大学大学院博士学位論文

Preparation and Characterization of Macromolecular Hydrogel Using

Cellulose as Cross-linker

セルロースの架橋作用による高分子ハイドロゲルの創製およびその性能評価

朱 龍祥

2018 年 3 月

Abstract

Hydrogels, as soft and wet materials, have attracted great attention in the field of functional materials. It has been used in the field of drug delivery system, superabsorbent, biosensor, tissue engineering, wound dressing, conductive device, and others. Conventional hydrogels show weak mechanical properties which greatly limits the application of hydrogel. Most recently, the designed hydrogels, according to the energy dissipation principle, overcome the low mechanical strength, poor toughness, and limited recoverability of common hydrogels and show excellent mechanical properties. In this work, the prepared hydrogels with cellulose as cross-linker possess instantaneous recovery, anti-fatigue, high modulus and thermal stability.

In chapter 1, the research background of hydrogel was introduced, including hydrogel types, hydrogel applications, research status of tough hydrogel and the purpose of this study.

In chapter 2, the properties of experiment materials, as well as experimental methods and characterizations are presented.

In chapter 3, a novel hydrogel with carboxymethyl cellulose as cross-linker was synthesized via visible-light-triggered polymerization. In this study, a mesoscopic inhomogeneous hydrogel consisting of carboxymethyl cellulose and polyacrylic acid is synthesized through a facile, one-pot, visible-light-triggered polymerization. The prepared hydrogel can be stretched over 700% with fracture strength as high as 850 kPa and shows a high elastic modulus (180 kPa). The microgel aggregated structure endows an efficient energy dissipation mechanism to the hydrogel. After the internal network structure stabilizing, the hydrogel exhibits a recovery time of 10 ms and over 92% resilience during impact and cyclic tensile tests, respectively. The hydrogel with such excellent mechanical properties can extend its application in biomaterial fields.

In chapter 4, a high resilience hydrogel was prepared depending on chapter 3. In this work, we synthesized a double cross-linking poly(acrylic acid) hydrogel via a simple,

one-pot, visible-light-trigger polymerization, with carboxymethyl cellulose as initiator and the first cross-linker, N,N′-methylene bis(acrylamide) (MBA) as the second cross-linker. The tensile strength and elastic modulus are in the range of 724−352 kPa and 115−307 kPa, respectively, depending on the MBA content. The swelling ratio of hydrogels dramatically decreased with increasing the MBA content. DMA results indicate that the internal friction between molecules within the hydrogel decreases with the increase of MBA content. Cyclic tensile tests show that after the structure stabilizes, the resilience, maximum stress, and residual strain of Gel-2 maintains over 93% (95% for successive cyclic tensile test), 115 kPa and less than 3%, respectively, at a strain of 125%. The values of resilience and residual strain are almost constant in both successive and intermittent cyclic tensile tests. Moreover, the swollen hydrogel has higher resilience and lower residual strain than the same hydrogel in the as-prepared state.

In chapter 5, a high modulus hydrogel was prepared based on chapter 3. The excellent biocompatibility and stimuli-responsiveness have made hydrogels excellent candidates in the field of materials science. However, most of the hydrogels are extremely soft (modulus of approximately 0.1 MPa) as compared to rubber materials; this greatly limits their application in the field of material engineering. In this study, an Al^{3+} reinforced carboxymethyl cellulose/polyacrylic acid hydrogel was first synthesized by a facile, visible-light-triggered, one-pot polymerization method. Subsequently, the as-prepared hydrogel was reinforced by evaporation-swelling (E-S) treatment to obtain a hydrogel (HM-Gel) with a 10-fold higher elastic modulus. This hydrogel exhibits a tensile strength of 1.26–1.74 MPa and an elastic modulus of 0.59–1.94 MPa. Moreover, the HM-Gel, with an excellent vibration absorption ability, can find applications in the field of industrial engineering and bioengineering.

In chapter 6, the oxidized multi-aldehyde cellulose nanofiber (CNF) was used as chemical cross-linker to fabricated CNF/PVA hydrogel. The obtained hydrogels were reinforced through evaporation-swelling method. The crystallinity and decomposition temperature of oxidized CNF is reduced from 65.9% to 26.1% and 323.2 to 248.0°C, respectively, with an increase in the amount of $NaIO_4$. The tensile strength and elastic

modulus of reinforced hydrogels are in the range of 0.25-3.13 MPa and 0.14-2.10 MPa, respectively, depending on various oxidized CNF. The chemical cross-linked hydrogels exhibit mechanical properties and water content closer to the natural soft tissue. In addition, the prepared hydrogels show thermal stability during the use of conventional high temperature autoclaving process.

In chapter 7, the present study is summarized.

Content

1. Introduction

1.1 Background

Hydrogels, which are soft and wet materials, usually composed of three-dimensional polymer network structure and a large amount of water (50 ~ 99%) inside the network structure. Besides their wide variety of applicability such as drug delivery system, superabsorbents, microfluidics, and contact lenses in the materials science field, they have become extensively attractive in tissue engineering because of their stimuli-responsive property. However, most of the synthetic hydrogel suffered from a lack of mechanical strength compared with the hydrogel-like bio-tissues such as cartilage, tendon, muscle, and blood vessel. These load-bearing soft tissues exhibit excellent mechanical performances, for example, cartilage tissue possesses high toughness, shock absorbing, low sliding friction. Seeking artificial tissues (excellent soft, wet, and tough hydrogel material) as a replacement of damaged tissues has been a challenging task for material scientists.

1.1.1 Definition

Like a solid, hydrogels do not flow. Like a liquid, small molecules diffuse through a hydrogel. So what is a hydrogel? In 1926, Dorothy Jordan Lloyd stated that "the colloidal condition, the gel, is one which is easier to recognize than to define" [1]. Hydrogels are currently considered to consist of three-dimensional network polymer chains plus water that fills the voids between polymer chains. Cross-linking networks can make hydrogels insoluble in water, and endow the hydrogel certain mechanical strength and toughness. The main component of the hydrogel is water (the mass fraction of water is much greater than that of polymer). Therefore, the ability of a hydrogel to hold a significant amount of water implies that the polymer chains must have moderate hydrophilic character.

1.1.2 Types of hydrogels

The polymer chains in the hydrogel are cross-linked. According to the type of cross-linking can generally be divided into two categories: physical cross-linking and chemical cross-linking. For the former, the connections are weaker and more reversible; for example, heat may break the chain-chain link. Polymers chains of physical hydrogels are held together by electrostatic forces, hydrogen bonds, hydrophobic interactions or chain entanglements. The other is a covalently cross-linked hydrogel, the polymer chains of the chemical hydrogel are connected by permanent covalent bonds.

A second way to categorize hydrogels is the starting point for synthesis (production). First, a polymer network may be prepared from monomers and cross-linkers. For example, networks made with PEG and PPO monomers are good carriers for drug delivery. Second, a polymer network may be prepared to start with prepolymers (oligomers that are capable of further polymerization). For example, polyurethane networks may be prepared using prepolymers. A non-medical application of a polyurethane hydrogel is entrapment (immobilization) of microbial cells for wastewater treatment. Third, polymer networks may be prepared to start with polymers. An example is chitosan cross-linked with glutaraldehyde, the prepared hydrogel can be used as scaffolding for soft tissue engineering and adhesive for peripheral nerve repair.

Another way to classify hydrogels is based on the polymer origin. Examples of polymers from the natural origin are proteins and polysaccharides such as collagen, chitosan, dextran, and alginate. Hydrogels from natural origin support cellular activity and are biocompatible and biodegradable. On the other hand, they may contain biological pathogens or evoke an immune response. Besides, the natural origin hydrogels generally show low mechanical strength. Synthetic polymers are made from monomers such as vinyl acetate, acrylamide, ethylene glycol and lactic acid. Not all monomers used in the synthesis of polymers are derived from petroleum; for example, lactic acid is made from plants such as corn and sugarcane. Synthesis of polymers can be precisely controlled and tailored to provide a wide range of performance. Moreover,

they have a low risk of biological pathogens and evoking an immune response. Disadvantages are low biodegradability and lack of inherent biological activity. Also, toxic substances may be present.

Classification may be based on the physical structure of the polymer chain: amorphous (random, noncrystalline), semi-crystalline (regions of partially ordered structure) or hydrogen-bonded (network held together by hydrogen bonds). Another way to classify hydrogels is by the method of preparation: homopolymer, copolymer, multi-polymer or interpenetrating polymer. Hydrogels may also be categorized based on ionic charges as follows: neutral (no charge) such as dextran; anionic (negative charge) such as carrageenan; cationic (positive charge) such as chitosan; and ampholytic (capable of behaving either positively or negatively) such as collagen.

1.2 Applications of hydrogels

1.2.1 Durg delivery system

Hydrogel delivery systems have found clinical use in the field of drug delivery. Hydrogels can provide spatial and temporal to control the release of various therapeutic agents, including small-molecule drugs, macromolecular drugs, and cells. Due to its tunable physical properties, controllable degradability and capability to protect labile drugs from degradation, hydrogels act as a platform for various physiochemical interactions with the encapsulated drugs to control drug release.

Hydrogels are a particularly attractive type of drug delivery system and have been used in many medical branches including immunology, cardiology, wound healing, oncology, and pain management. Hydrogels consist of a large amount of water and a cross-linked polymer network. High water content (70–99%) provides physical similarity to tissues and can give the hydrogel excellent biocompatibility and the ability to easily encapsulate hydrophilic drugs. In addition, since they are commonly formed in aqueous solutions, the risk of drug denaturation and aggregation upon exposure to organic solvents is minimized. Hydrogels differ in size, structure, and function, and

these features together determine how the hydrogel is used for drug delivery. In hydrogels, there are features of length scales spanning from centimeters to subnanometers (Fig. 1.1) [2]. The macroscopic design largely determines the way hydrogels can be delivered into the human body. In addition, hydrogels can form almost any overall size and shape.
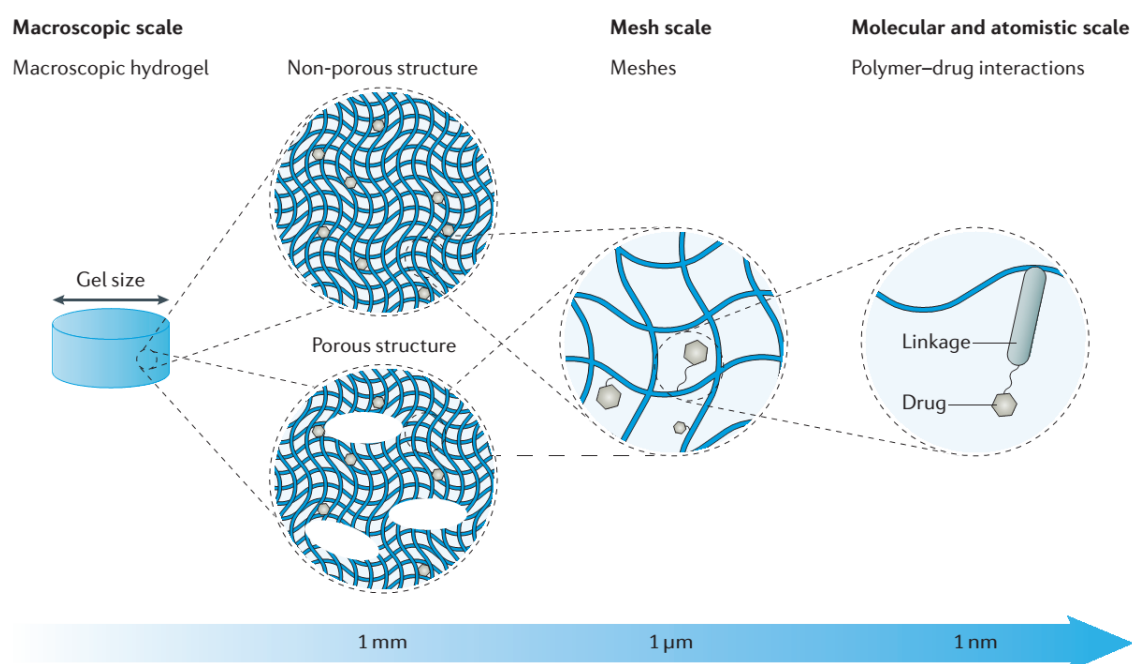
Fig. 1.1 Multiscale properties of hydrogels [2].

Hydrogels can be formed into almost any shape and size according to the requirements of the delivery route into the body. Hydrogel delivery systems can be classified into three main categories based on their size: macroscopic hydrogels, microgels, and nanogels. Microgels and nanogels are particulate hydrogels with dimensions on the order of micrometers and nanometers, respectively. Advances in biomaterials have broadened the repertoire of hydrogels designed for controlled drug delivery. The impact of hydrogel drug delivery systems is expected to increase in the coming years with the continuous expansion of material systems and target applications, and increasing fundamental understanding. Hydrogel drug delivery systems may further alter the scale, efficacy, and cost of therapeutics, and continue to improve human health care.

1.2.2 Superabsorbent
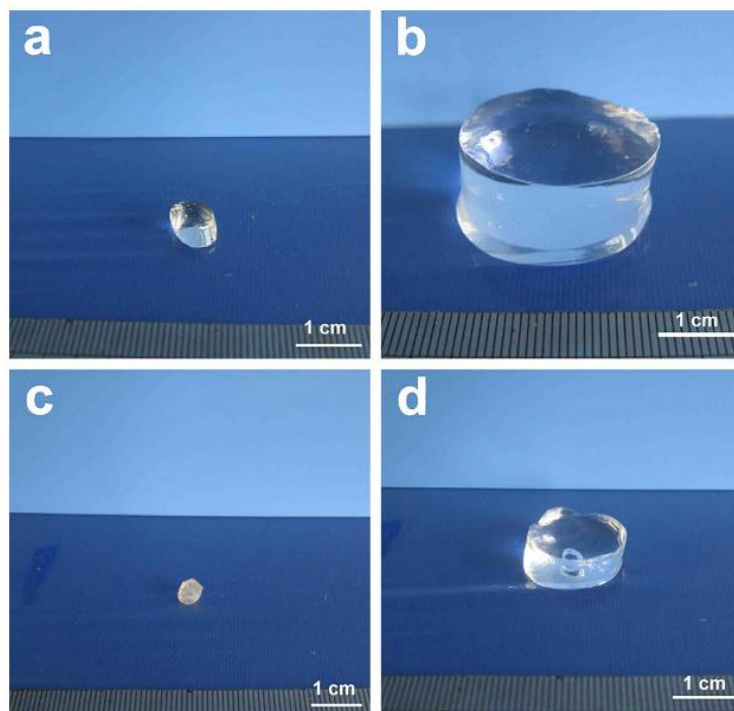
Fig. 1.2 Photographs of GEL91: (a) original hydrogel, (b) swollen hydrogel, (c) dried
hydrogel and (d) hydrogel after swelling in NaCl solution for a week [5].

Cross-linked polymeric gels are a class of materials which can absorb a large volume of solvent molecules in their three-dimensional network structure without dissolution. These materials can be classified into two types: organogels (absorbing media is organic solvent) and hydrogels (absorbing media is water), depending on the absorbing solvent media that can be penetrated into cross-linked polymer gels. In recent years, design and synthesis of superabsorbent polymeric (SAP) organogels are gaining increasing interest in industry and academia due to their application for the recovery of volatile organic compound (VOC) and oil spill in water to protect our environment and marine life from their catastrophic impact [3]. Among various stimuli-responsive hydrogels, pH and salt responsive hydrogels are mostly investigated due to their applications in the field of pharmacy, medicine, and biotechnology [4]. Such as Chang et al. have successfully prepared a novel superabsorbent hydrogel from carboxymethyl cellulose sodium and cellulose in the NaOH/urea aqueous system by using epichlorohydrin as cross-linker. Their equilibrium swelling ratio in distilled water and different physiological fluids

were evaluated, indicating the maximum swelling ratio in water reached an exciting level of 1000 as the hydrogels still keeping a steady appearance (Fig. 1.2) [5].

1.2.3 Biosensor

By interconnecting (cross-linking) either small aggregating molecules [6], particles, or polymers, it is possible to form a material with an extended elongated structure. The crosslinks can be of either chemical nature, in the form of covalent bonds, or of physical nature in the form of coordinative, electrostatic, hydrophobic, dipole-dipole interactions or chain entanglements between the network segments. Due to the highly open structure and the large inner surface, hydrogels can hold large amounts of molecules with specific functions and are becoming irreplaceable materials in biosensing technology for the detection of chemical or biological analytes [7-11]. In many biosensor applications, a hydrogel material is used at the interface between the to-be-analyzed aqueous sample fluid and the sensor signal transducer (Fig. 1.3) [12]. Typically, the hydrogel interface is modified with biomolecular recognition elements (BREs) such as enzymes, antibodies or with biomimetic molecular imprinted moieties in order to selectively recognize specific target analytes. Compared to other types of biointerfaces (for example, based on 2D self-assembled monolayers—SAMs), the 3D nature of the hydrogel networks allows to accommodate orders of magnitude larger amounts of recognition elements [13], provides a more natural microenvironment for biomolecules that increases their stability [14] and offers ways to implement additional functionalities (for example, separation of target analyte from other molecules in a sample) [15]. In addition, the class of "smart" gels that respond to external stimuli become of increasing interest in biosensor research. For instance, miniature holographic diffraction elements based on these responsive hydrogel materials were integrated into a contact lens for the real-time monitoring of glucose levels in an artificial tear fluid by a diffracting wavelength shift [16]. Moreover, appropriate selection of polymer building blocks and the introduction of suitable functional groups can modulate the response behavior. In addition, the mechanical work that can be performed by the swelling and collapse

process is utilized in actuation, which forms the basis for valves, pumps and potentially for micromachines.
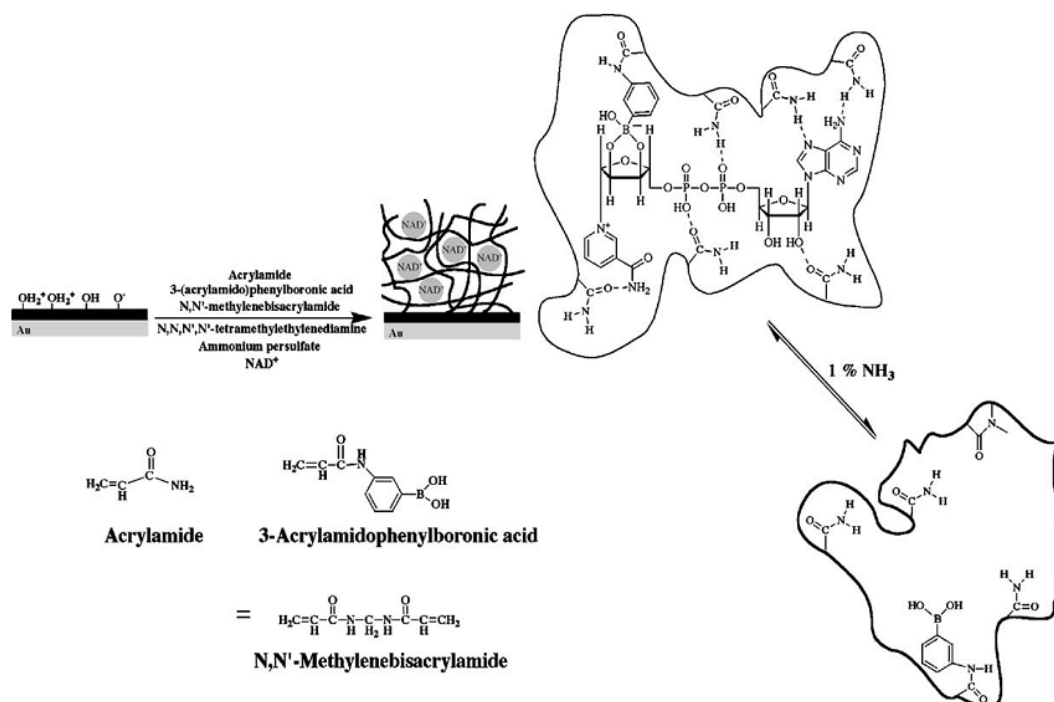
Fig. 1.3 NAD(P)+/NAD(P)H cofactors-imprinted hydrogel with an acrylamide-acrylamidophenylboronic acid copolymer on an Au-coated glass for SPR-based detection [12].

1.2.4 Tissue engineering

Hydrogels have been used as an important class of tissue engineering scaffolds because they provide a soft tissue-like environment for cell growth and allow diffusion of nutrients and cellular waste through the elastic hydrogel network (Fig. 1.4). Compared with other types of polymer scaffolds, it has advantages of easy control of structural parameters, high water content, promising biocompatibility and adjustable scaffold architecture.

Currently, synthetic polymers have become an important alternative choice for fabricating hydrogel tissue-engineering scaffolds because they can be molecularly tailored with block structures, molecular weights, mechanical strength, and biodegradability [17-23]. Synthetic polymers used for preparing synthetic hydrogels

can be classified into three main types, including nonbiodegradable [24-26], biodegradable [27-32] and bioactive polymers [33-35]. For example, Poly(*N*-isopropylacrylamide) (PNIPAm) has been investigated extensively as a thermo-sensitive polymer, which can form thermo-sensitive hydrogels from the free radical polymerization of NIPAm with cross-linkers; PNIPAm hydrogels swell in water at temperatures less than the lower critical solution temperature (~32°C) [35]. Hydrogen bonding between water molecules and the amide groups of PNIPAm plays a dominant role in the intermolecular association. This unique property of temperature-responsive swelling/de-swelling can be used to isolate the cellular layers of engineered special tissues such as cornea or cell sheets [36].
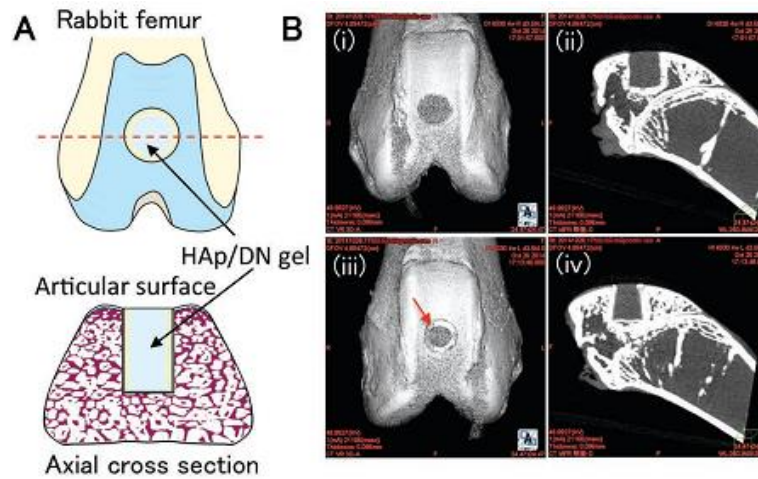
Fig.1.4 Schematic of HAp/DN gel plugs implanted in rabbit femurs [37].

1.2.5 Wound dressing

Burn wound infection is one of the most important and potentially serious complications that occur during the acute period following injury. Although burn wound surfaces are sterile immediately following thermal injury, colonization with autogenous micro-organisms (originating from the skin, gastrointestinal and respiratory flora) or through contact with the contaminated environment (water, air, and healthcare workers) generally occurs within 48 h [38, 39]. The typical burn wound is initially colonized predominantly with Gram-positive organisms, which are replaced by antibiotic-susceptible Gram-negative organisms within 1 week after the burn injury. If

wound closure is delayed and the patient becomes infected, thus requiring treatment with broad-spectrum antibiotics, this flora may be replaced by yeasts, fungi and antibiotic-resistant bacteria. Therefore, much attention has been given to the use or modification of different polymeric materials currently available for biomedical devices to meet the demands of medical applications for over-increasing these materials [40].

At present, PVA is one of the most frequent and the oldest synthetic polymer hydrogels that due to its good biocompatibility has been applied in several advanced biomedical applications (Fig. 1.5) [41]. Such as wound dressing [42], wound management [43].
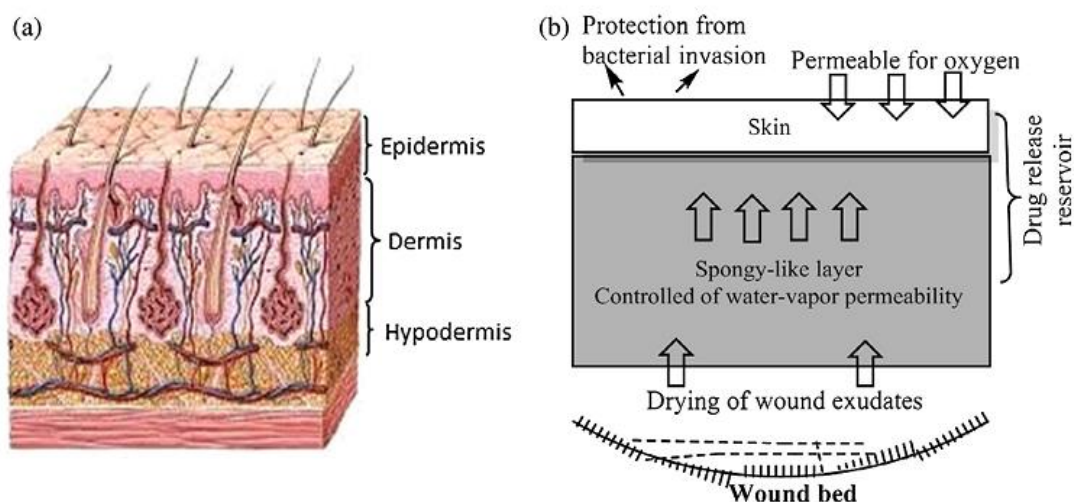
Fig. 1.5 Schematic representation of normal skin structure (a) and design of an ideal wound dressing membrane (b) [41].

1.2.6 Conductive device

In recent years, the rapid development of nanoscience and technology has promoted the development of nanostructured conductive polymers [44-46]. Due to the unusual physical/chemical properties associated with confined dimensions of nanoscale structure[47-49] and conjugated polymer chains, nanostructured conductive polymers have been used in applications ranging from energy conversion and storage, electronics, and biological and chemical sensors to medical science [50-53]. Among these diverse nanostructures, conductive polymer gels (CPGs) with three-dimensional (3D) hierarchical structures constructed by highly cross-linked networks of polymer chains

are of particular interest since they possess hierarchically porous microstructure, high surface area (40−100 m^2/g), exceptional compatibility with bio- or other hydrophilic molecules, and tunable chemical/physical properties (Fig. 1.6) [54]. The porous structure of CPGs can also help accommodate the strain induced by volume change during electrochemical reaction and offer the possibility of making lightweight flexible devices [46, 55]. CPGs have recently been converted to carbon framework materials by thermal treatment and activation [56, 57]. The resulting carbon materials have been demonstrated to be promising for energy storage and conversion owing to their high electrocatalytic activity.
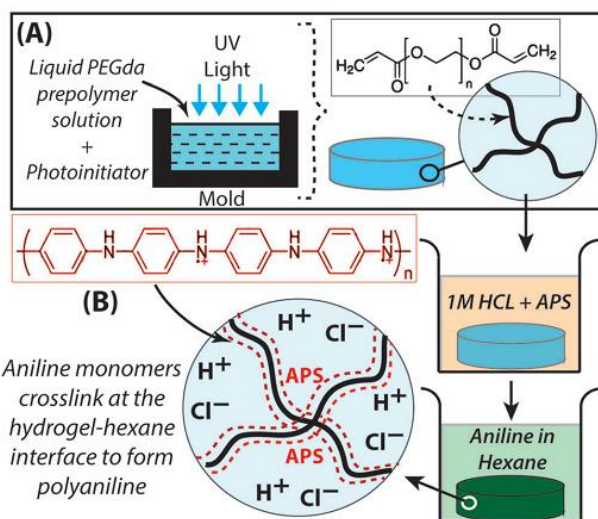
Fig. 1.6 Synthesis and formation of polyethylene glycol–polyaniline (PEGda–PANI) conductive hydrogels using interfacial polymerization process [45].

1.2.7 Others

Owing to their unique integration of solid and liquid properties, hydrogels also have the application in the field of contact lenses [58], and actuators in soft machines [59, 60].

1.3 Benefits and limitations of hydrogels

The conventional hydrogels have their unique benefits:

- Biocompatible

- Can be injected in vivo as a liquid that then hydrogels at body
- Protect cells
- Good transport properties
- Timed released of medicines or nutrients
- Easy to modify
- Can be biodegradable or bioabsorbable

However, the conventional hydrogels also have some limitations:

- High cost
- Low mechanical strength
- Can be hard to handle
- May be difficult to sterilize
- Non-adherent

At present, the mechanical properties of hydrogels cannot meet the needs of tissue engineering, scaffold replacement, and other fields. The defect greatly limits the application of hydrogels in the field of biology and medicine. Therefore, scientists have shown great interest in how to improve the mechanical properties of hydrogels.

1.4 Multi-mechanism design of tough hydrogels

Most of the hydrogels show poor mechanical properties, and the mechanical properties greatly decreased with increasing the water content. For example, when the water absorption of a gelatin hydrogel is 5 times the weight of the dry hydrogel, the tensile strength is about 70 kPa, and the fracture elongation is 10%. However, when the water absorption of the gelatin hydrogel is 40 times the weight of the dry hydrogel, the tensile strength and fracture elongation is only 6 kPa and 11%, respectively [61]. The poor mechanical properties have seriously affected the possible application of the hydrogel. Traditionally, the strategies of increasing the tensile strength have been mainly focused on improving the cross-linking density of hydrogels. However, the tensile strength of hydrogels can not be improved by only increasing the crosslink density. Meanwhile, the stiffness, permeability, and diffusion of the hydrogel will

reduce by increasing the cross-linking density.

In recent years, due to tremendous demands for tough hydrogels in various applications, intensive research has been going on to improve mechanical strengths of hydrogels over the last few decades. Many hydrogels have shown significant enhancements of fracture toughness over their conventional counterparts. Strategies and concepts developed to make tough hydrogels capable of large deformation include Double-network hydrogel, Nanocomposite hydrogel, Topological hydrogel, Resilin-based hydrogel, Macromolecule cross-linking hydrogel, Covalently and physically cross-linked hydrogel, Slide ring hydrogel, Tetra-PEG hydrogel, Freeze-thaw technique, and so on.

1.4.1 Double-network hydrogel

Double-network hydrogels usually contain 80 to 90 weight percent (wt %) of water, yet are both hard and strong, with comparable mechanical properties to that of rubbers and cartilages [62, 63]. The hydrogels consist of two interpenetrating polymer networks with contrasting mechanical properties. The design principle can be summarized as follows: first, rigid and brittle polyelectrolyte serves as the first network, while soft and ductile neutral polymer serves as the second network; second, the molar concentration of the second network is 20–30 times that of the first network; third, the first network is tightly (making it stiff and brittle) while the second network is loosely cross-linked (making it soft and stretchable) to achieve a strong asymmetric gel structure.

The toughness is the ability of a material to absorb mechanical energy and deform without rupture. One of the definitions of material toughness is the fracture energy, which is the energy per unit area required to propagate a notch crack. Double-network gels are tough because the internal fracture of the brittle network dissipates substantial amounts of energy under large deformation, while the elasticity of the second network is able to return to its original shape after deformation. The fracture energy of the double network can always be much larger than those of either of the corresponding single networks (Fig. 1.7). Therefore, the material gains toughness by sacrificing the rupture

of the covalent bonds of the brittle first network. The covalent bonds serve as "sacrificial bonds," which used to describe how bones fracture [64].
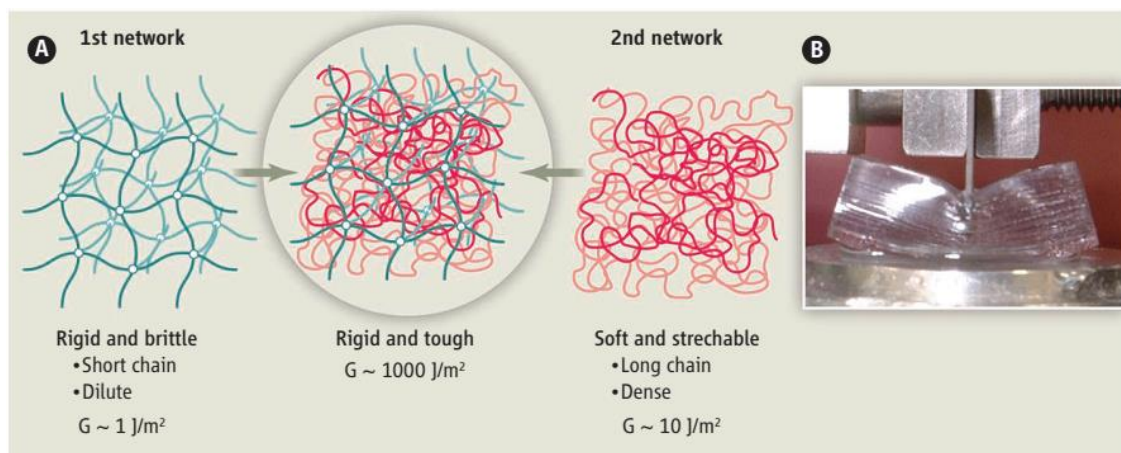
Fig. 1.7 The reinforce mechanism of the double-network hydrogel [64].

The double-network concept presents an overarching strategy for designing tough soft materials: incorporation of a mechanically fragile structure to toughen the material as a whole. This strategy is not limited to double- or multiple-network systems but also applies to single-network systems, as long as they have sacrificial bonds to dissipate energy and can retain the original configurations of the material after large deformation [65].

1.4.2 Nanocomposite hydrogel

Nanoparticles find their applications in common consumer products and appliances due to their differences in properties compared to bulk materials. This trend has raised public debate over the safety of nanoparticle technology, with regulators intervening in several countries. The challenges of nanoparticles application could potentially be overcome by incorporation into hydrogels, which resulting in decreased risks to human health and the environment. In addition, the innovative combination of these two completely different types of materials was not only thought of as creating structural diversity but also generating a plurality of property enhancements. These performance enhancements were the main focus of hydrogel-nanoparticle composite materials research leading to improved mechanical strength and stimuli response. For example, recently reported silica nanoparticle-hydrogel composite made of silica nanoparticles

and modified polyethylene glycol demonstrated remarkable improvements in tissue adhesive property, mechanical stiffness and bioactivity compared to hydrogel without nanoparticles [66, 67].

So far, researchers have reported three different supramolecular hydrogel-nanoparticle. i) micro or nano-gels stabilizing single/multiple nanoparticles, ii) nanoparticles non-covalently immobilized in a hydrogel matrix, and iii) nanoparticles covalently immobilized in a hydrogel matrix (Fig. 1.8). There are reviews on type (i) structures covering their applications in biomedicine, catalysis, and electronics [68]. Bulk hydrogels of type (ii) and (iii) have been reviewed by Schexnailder and Schmidt [69], but since then there have been few accounts covering only very specific applications [70].
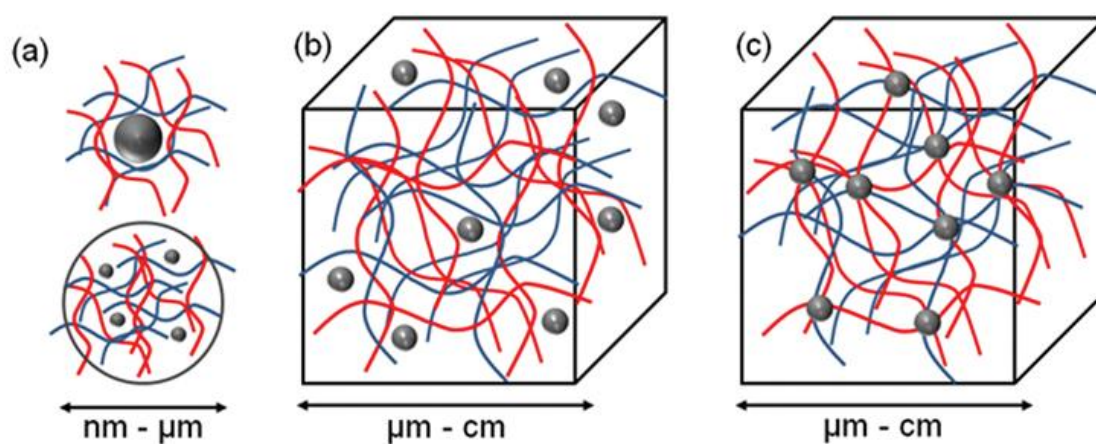
Fig. 1.8 Concept for combination of nanoparticles and hydrogel to form new functional materials [71].

1.4.3 Resilin-based hydrogel

Due to their potential applications in biomedical and tissue engineering, protein-based hydrogels have attracted considerable interest [72,73]. Most synthetic proteinaceous hydrogels are constructed from unstructured or non-globular proteins[74-76] and often do not have high stretchability or toughness, significantly limiting their scope of applications. However, folded globular proteins are found in a wide range of naturally occurring biological materials. The force-induced unfolding of

proteins can lead to a large extension of the polypeptide chain and result in effective energy dissipation [77-79]. Many biological systems, such as fibrin clots16, muscles [77, 80, 81] and extracellular matrices [79, 82] have effectively exploited such features to achieve desirable mechanical properties and regulate their biological functions.

Unfolding a small number of folded domains in the giant muscle protein titin effectively dissipates energy and prevents damage to the tissues by overstretching [81]. For example, Fang et al. report the engineering of a chemically cross-linked, highly elastic and tough protein hydrogel using a mechanically extremely labile, de novo-designed protein that assumes the classical ferredoxin-like fold structure. These hydrogels can withstand an average strain of 450% before breaking and show massive energy dissipation. Upon relaxation, refolding of the ferredoxin-like domains enables the hydrogel to recover its massive hysteresis. This novel biomaterial may expand the scope of hydrogel applications in tissue engineering (Fig. 1.9) [83].
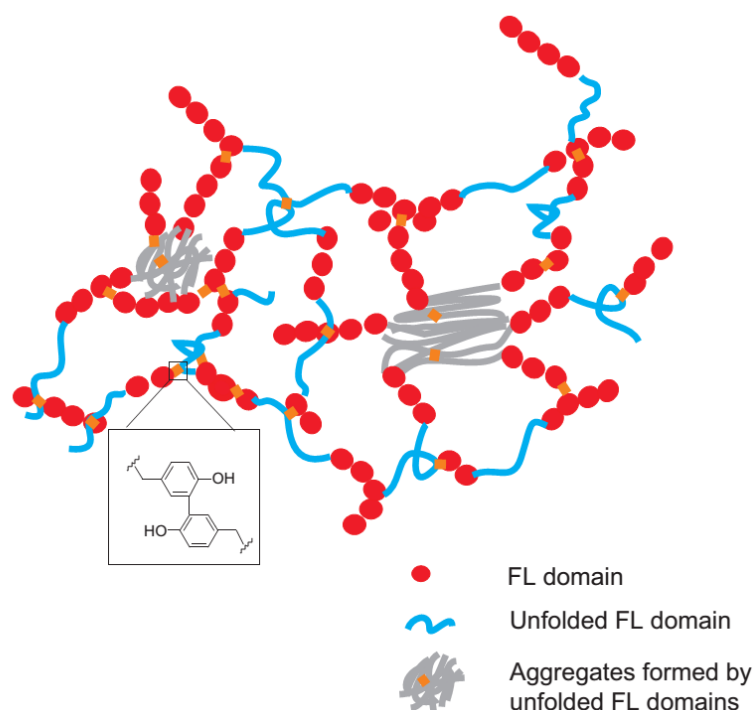
Fig. 1.9 Schematics of the structure of (FL)8-based hydrogels [83].

1.4.4 Macromolecule cross-linking hydrogel

The macromolecule cross-linking hydrogel is a hydrogel which macromolecular

polymer or macromolecular microsphere as covalent or physical cross-linker. The macromolecular cross-linker usually has two typical types. (i) The cross-linker contains many cross-linking sites (e.g. vinyl group), and act as multi-cross-linker in the hydrogel during the polymerization. (ii) Generating the free radical in the macromolecule chains through radiation, chemical reactions, ionization and so on; and then initiate the monomer polymerization.
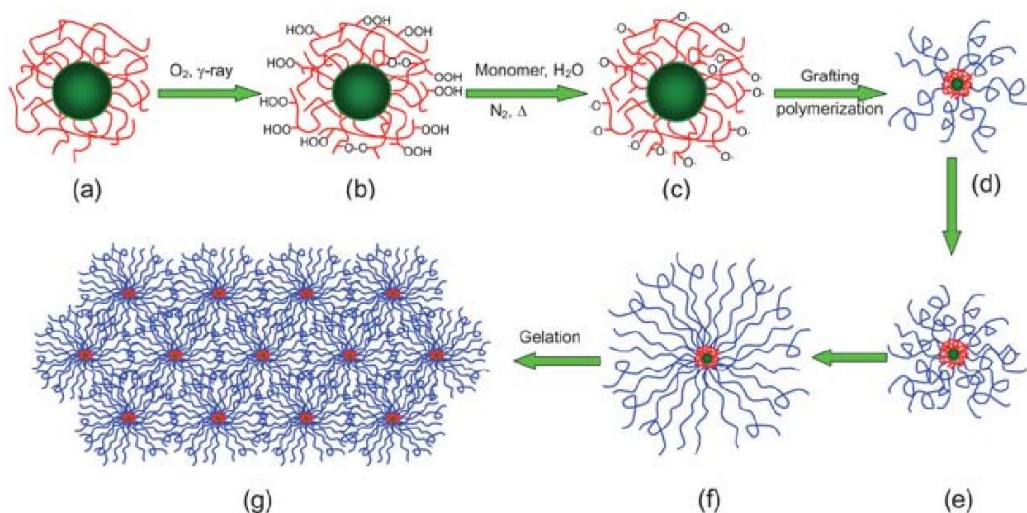
Fig. 1.10 Schematic representation of the formation of nanoparticles, microgels and a bulk hydrogel from micelles [84].

For example, Wang et al use peroxidized macromolecular microspheres (MMSs) as polyfunctional initiating and cross-linking centers (PFICC) [84]. Grafted polymer chains are covalently attached to the evenly distributed MMSs, and they can be chemically cross-linked by the mutual combination of growing grafted chains or be physically cross-linked by chain entanglement and hydrogen bonding among the polymer chains on vicinal MMSs (Fig. 1.10). Due to the even distribution of the cross-linking centers (MMSs) and the long grafted polymer chains with a similar length, the load applied on a gel sample can be evenly shared by all the polymer chains, leading to the high mechanical strengths. Due to this strategy, tough hydrogels are also obtained by using peroxidized micelles [84, 85], and graphene peroxide (GPO) sheets [86] as PFICC. The hydrogels exhibit excellent mechanical properties, namely, very high extensibility, tensile strengths and compressive strengths. In addition, the MMC gels

16

and the gels initiated and cross-linked by peroxidized micelles show good deformation recoverability in compression tests.

1.4.5 Covalently and physically cross-linked hydrogel

Covalently and physically cross-linked hydrogels are often termed as double cross-linked hydrogels. Several research groups have observed that the presence of network inhomogeneities and clusters of high cross-link densities reduce the strength of tough hydrogels [87, 88]. However, this trend might not apply to hydrogels that are both covalently and physically cross-linked. Multifunctional and reversible cross-linkers allow the hydrogel network to move during hydrogel stretching. Chain rearrangement is possible between the networks, which may reduce the number of defects [89]. Once the strain is released, the material may then self-heal to a certain degree. Polymer can reversibly attach and detach charged nanoparticle within the constraints of a covalently cross-linked network to form a tough nanocomposite polymer hydrogel.

Nanocomposite hydrogels prepared with PEG-DA and hydroxyapatite nanoparticles were observed to be very similar to the one found in the polymer–Laponite system [90]. The resulting tough materials are highly extensible (2000 %) and reach fracture stresses near 1 MPa (engineering values). Within a covalently cross-linked PEG network, the charged hydroxyapatite interacts with PEG through non-covalent interactions including ionic, dipole and hydrogen bonding schemes. These tough hydrogels have much in common with elastomers. The toughest samples are translucent to almost opaque. Therefore, photo cross-linking reactants require thinner samples and longer polymerization times. Since these materials were only recently discovered, more needs to be done to optimize the mechanical properties.

1.4.6 Slide ring hydrogel

"Slip-link" or slide ring polymer hydrogels are topological materials made from necklace-like macromolecules [91]. These hydrogels have been compared to pulleys and chains with knots. Moreover, cyclic cross-links can slide along a polymer chain and

thus allow for extensive stretching. The chain ends have stopper molecules (topological restrictions) that prevent dissociation of the cyclic molecules from the axis. The cyclic molecules are polyrotaxane or catenane rings that can be chemically modified to better suit specific applications.
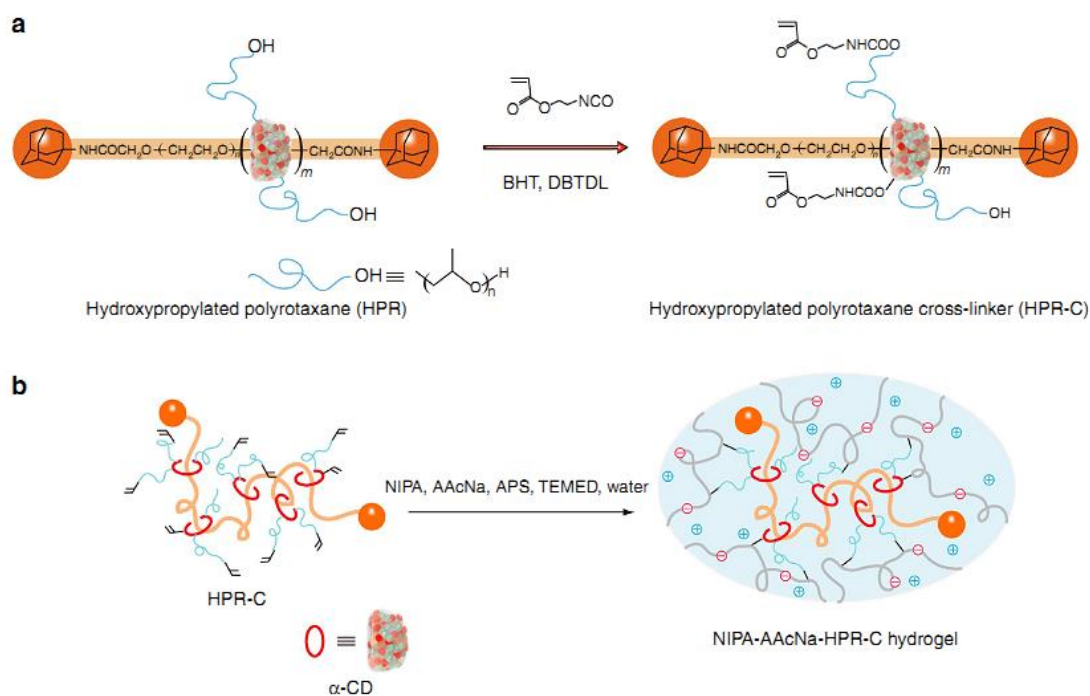
Fig. 1.11 Preparation of the polyelectrolyte hydrogels using

nonionic PR cross-linker [92].

Imran et al prepare extremely stretchable thermosensitive hydrogels with good toughness by using polyrotaxane derivatives composed of a-cyclodextrin and polyethylene glycol as cross-linkers and introducing ionic groups into the polymer network (Fig. 1.11). The ionic groups help the polyrotaxane cross-linkers to become well extended in the polymer network. The resulting hydrogels are surprisingly stretchable and tough because the cross-linked a-cyclodextrin molecules can move along the polyethylene glycol chains. In addition, the polyrotaxane cross-linkers can be used with a variety of vinyl monomers; the mechanical properties of the wide variety of polymer gels can be improved by using these cross-linkers [92].

1.4.7 Tetra-PEG hydrogel

Tetra-PEG hydrogels can be made from tetra-PEG macromers containing functional groups such as amines and esters [93, 94]. These hydrogels are a different and unique class of tough materials. In this hydrogel, network defects are negligible and there are no trapped entanglements between the polymer chains [95]. Mechanical testing and scattering experiments suggest that the hydrogels consist of elastic polymer "blobs" (i.e., coils) that are packed within the hydrogels. For example, cross-end coupling of tetra-amine-terminated PEG and tetra-N-hydroxysuccinimide-glutaraldehyde-terminated PEG leads to hydrogel networks with high cross-linking efficiency and little hysteresis. This behavior is very similar to that of an elastic rubber.
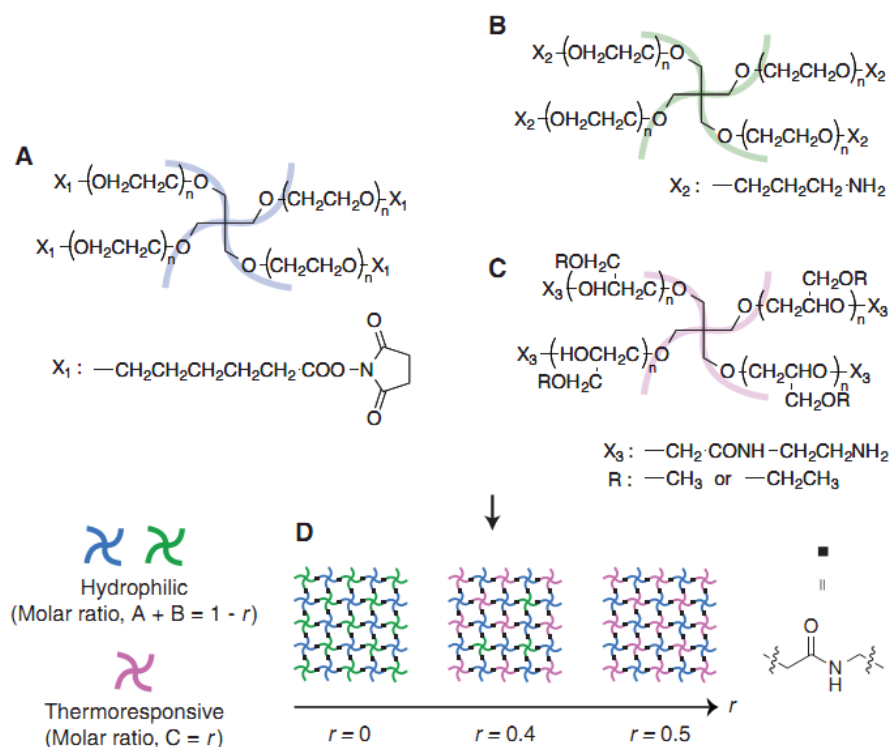
Fig. 1.12 Schematic of the Tetra-PEG hydrogel system [99].

Scattering studies show that these tetra-PEG hydrogels are mostly homogeneous with low concentration fluctuations comparable to those of the corresponding solutions [93, 96]. Concentration fluctuations are changes in density within the same hydrogel. When the ratio of the reacting macromonomers is not stoichiometric ratio, heterogeneity will occur due to an increase in structural defects [97, 98]. Kamata et al. report the synthesis

of injectable "nonswellable" hydrogels from hydrophilic and thermoresponsive polymers, in which two independently occurring effects (swelling and shrinking) oppose each other (Fig. 1.12). The hydrogels can endure a compressive stress up to 60 MPa and can be stretched more than sevenfold without hysteresis [99].

1.4.8 Freeze-thaw technique

Freeze-thaw technology (Freeze-thaw technique) is a physical cross-linking method for the preparation of hydrogels. The hydrogels prepared by this method can have good mechanical strength at higher water content [100, 101]. The molecular motion of the aqueous solution can be fixed by van der waals forces and/or hydrogen bonds, and some molecular segments in a certain region can even form an ordered structure. After thawing, these closely bound ordered domains are no longer separated, and when re-frozen, a newly ordered micro-domain is generated. So the use of repeated freezing and thawing method can promote molecular movement, rearrangement, so as to obtain a crystalline or semi-crystalline structure of the hydrogel. Only the absorbent polymer can form a semi-crystalline or crystalline region to use this method. Thus, so far, this method can be only applied to PVA hydrogel system.

1.4.9 Prospect

The next-generation tough hydrogels should be able to maintain high toughness in various environments and under various loading conditions. However, as discussed above, hydrogels that rely on a single pair of mechanisms may lose their toughness due to environmental and loading effects. A promising strategy to design next-generation tough hydrogels is to integrate multiple pairs of mechanisms across multiple length scales into a hydrogel. In this way, if one pair of mechanisms becomes ineffective, other pairs can still maintain high toughness of the hydrogel [65].

1.5 Purpose of this research

Hydrogels have become very popular due to their unique properties such as high

water content, softness, flexibility, and biocompatibility. Natural and synthetic hydrophilic polymers can be physically or chemically cross-linked in order to produce hydrogels. Their resemblance to living tissue opens up many opportunities for applications in biomedical areas. Currently, hydrogels are used for manufacturing contact lenses, hygiene products, tissue engineering scaffolds, drug delivery systems and wound dressings. Although hydrogels have brilliant future in the next decade, the mechanical properties of the hydrogel have some distance from their final application. Therefore, our goal is to design a hydrogel with the required mechanical properties to meet the requirements of various application fields. In this study, we used cellulose derivatives (carboxymethyl cellulose, nano-cellulose fiber) as macromolecule cross-linker to prepare a series of hydrogels with special mechanical properties by polymerization or condensation reaction. These hydrogels are expected to be used in the fields of biomedicine, mechanical engineering and so on.

References

[1] Lloyd DJ. Chemistry of the Proteins and its Economic Applications. Chemistry of the Proteins and its Economic Applications. 1926.

[2] Li J, Mooney DJ. Designing hydrogels for controlled drug delivery. Nature Reviews Materials. 2016;1(12):16071.

[3] Basak S, Nanda J, Banerjee A. A new aromatic amino acid based organogel for oil spill recovery. Journal of Materials Chemistry. 2012;22(23):11658.

[4] Peppas NA, Huang Y, Torres-Lugo M, Ward JH, Zhang J. Physicochemical foundations and structural design of hydrogels in medicine and biology. Annual review of biomedical engineering. 2000;2:9-29.

[5] Chang C, Duan B, Cai J, Zhang L. Superabsorbent hydrogels based on cellulose for smart swelling and controllable delivery. European Polymer Journal. 2010;46(1):92-100.

[6] Estroff LA, Hamilton AD. Water gelation by small organic molecules. Chemical reviews. 2004;104(3):1201-18.

[7] Richter A. Hydrogels for Actuators. 2009;6:221-48.

[8] Gerlach G, Arndt K-F. <Hydrogel Sensors and Actuators.pdf>. 2010;6.

[9] Davies ML, Murphy SM, Hamilton CJ, Tighe BJ. Polymer membranes in clinical sensor applications. Biomaterials. 1992;13(14):991-9.

[10] Richter A, Paschew G, Klatt S, Lienig J, Arndt KF, Adler HP. Review on Hydrogel-based pH Sensors and Microsensors. Sensors. 2008;8(1):561-81.

[11] Tokarev I, Minko S. Stimuli-responsive hydrogel thin films. Soft Matter. 2009;5(3):511-24.

[12] Wicklein B, Kocjan A, Salazar-Alvarez G, Carosio F, Camino G, Antonietti M, et al. Thermally insulating and fire-retardant lightweight anisotropic foams based on nanocellulose and graphene oxide. Nature nanotechnology. 2015;10(3):277-83.

[13] Wang Y, Brunsen A, Jonas U, Dostalek J, Knoll W. Prostate specific antigen biosensor based on long range surface plasmon-enhanced fluorescence spectroscopy and dextran hydrogel binding matrix. Analytical chemistry. 2009;81(23):9625-32.

[14] Gehrke SH, Uhden LH, McBride JF. Enhanced loading and activity retention of bioactive proteins in hydrogel delivery systems. Journal of Controlled Release. 1998;55(1):21-33.

[15] Andersson O, Larsson A, Ekblad T, Liedberg B. Gradient hydrogel matrix for microarray and biosensor applications: an imaging SPR study. Biomacromolecules. 2009;10(1):142-8.

[16] Yang X, Pan X, Blyth J, Lowe CR. Towards the real-time monitoring of glucose in tear fluid: holographic glucose sensors with reduced interference from lactate and pH. Biosensors & bioelectronics. 2008;23(6):899-905.

[17] Drury JL, Mooney DJ. Hydrogels for tissue engineering: scaffold design variables and applications. Biomaterials. 2003;24(24):4337-51.

[18] Brandl F, Sommer F, Goepferich A. Rational design of hydrogels for tissue engineering: impact of physical factors on cell behavior. Biomaterials. 2007;28(2):134-46.

[19] Cushing MC, Anseth KS. Materials science. Hydrogel cell cultures. Science. 2007;316(5828):1133-4.

[20] Nuttelman CR, Rice MA, Rydholm AE, Salinas CN, Shah DN, Anseth KS. Macromolecular Monomers for the Synthesis of Hydrogel Niches and Their Application in Cell Encapsulation and Tissue Engineering. Prog Polym Sci. 2008;33(2):167-79.

[21] Slaughter BV, Khurshid SS, Fisher OZ, Khademhosseini A, Peppas NA. Hydrogels in regenerative medicine. Advanced materials. 2009;21(32-33):3307-29.

[22] Liu SQ, Tay R, Khan M, Rachel Ee PL, Hedrick JL, Yang YY. Synthetic hydrogels for controlled stem cell differentiation. Soft Matter. 2010;6(1):67-81.

[23] Zhu J. Bioactive modification of poly(ethylene glycol) hydrogels for tissue engineering. Biomaterials. 2010;31(17):4639-56.

[24] Beamish JA, Zhu J, Kottke‑Marchant K, Marchant RE. The effects of monoacrylated poly (ethylene glycol) on the properties of poly (ethylene glycol) diacrylate hydrogels used for tissue engineering. Journal of Biomedical Materials Research Part A. 2010;92(2):441-50.

[25] Schneider GB, English A, Abraham M, Zaharias R, Stanford C, Keller J. The effect of hydrogel charge density on cell attachment. Biomaterials. 2004;25(15):3023-8.

[26] Vihola H, Laukkanen A, Valtola L, Tenhu H, Hirvonen J. Cytotoxicity of thermosensitive polymers poly(N-isopropylacrylamide), poly(N-vinylcaprolactam) and amphiphilically modified poly(N-vinylcaprolactam). Biomaterials. 2005;26(16):3055-64.

[27] Zustiak SP, Leach JB. Hydrolytically degradable poly (ethylene glycol) hydrogel scaffolds with tunable degradation and mechanical properties. Biomacromolecules. 2010;11(5):1348-57.

[28] Malkoch M, Vestberg R, Gupta N, Mespouille L, Dubois P, Mason AF, et al. Synthesis of well-defined hydrogel networks using click chemistry. Chemical communications. 2006(26):2774-6.

[29] Hauser CA, Zhang S. Designer self-assembling peptide nanofiber biological materials. Chemical Society reviews. 2010;39(8):2780-90.

[30] Jayawarna V, Richardson SM, Hirst AR, Hodson NW, Saiani A, Gough JE, et al. Introducing chemical functionality in Fmoc-peptide gels for cell culture. Acta biomaterialia. 2009;5(3):934-43.

[31] Galler KM, Aulisa L, Regan KR, D'Souza RN, Hartgerink JD. Self-assembling multidomain peptide hydrogels: designed susceptibility to enzymatic cleavage allows enhanced cell migration and spreading. Journal of the American Chemical Society. 2010;132(9):3217-23.

[32] Deshmukh M, Singh Y, Gunaseelan S, Gao D, Stein S, Sinko PJ. Biodegradable poly(ethylene glycol) hydrogels based on a self-elimination degradation mechanism. Biomaterials. 2010;31(26):6675-84.

[33] Salinas CN, Anseth KS. Decorin moieties tethered into PEG networks induce chondrogenesis of human mesenchymal stem cells. Journal of Biomedical Materials Research Part A. 2009;90(2):456-64.

[34] Cheung CY, McCartney SJ, Anseth KS. Synthesis of polymerizable superoxide dismutase mimetics to reduce reactive oxygen species damage in transplanted biomedical devices. Advanced Functional Materials. 2008;18(20):3119-26.

[35] Jing P, Rudra JS, Herr AB, Collier JH. Self-assembling peptide-polymer hydrogels designed from the coiled coil region of fibrin. Biomacromolecules. 2008;9(9):2438-46.

[36] Higuchi A, Aoki N, Yamamoto T, Miyazaki T, Fukushima H, Tak TM, et al. Temperature‐induced cell detachment on immobilized pluronic surface. Journal of Biomedical Materials Research Part A. 2006;79(2):380-92.

[37] Nonoyama T, Wada S, Kiyama R, Kitamura N, Mredha MT, Zhang X, et al. Double-Network Hydrogels Strongly Bondable to Bones by Spontaneous Osteogenesis Penetration. Advanced materials. 2016;28(31):6740-5.

[38] Altoparlak U, Erol S, Akcay MN, Celebi F, Kadanali A. The time-related changes of antimicrobial resistance patterns and predominant bacterial profiles of burn wounds and body flora of burned patients. Burns : journal of the International Society for Burn Injuries. 2004;30(7):660-4.

[39] Erol S, Altoparlak U, Akcay MN, Celebi F, Parlak M. Changes of microbial flora and wound colonization in burned patients. Burns : journal of the International Society for Burn Injuries. 2004;30(4):357-61.

[40] Sharma B. Infection in patients with severe burns: causes and prevention thereof. Infectious disease clinics of North America. 2007;21(3):745-59.

[41] Kamoun EA, Kenawy ES, Chen X. A review on polymeric hydrogel membranes for wound dressing applications: PVA-based hydrogel dressings. Journal of advanced research. 2017;8(3):217-33.

[42] Kenawy E-R, Kamoun EA, Eldin MSM, El-Meligy MA. Physically crosslinked poly (vinyl alcohol)-hydroxyethyl starch blend hydrogel membranes: Synthesis and characterization for biomedical applications. Arabian Journal of Chemistry. 2014;7(3):372-80.

[43] Zhao L, Mitomo H, Zhai M, Yoshii F, Nagasawa N, Kume T. Synthesis of antibacterial PVA/CM-chitosan blend hydrogels with electron beam irradiation. Carbohydrate Polymers. 2003;53(4):439-46.

[44] Shi Y, Peng L, Ding Y, Zhao Y, Yu G. Nanostructured conductive polymers for advanced energy storage. Chemical Society reviews. 2015;44(19):6684-96.

[45] Yin Z, Zheng Q. Controlled Synthesis and Energy Applications of One‑Dimensional Conducting Polymer Nanostructures: An Overview. Advanced Energy Materials. 2012;2(2):179-218.

[46] Tran HD, Li D, Kaner RB. One‑Dimensional Conducting Polymer Nanostructures: Bulk Synthesis and Applications. Advanced materials. 2009;21(14‑15):1487-99.

[47] Joshi RK, Schneider JJ. Assembly of one dimensional inorganic nanostructures into functional 2D and 3D architectures. Synthesis, arrangement and functionality. Chemical Society reviews. 2012;41(15):5285-312.

[48] Tran HD, Shin K, Hong WG, D'Arcy JM, Kojima RW, Weiller BH, et al. A Template‑Free Route to Polypyrrole Nanofibers. Macromolecular rapid communications. 2007;28(24):2289-93.

[49] Qu L, Shi G, Chen Fe, Zhang J. Electrochemical growth of polypyrrole microcontainers. Macromolecules. 2003;36(4):1063-7.

[50] Li D, Huang J, Kaner RB. Polyaniline nanofibers: a unique polymer nanostructure for versatile applications. Accounts of chemical research. 2008;42(1):135-45.

[51] Lei Z, Wang Q, Sun S, Zhu W, Wu P. A Bioinspired Mineral Hydrogel as a Self-Healable, Mechanically Adaptable Ionic Skin for Highly Sensitive Pressure Sensing. Advanced materials. 2017;29(22).

[52] Tai Y, Mulle M, Aguilar Ventura I, Lubineau G. A highly sensitive, low-cost, wearable pressure sensor based on conductive hydrogel spheres. Nanoscale. 2015;7(35):14766-73.

[53] Jung BC, Lee D, Youn BD, Lee S. A statistical characterization method for damping material properties and its application to structural-acoustic system design. Journal of Mechanical Science and Technology. 2011;25(8):1893-904.

[54] Wu Y, Chen YX, Yan J, Yang S, Dong P, Soman P. Fabrication of conductive polyaniline hydrogel using porogen leaching and projection microstereolithography. J Mater Chem B. 2015;3(26):5352-60.

[55] Wu Z-Y, Liang H-W, Chen L-F, Hu B-C, Yu S-H. Bacterial Cellulose: A Robust Platform for Design of Three Dimensional Carbon-Based Functional Nanomaterials. Accounts of Chemical Research. 2016;49(1):96-105.

[56] Wang W, Zhang Y, Liu W. Bioinspired fabrication of high strength hydrogels from non-covalent interactions. Progress in Polymer Science. 2017.

[57] Hayes JC, Curley C, Tierney P, Kennedy JE. Biomechanical analysis of a salt-modified polyvinyl alcohol hydrogel for knee meniscus applications, including comparison with human donor samples. Journal of the mechanical behavior of biomedical materials. 2016;56:156-64.

[58] Karlgard C, Wong N, Jones L, Moresoli C. In vitro uptake and release studies of ocular pharmaceutical agents by silicon-containing and p-HEMA hydrogel contact lens materials. International journal of pharmaceutics. 2003;257(1):141-51.

[59] Yoshida R. Self-Oscillating Gels Driven by the Belousov-Zhabotinsky Reaction as Novel Smart Materials. Advanced materials. 2010;22(31):3463-83.

[60] Maeda S, Hara Y, Yoshida R, Hashimoto S. Active polymer gel actuators. International journal of molecular sciences. 2010;11(1):52-66.

[61] Calvert P. Hydrogels for Soft Machines. Advanced materials. 2009;21(7):743-56.

[62] Gong JP, Katsuyama Y, Kurokawa T, Osada Y. Double-Network Hydrogels with Extremely High Mechanical Strength. Advanced materials. 2003;15(14):1155-8.

[63] Gong JP. Why are double network hydrogels so tough? Soft Matter. 2010;6(12):2583.

[64] Zhao X, Zhou H, Sikarwar VS, Zhao M, Park A-HA, Fennell PS, et al. Biomass-based chemical looping technologies: the good, the bad and the future. Energy Environ Sci. 2017.

[65] Zhao X. Multi-scale multi-mechanism design of tough hydrogels: building dissipation into stretchy networks. Soft Matter. 2014;10(5):672-87.

[66] Liu Y, Meng H, Konst S, Sarmiento R, Rajachar R, Lee BP. Injectable dopamine-modified poly (ethylene glycol) nanocomposite hydrogel with enhanced adhesive property and bioactivity. ACS applied materials & interfaces. 2014;6(19):16982-92.

[67] Skelton S, Bostwick M, O'Connor K, Konst S, Casey S, Lee BP. Biomimetic adhesive containing nanocomposite hydrogel with enhanced materials properties. Soft Matter. 2013;9(14):3825-33.

[68] Li J, Mooney DJ. Designing hydrogels for controlled drug delivery. Nature Reviews Materials. 2016;1(12):16071.

[69] Silva RM, Rodrigues JL, Pinto VV, Ferreira MJ, Russo R, Pereira CM. Evaluation of shock absorption properties of rubber materials regarding footwear applications. Polymer Testing. 2009;28(6):642-7.

[70] Zhang L, Wang Z, Xu C, Li Y, Gao J, Wang W, et al. High strength graphene oxide/polyvinyl alcohol composite hydrogels. Journal of Materials Chemistry. 2011;21(28):10399.

[71] Thoniyot P, Tan MJ, Karim AA, Young DJ, Loh XJ. Nanoparticle-Hydrogel Composites: Concept, Design, and Applications of These Promising, Multi-Functional Materials. Advanced Science. 2015;2(1-2):n/a-n/a.

[72] Lutolf M, Hubbell J. Synthetic biomaterials as instructive extracellular microenvironments for morphogenesis in tissue engineering. Nature biotechnology. 2005;23(1):47.

[73] Langer R, Tirrell DA. Designing materials for biology and medicine. Nature. 2004;428(6982):487.

[74] Petka WA, Harden JL, McGrath KP, Wirtz D, Tirrell DA. Reversible hydrogels from self-assembling artificial proteins. Science. 1998;281(5375):389-92.

[75] Kopeček J. Hydrogel biomaterials: a smart future? Biomaterials. 2007;28(34):5185-92.

[76] Nagapudi K, Brinkman WT, Leisen J, Thomas BS, Wright ER, Haller C, et al. Protein-based thermoplastic elastomers. Macromolecules. 2005;38(2):345-54.

[77] Rief M, Gautel M, Oesterhelt F, Fernandez JM, Gaub HE. Reversible unfolding of individual titin immunoglobulin domains by AFM. science. 1997;276(5315):1109-12.

[78] Cao Y, Li H. Polyprotein of GB1 is an ideal artificial elastomeric protein. Nature materials. 2007;6(2):109.

[79] Klotzsch E, Smith ML, Kubow KE, Muntwyler S, Little WC, Beyeler F, et al. Fibronectin forms the most extensible biological fibers displaying switchable force-exposed cryptic binding sites. Proceedings of the National Academy of Sciences. 2009;106(43):18267-72.

[80] Li H, Linke WA, Oberhauser AF, Carrion-Vazquez M. Reverse engineering of the giant muscle protein titin. Nature. 2002;418(6901):998.

[81] Minajeva A, Kulke M, Fernandez JM, Linke WA. Unfolding of titin domains explains the viscoelastic behavior of skeletal myofibrils. Biophysical journal. 2001;80(3):1442-51.

[82] Lemmon CA, Ohashi T, Erickson HP. Probing the folded state of fibronectin type III domains in stretched fibrils by measuring buried cysteine accessibility. Journal of biological chemistry. 2011;286(30):26375-82.

[83] Fang J, Mehlich A, Koga N, Huang J, Koga R, Gao X, et al. Forced protein unfolding leads to highly elastic and tough protein hydrogels. Nature communications. 2013;4:2974.

[84] He C, Jiao K, Zhang X, Xiang M, Li Z, Wang H. Nanoparticles, microgels and bulk hydrogels with very high mechanical strength starting from micelles. Soft Matter. 2011;7(6):2943-52.

[85] Sun Y-n, Gao G-r, Du G-l, Cheng Y-j, Fu J. Super tough, ultrastretchable, and thermoresponsive hydrogels with functionalized triblock copolymer micelles as macro-cross-linkers. ACS Macro Letters. 2014;3(5):496-500.

[86] Liu J, Chen C, He C, Zhao J, Yang X, Wang H. Synthesis of graphene peroxide and its application in fabricating super extensible and highly resilient nanocomposite hydrogels. Acs Nano. 2012;6(9):8194-202.

[87] Webber RE, Creton C, Brown HR, Gong JP. Large strain hysteresis and mullins effect of tough double-network hydrogels. Macromolecules. 2007;40(8):2919-27.

[88] Naseri N, Deepa B, Mathew AP, Oksman K, Girandon L. Nanocellulose-Based Interpenetrating Polymer Network (IPN) Hydrogels for Cartilage Applications. Biomacromolecules. 2016;17(11):3714-23.

[89] Wu C-J, Gaharwar AK, Chan BK, Schmidt G. Mechanically tough pluronic F127/laponite nanocomposite hydrogels from covalently and physically cross-linked networks. Macromolecules. 2011;44(20):8215-24.

[90] Javadi A, Zheng Q, Payen F, Javadi A, Altin Y, Cai Z, et al. Polyvinyl alcohol-cellulose nanofibrils-graphene oxide hybrid organic aerogels. ACS applied materials & interfaces. 2013;5(13):5969-75.

[91] Abraham A, Mathew AK, Sindhu R, Pandey A, Binod P. Potential of rice straw for bio-refining: An overview. Bioresource technology. 2016;215:29-36.

[92] Bin Imran A, Esaki K, Gotoh H, Seki T, Ito K, Sakai Y, et al. Extremely stretchable thermosensitive hydrogels by introducing slide-ring polyrotaxane cross-linkers and ionic groups into the polymer network. Nature communications. 2014;5:5124.

[93] Zhang L, Shi G. Preparation of Highly Conductive Graphene Hydrogels for Fabricating Supercapacitors with High Rate Capability. The Journal of Physical Chemistry C. 2011;115(34):17206-12.

[94] Matsuhisa N, Inoue D, Zalar P, Jin H, Matsuba Y, Itoh A, et al. Printable elastic conductors by in situ formation of silver nanoparticles from silver flakes. Nature materials. 2017.

[95] Butylina S, Geng S, Oksman K. Properties of as-prepared and freeze-dried hydrogels made from poly(vinyl alcohol) and cellulose nanocrystals using freeze-thaw technique. European Polymer Journal. 2016;81:386-96.

[96] Abitbol T, Johnstone T, Quinn TM, Gray DG. Reinforcement with cellulose nanocrystals of poly(vinyl alcohol) hydrogels prepared by cyclic freezing and thawing. Soft Matter. 2011;7(6):2373.

[97] Akagi Y, Matsunaga T, Shibayama M, Chung U-i, Sakai T. Evaluation of topological defects in tetra-PEG gels. Macromolecules. 2009;43(1):488-93.

[98] Millon LE, Wan WK. The polyvinyl alcohol-bacterial cellulose system as a new nanocomposite for biomedical applications. Journal of biomedical materials research Part B, Applied biomaterials. 2006;79(2):245-53.

[99] Kamata H, Akagi Y, Kayasuga-Kariya Y, Chung UI, Sakai T. "Nonswellable" hydrogel without mechanical hysteresis. Science. 2014;343(6173):873-5.

[100] Ricciardi R, Auriemma F, Gaillet C, De Rosa C, Lauprêtre F. Investigation of the crystallinity of freeze/thaw poly (vinyl alcohol) hydrogels by different techniques. Macromolecules. 2004;37(25):9510-6.

[101] Ricciardi R, D'Errico G, Auriemma F, Ducouret G, Tedeschi AM, De Rosa C, et al. Short time dynamics of solvent molecules and supramolecular organization of poly (vinyl alcohol) hydrogels obtained by freeze/thaw techniques. Macromolecules. 2005;38(15):6629-39.

Chapter 2 Materials, Experiment and Characterizations

2.1 Materials

Cellulose is considered the most abundant, renewable polymer resource on earth. It has been estimated that 10^{11} - 10^{12} tons cellulose are produced by photosynthesis every year. The most famous is the seed hairs of the cotton plant but mostly are combined with lignin and hemicelluloses in the cell wall of woody plants [1, 2]. Cellulose is a natural polymer raw material generally used for two purposes. (i) Cellulose has served as a construction material, mainly in the form of intact wood and textile fibers, or in the form of paper and board [3]. (ii) In recent centuries, cellulose is a versatile raw material for chemical conversions, such as cellulose-based threads or films as well as a variety of cellulose derivatives (carboxymethyl cellulose, cellulose acetate, hydroxypropyl cellulose and nano-cellulose etc.) [4, 5].

2.1.1 Carboxymethyl cellulose (CMC)

CMC is a cellulose derivative with carboxymethyl groups (-CH2-COOH) bound to some of the hydroxyl groups of the glucopyranose monomers that make up the cellulose backbone (Fig. 2.1). It is often used as its sodium salt, sodium carboxymethyl cellulose. It is synthesized by the alkali-catalyzed reaction of cellulose with chloroacetic acid [6]. The polar (organic acid) carboxyl groups render the cellulose soluble and chemically reactive. It has been widely used due to its high viscosity, nontoxic and hypoallergenic [7].
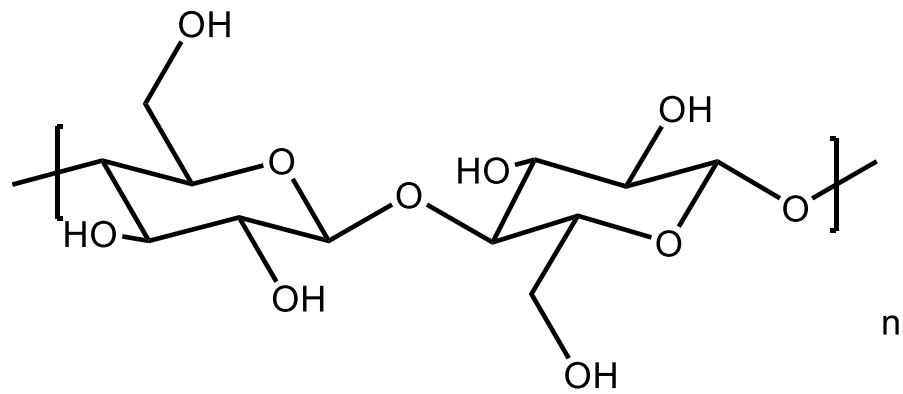
Cellulose, Nano-cellulose
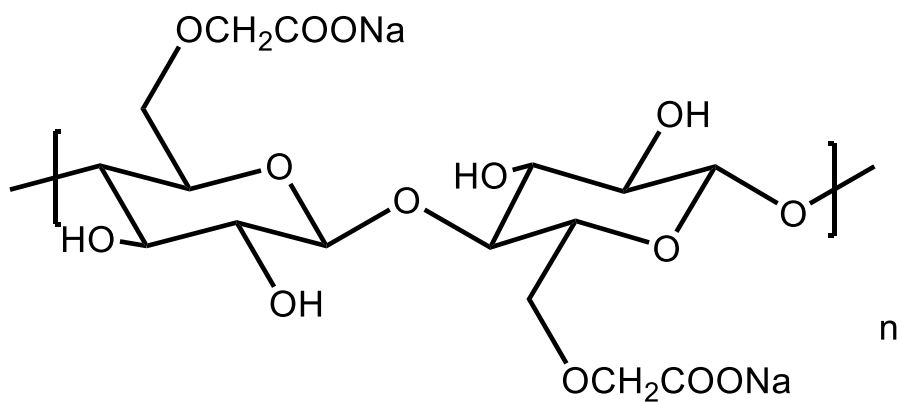
Carboxymethyl cellulose

Fig. 2.1 Chemical structure of cellulose, cellulose nanofiber and carboxymethyl cellulose.

2.1.2 Cellulose nanofiber (CNF)

Nanocellulose is a term referring to nano-structured cellulose. This may be either cellulose nanofibers (CNF) also called microfibrillated cellulose (MFC), nanocrystalline cellulose (NCC or CNC), or bacterial nanocellulose, which refers to nano-structured cellulose produced by bacteria.[8] CNF is a material composed of nanosized cellulose fibrils with a high aspect ratio (length to width ratio). Typical fibril widths are 5–20 nanometers with a wide range of lengths, typically several micrometers [9]. It is pseudo-plastic and exhibits thixotropy, the property of certain gels or fluids that are thick (viscous) under normal conditions, but become less viscous when shaken

or agitated. When the shearing forces are removed the gel regains much of its original state. The fibrils are isolated from any cellulose containing source including wood-based fibers (pulp fibers) through high-pressure, high temperature and high velocity impact homogenization, grinding or microfluidization [10].

2.1.3 Other chemical reagents

In this research, ceric ammonium nitrate (CAN), acrylic acid (AA), *N,N′*-methylene bis(acrylamide) (MBA), sodium chloride (NaCl), aluminium chloride hexahydrate (AlCl$_3$·6H$_2$O), Sodium periodate (NaIO$_4$), Nitric acid (HNO$_3$)，were purchased from Nacalai Tesque, Inc. All chemical reagents were used as received. Distilled water was used in all experiments.

2.2 Experiment method

2.2.1 Visible-light-trigger polymerization

In the following series experiments, it is found that carboxymethyl cellulose has a characteristic oxidation phenomenon in the presence of cerium ions under visible light (Fig. 2.2).
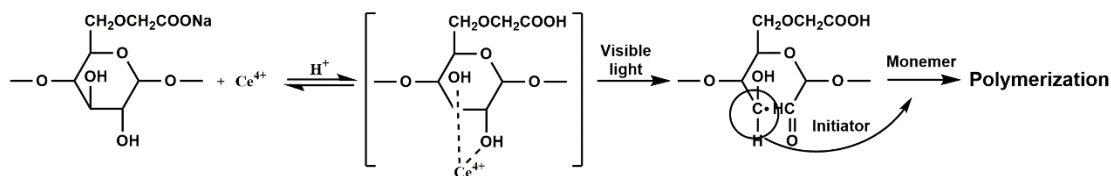
Fig. 2.2 Mechanism of visible-light-trigger polymerization.

(a) Preparation of carboxymethyl cellulose/polyacrylic acid (CMC/PAA) hydrogel

A certain amount of carboxymethyl cellulose was slowly added to the mixture under strong magnetic stirring. After vigorous stirring for 1 h, the CMC was stably dispersed. We then poured the hydrogel precursor into a transparent glass mold and covered it with a glass plate. The mold was immersed in an ice-water bath and was placed 25 cm below a visible light source (LS-M210, Sumita) with 50% power output. The process of

hydrogel formation required only a few minutes. The transparent carboxymethyl cellulose/polyacrylic acid (CMC/PAA) hydrogel was then sealed and stored at 4 °C for future testing.

(b) Synthesis of high resilience Gel with adding molecule cross-linker

The hydrogel synthesis method was modified from 2.2.1 (a). In brief, the hydrogels were prepared as follows: 40 mg CAN, 4.00 g AA, and 10.0 mL of a series MBA aqueous solutions were added to a vial step by step, and mixed by magnetic stirring in an ice bath. After that, 0.40 g CMC was slowly added to the mixture with strong magnetic stirring. The precursor hydrogel was stably dispersed for 1 h with vigorous stirring. The viscous precursor hydrogel was transferred into a transparent glass mold and covered with a glass plate. Finally, the glass mold was placed 20 cm below a visible light (LS-M210, Sumita, 50% output) for 5 min. The obtained hydrogels were cut into different sizes for further testing.

(c) Preparation of high modulus hydrogel (HM-Gel) via evaporation-swelling method

The HM-Gels were prepared *via* two steps consisting of visible-light-triggered polymerization and evaporation-swelling. The synthesis of hydrogel part also referenced 2.2.1 (a). On this basis, one more operation was carried out: a range of concentrations of $AlCl_3 \cdot 6H_2O$ (0–1.5 mol%, Al^{3+} to AA) was added to a series of vials, and the mixtures were stirred for 20 min. The prepared carboxymethyl cellulose/polyacrylic acid hydrogels were named Gel-*X*, where *X* denoted the Al^{3+} concentration (mol%) relative to that of monomer (AA). The obtained Gels were placed in a dry oven and dried at various temperatures for 24 h (for 25 °C, the hydrogel was dried at room temperature for 3 days). The dried Gels were immersed in distilled water for 50 h to obtain a swelling equilibrium. The swollen hydrogels at equilibrium with a high modulus were named HM-Gel. All hydrogels were dried in air at 60 °C.

2.2.2 Aldolization cross-linking

(a) Cellulose oxidation

2 g cellulose nanofiber (solid content) and 60 mL distilled water were added in 250 mL conical flask. The mixture was magnetically stirred for 10 minutes to disperse the CNF. Then a certain amount of $NaIO_4$ was added into the conical flask, the mixture was magnetically stirred for 48 h under a dark environment. The oxidation products were separated by centrifugation and washing with distilled water for three times to removal the excess raw materials and reduced impurity ions (Fig. 2.3 a).
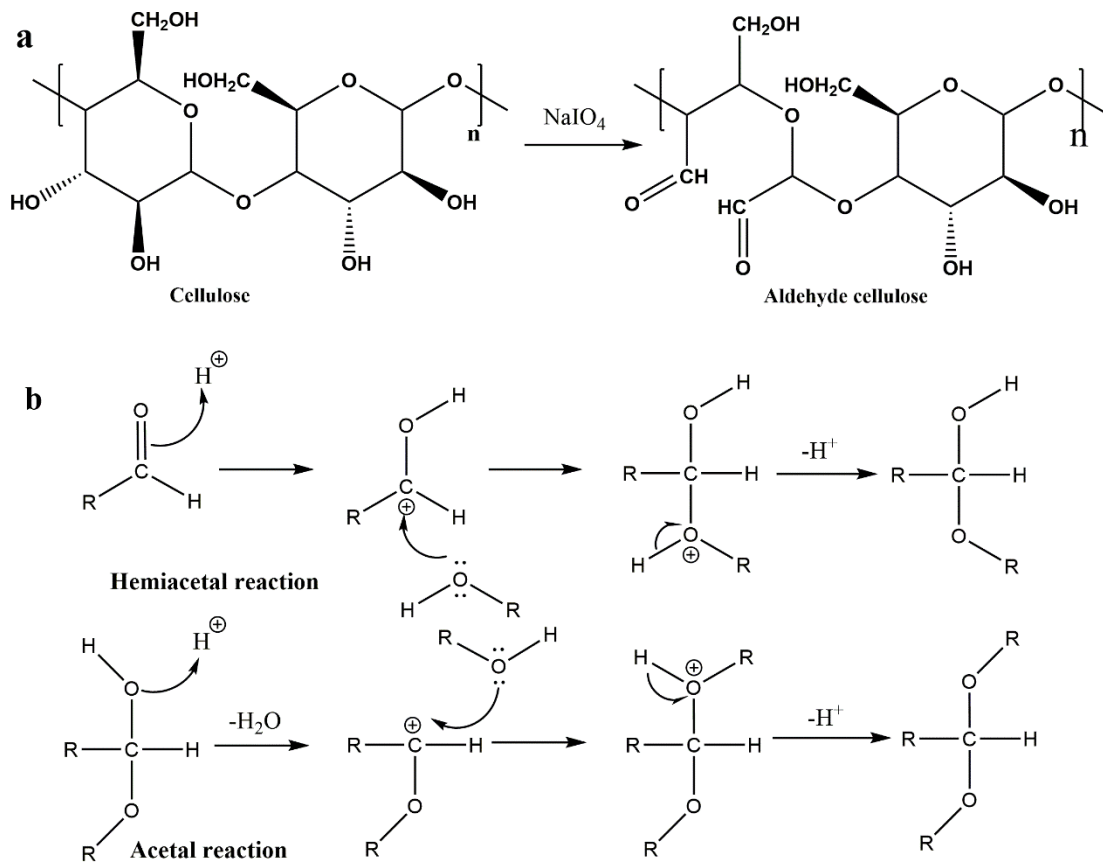
Fig. 2.3 Mechanism of cellulose oxidation (a) and aldolization reaction (b).

(b) Preparation of hydrogel through aldolization reaction

0.60 g of the oxide-CNF and 2 g PVA were dispersed into 30 mL water. The mixture was magnetically stirred for 1 h at 95 °C to ensure that the PVA dissolved completely and the CNF homogeneous dispersed. 5 drops of 0.5 M HNO_3 were added as a catalyst to the mixture after it was cooled to 60 °C. The hydrogel precursor was transferred into a sealed transparent mold before it was stirred for 10 min. Finally, the mold was placed in oven at 80 °C for 24 h (Fig. 2.3 b). Evaporation-swelling method was used to reinforce the mechanical performance of the hydrogel. In brief, the hydrogel was

evaporation at 40 °C in electric blast drying oven for 24 h. After that, the CNF/PVA hydrogel was obtained after the dried hydrogel was swollen in distilled water for 60 h.

2.3 Instruments and Characteristics

2.3.1 Tensile tests

The uniaxial elongation properties were tested at room temperature using a universal testing machine (Instron, 3385, extra 50 N load cell, Instron Co., Ltd., Canton, USA) in accordance with standard JIS K6251. For the cyclic tensile test, loading–unloading measurements were performed using the same universal testing machine at constant velocity of 100 mm/min.

2.3.2 Compression tests

The compressive properties were measured using a universal testing machine (Instron, 3365, Instron Co., Ltd., Canton, USA) at a cross-head speed of 1 mm/min. The cyclic compressive properties were measured using the same universal testing machine at a cross-head speed of 1 mm/min.

2.3.3 Internal network of hydrogel

The dispersion of CMC in hydrogel in the original state was investigated using an optical microscope (Eclipse model ME 600D, Nikon, Japan). The thin hydrogel film was obtained by shock-frozen section using a microtome (RM2145, Leica Microsystems, Japan).

The microgel microstructure was also observed using a scanning electron microscope (SEM) (Hitachi, Ltd S-4300, Japan). The freeze-dried samples were sputter coated with gold using an ion sputtering apparatus prior to the test.

2.3.4 DMA

The storage modulus and loss modulus of the hydrogel specimens were measured as

a function of frequency using a dynamic mechanical analysis (DMA, RSA-G2, TA Instrument, New Castle, DE, U.S.A.). Before measurement, the specimens were applied an axial force (0.981 N). The frequency sweeping experiments were performed under constant strain amplitude (1%) at a frequency range of 100 – 0.1 Hz.

2.3.5 Gelation time

The phase transition time of the hydrogels was determined by dynamic mechanical analysis (DMA, RSA-G2, TA Instrument, New Castle, DE, USA). The improved experimental set-up is shown below (Fig. 2.4):
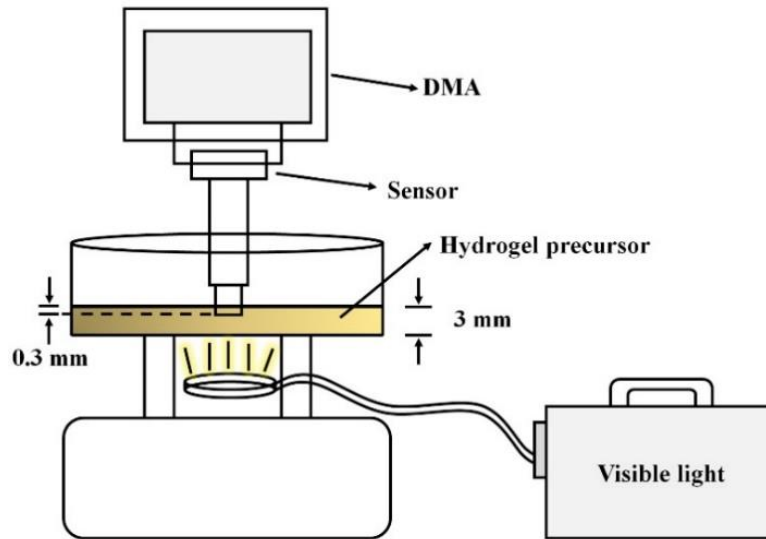
Fig. 2.4 Modified DMA instrument for gelation time test.

We used a stress relaxation modulus program for the hydrogel gelation time tests using a disc model at 25 °C, 1 Hz, and 1% strain. The program and light were turned on at the same time.

2.3.6 Swelling experiments

Swelling experiments were performed by immersing the Gels and dried-Gels in conical flasks filled with distilled water. The flasks were placed in a temperature-controlled bath at 25 °C for 50 hours. The swelling ratio (Q_m) was calculated by the following equation:

$$Q_m = W_s/W_a \text{ (2-1)}$$

where W_s is the weight of the swollen hydrogel and W_a is the weight of the as-prepared Gels. For the swelling experiment, all samples were measured 3 times.

2.3.7 Thermal property

Thermal gravimetric analyzer (TGA) and Differential Thermal Analysis (DTA) of the samples were performed with TG instrument (DTG-60, Shimadzu Co., Ltd., Kyoto, Japan) at a scan rate of 10 °C min^{-1} from room temperature to 600 °C in N$_2$ atmosphere (flow rate of 50 mL/min). Sample (4-6 mg) were placed in aluminum crucibles by using an empty aluminum crucible as a reference. All of the samples were obtained from freeze-drying.

2.3.8 FT-IR

A Thermo Scientific Nicolet iN 10 infrared spectrometer was used for the analysis of FT-IR. The sample was measured in the range of 650 – 4000 cm^{-1} with a resolution of 4 cm^{-1}. Both KBr pellet and ATR technique were adopted in the test. A total of 32 scans were accumulated.

2.3.9 XRD

The crystallographic structure of samples was obtained by X-ray diffraction system with a diffractometer (XRD 6000, Shimadzu Corporation, Japan) in range of 5~90° by step scanning. Nickel-filter Cu Kα radiation (λ=0.15417 nm) was used with a generator voltage of 40 kV and a current of 30 mA.

2.3.10 Vibration experiment

For the experiments evaluating the damping performance, a commercially available test tube mixer was used as the vibration source; the vibration machine was equipped with a hydrogel vibration damper, a support plate, and a force sensor. The sampling

frequency was set at 20 points per second.

2.4 Conclusion

The experimental procedure was displayed as Fig. 2.5.
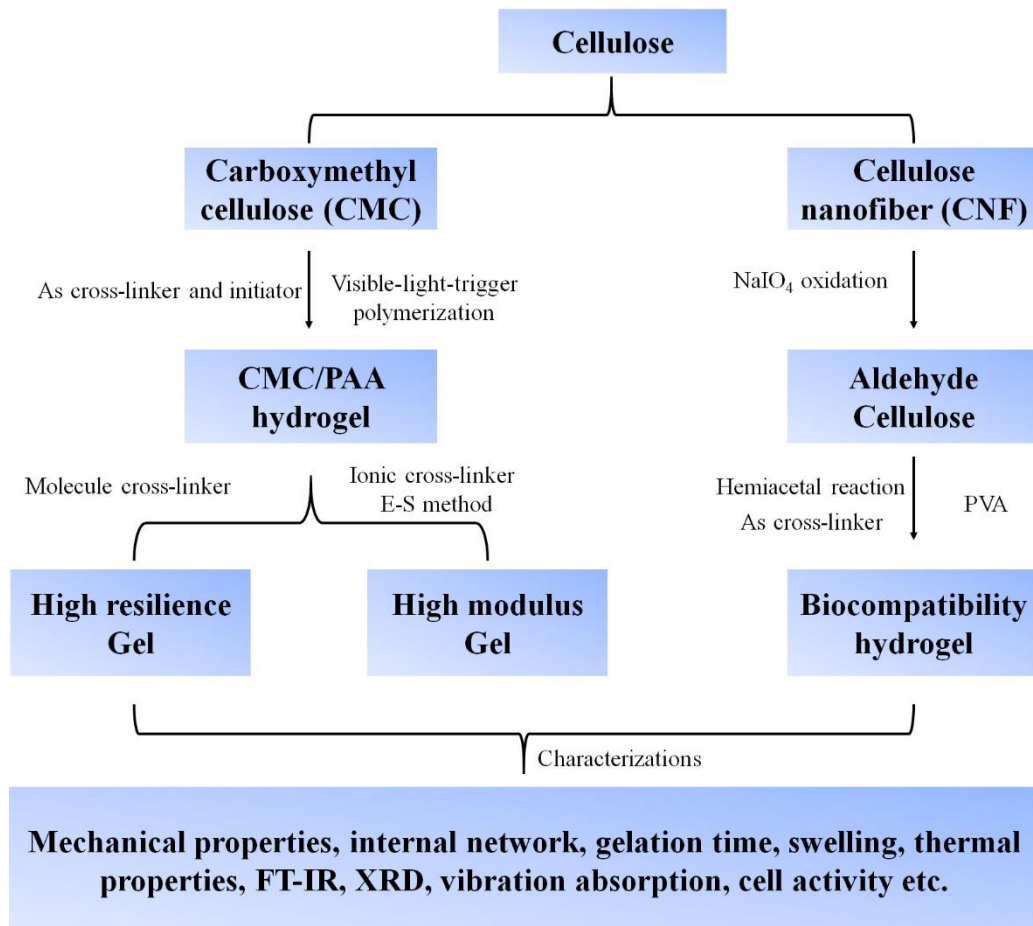
Fig. 2.5 The experimental procedure.

References

[1] Moon RJ, Martini A, Nairn J, Simonsen J, Youngblood J. Cellulose nanomaterials review: structure, properties and nanocomposites. Chemical Society reviews. 2011;40(7):3941-94.

[2] Khalil HA, Bhat A, Yusra AI. Green composites from sustainable cellulose nanofibrils: A review. Carbohydrate Polymers. 2012;87(2):963-79.

[3] Basta A, El‑Saied H. Performance of improved bacterial cellulose application in the production of functional paper. Journal of applied microbiology. 2009;107(6):2098-107.

[4] Young R, Rowell RM. Cellulose: structure, modification and hydrolysis: John Wiley & Sons; 1986.

[5] Zhifeng Z. Research progress in cellulose modification [J]. Chemical Industry and Engineering Progress. 2010;8:025.

[6] Hollabaugh C, Burt LH, Walsh AP. Carboxymethylcellulose. Uses and applications. Industrial & Engineering Chemistry. 1945;37(10):943-7.

[7] Nadagouda MN, Varma RS. Synthesis of thermally stable carboxymethyl cellulose/metal biodegradable nanocomposites for potential biological applications. Biomacromolecules. 2007;8(9):2762-7.

[8] Siró I, Plackett D. Microfibrillated cellulose and new nanocomposite materials: a review. Cellulose. 2010;17(3):459-94.

[9] Iwamoto S, Isogai A, Iwata T. Structure and mechanical properties of wet-spun fibers made from natural cellulose nanofibers. Biomacromolecules. 2011;12(3):831-6.

[10] Siqueira G, Bras J, Dufresne A. Cellulosic bionanocomposites: a review of preparation, properties and applications. Polymers. 2010;2(4):728-65.

Chapter 3 Design of a Rubbery Carboxymethyl Cellulose/Polyacrylic Acid Hydrogel via Visible-Light-Triggered Polymerization

3.1 Introduction

Artificial hydrogels are a class of soft materials with biocompatibility [1] and/or external stimuli-responsive properties [2]; they have been used in a wide range of applications in biological fields [3], in tissue engineering [4], and as soft machines [5]. However, most reported hydrogels exhibit poor mechanical strength and toughness, seriously limiting their applications [6]. In recent years, researchers have intensively investigated different mechanisms to synthesize hydrogels with innovative network structure and largely improved mechanical properties, including double-network [7], nanocomposite [8], topological structure [9], resilin [10], macromolecular cross-linking [11] and other hydrogels. The reported tough hydrogels exhibit remarkable comprehensive mechanical properties: high strength (tensile strength: 0.2-10 MPa; fracture elongation: 100-6000%), rigidity (elastic modulus: 0.05-1.0 MPa) and toughness (fracture energy: 100-15000 J m^{-2}) [12]. However, some of these hydrogels show a lack of instantaneous recovery and fatigue resistance properties. For example, a double-network hydrogel consisting of interpenetrating reversible brittle and ductile networks show internal fracturing of the brittle network and effectively dissipates energy to obtain high toughness [13, 14]. Nevertheless, the reversible brittle network re-formation process requires a suitable long time (minutes or hours), resulting in an obvious residual strain (approximately 100%) and fatigue in cyclic tensile experiments [15-17]. Biomedical and industrial application of hydrogels require to have excellent instantaneous recovery and anti-fatigue properties during deformation due to mechanical parts (eg. soft robot) or artificial organs (eg. artificial muscles) made of

hydrogels generally should be able to withstand repeated deformation at different rates and sustain a long time.

To date, topological hydrogels and resilin hydrogels show excellent rapid recovery and fatigue resistance [9, 10]. In addition to these two kinds of hydrogels, macromolecular crosslinked hydrogels have received more and more attentions from researchers due to the special cross-linking network structure. Macromolecular cross-linking hydrogels with functional macromolecules as cross-linker and/or initiator endow hydrogels with an effective energy dissipation mechanism, leading to excellent mechanical performance [18-21]. There are two main approaches for obtaining such a structure: (i) macromolecules not only as an initiator but also as a cross-linker, in this case, the activation of the functional macromolecule generally requires a harsh condition where the macromolecule is irradiated with ^{60}Co γ-rays [11, 21]. (ii) macromolecules containing a large number of double bonds act only as a cross-linker. In this case, the stereo-hindrance effect of macromolecule significantly limits the activity of the double bond, leading to a low tensile strength (30-213 kPa) [22, 23]. Moreover, these strategies for preparing hydrogels generally require multiple steps, including the synthesis of complex macromolecular cross-linker. Due to these limitations, it is our goal to explore novel synthetic methods and/or novel structures to achieve better mechanical performance of macromolecular hydrogels.

Herein we report a method of preparing a rubbery carboxymethyl cellulose/polyacrylic acid (CMC/PAA) hydrogel through a facile, one-pot, visible-light-triggered polymerization. The rubbery hydrogel with mesoscopic movable inhomogeneous cross-linking network consists of "microgel". The hydrogel with special "microgel" aggregated structure possesses an effective energy dissipation mechanism through the deformation of interlinked "microgel". This structure endows the hydrogel with instantaneous recovery, anti-fatigue and over 92% resilience. We anticipate that the simple preparation method and the particular structure can be further applied to hydrogel design and open up new potential applications for both biomaterials, and engineering, such as tissue scaffold, building and agriculture.

3.2 Experimental

3.2.1 Materials

Carboxymethyl cellulose sodium salt (CMC, EP), acrylic acid (AA, EP), ceric ammonium nitrate ($(NH_4)_2Ce(NO_3)_4$, CAN, GR) were purchased from Nacalai Tesque, Inc.. All of the chemical reagents were used as received. Distill water was used for all experiments.

3.2.2 Fabrication of hydrogels

All reactants including ceric ammonium nitrate, acrylic acid and cool water were sequentially added to a vial and subsequently mixed by magnetic stirring while immersed in an ice bath. A certain amount of carboxymethyl cellulose was slowly added to the mixture under strong magnetic stirring. After vigorous stirring for 1 h, the CMC was stably dispersed. We then poured the hydrogel precursor into a transparent glass mold and covered it with a glass plate. The mold was immersed in an ice-water bath and was placed 25 cm below a visible light source (LS-M210, Sumita) with 50% power output. The process of hydrogel formation required only a few minutes. The transparent carboxymethyl cellulose/polyacrylic acid (CMC/PAA) hydrogel was then sealed and stored at 4 °C for future testing. For comparison, the hydrogel precursor was also immersed in a water bath at 60 °C for 1 or 4 h. All of the reactants were used without further treatment. Unless otherwise specified, the CMC/PAA hydrogel precursor consisted of 40 mg CAN, 4.00 g AA, 0.40 g CMC and water content was fixed at 69.4 wt.%.

3.2.3 Characterization

The uniaxial elongation properties were tested at room temperature using a universal testing machine (Instron, 3385, extra 50 N load cell, Instron Co., Ltd., Canton, USA) in accordance with standard JIS K6251. The measurement procedure was as follows:

Hydrogels were cut into a dumbbell-shape with a size of length of 75.0 mm (L), gauge length of 20.0 mm (L_o), width of 4.0 mm (W) and height of 2.0 mm (H) (Fig. 3.5d); tests were conducted at a cross-head speed of 500 mm/min. For the cyclic tensile tests, loading-unloading measurements were carried out using the same machine at a constant speed of 100 mm/min. The hydrogels' dimensions were L = 50.0 mm, W = 10.0 mm, H = 2.0 mm and L_o = 30.0 mm. The samples were covered with oil to prevent the water from evaporating. The compressive properties were measured using a universal testing machine (Instron, 3365, Instron Co., Ltd., Canton, USA) at a cross-head speed of 1 mm/min. Hydrogels were cut into disc shapes with a diameter 11.0 mm and height of 2.0 mm. All samples were tested at room temperature.

The dispersion of CMC in hydrogel in the original state was investigated using an optical microscope (Eclipse model ME 600D, Nikon, Japan). The thin hydrogel film was obtained by shock-frozen section using a microtome (RM2145, Leica Microsystems, Japan). The length, width and thickness of the hydrogel film were 15 mm, 2 mm and 200 μm, respectively. The microgel microstructure was also observed using a scanning electron microscope (Hitachi, Ltd S-4300, Japan). The freeze-dried samples were sputter coated with gold using an ion sputtering apparatus prior to the test.

3.3 Results and discussion

3.3.1 Hydrogel fabrication

Cerium (IV) ammonium nitrate (CAN), due to its large reduction potential value (+1.61 V vs normal hydrogen electrode), low toxicity, ease of handling and experiment simplicity, is usually accepted as an oxidizing agent [24]. It has acted as an initiator for a large number of polymerization reactions, particularly for modification of biopolymers such as cellulose, starch, chitosan, [25-28] etc. In previous reports, the researchers believe that temperature, pH, monomer concentration, initiator concentration and reaction time are the major factors affecting the graft modification reaction [27-29]. In their opinions, the temperature is the triggering factor for this

polymerization. However, we dramatically find that visible light (wavelength: 380-760 nm) is a more effective trigger than temperature. Fig. 3.1a shows that the hydrogel precursor is quickly polymerized into a hydrogel within 1 minute by triggering with visible light. In contrast, the same hydrogel precursor is partly polymerized into viscous state within 1 hour in a water bath at 60 ℃, and after 4 hours the gelation is completed (Fig. 3.1b). The temperature triggered hydrogel emits an acrylic acid odor and can be partially dissolved in the weak base solution, however, visible-light-triggered hydrogel swells only in the base solution.
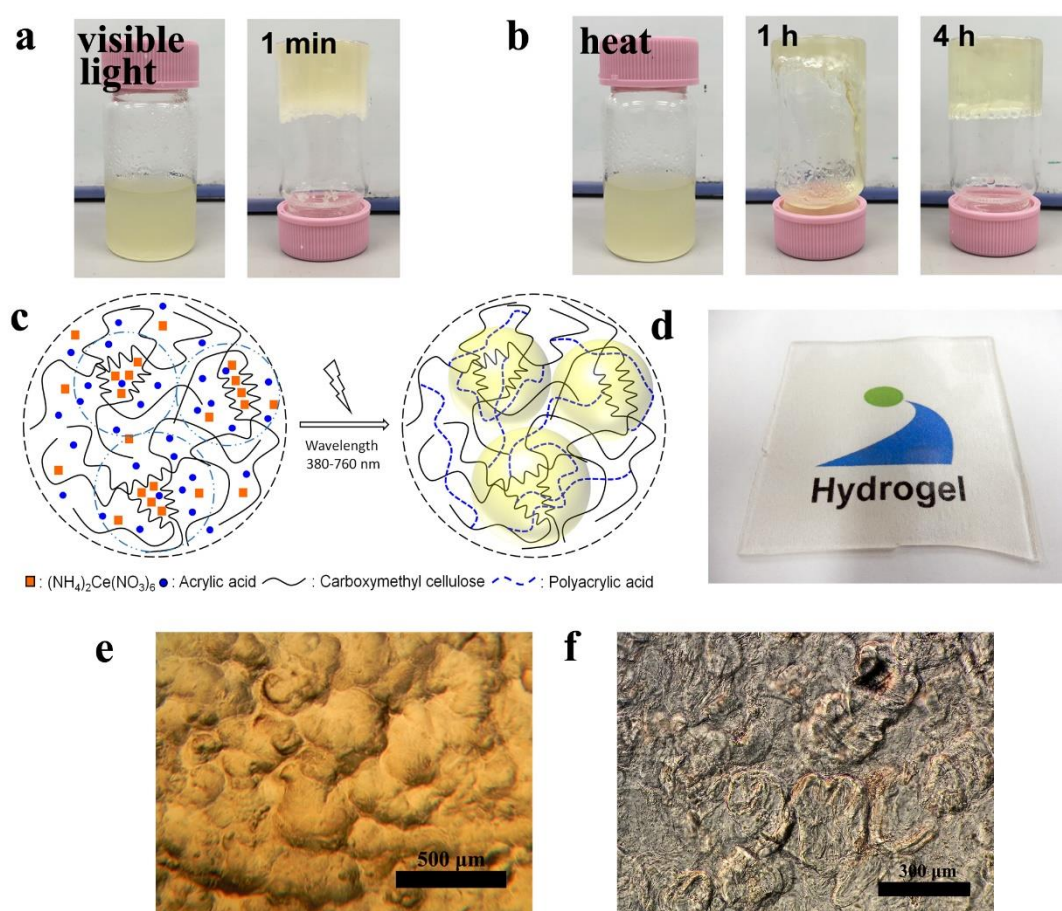

Fig. 3.1 a, b) Photographs of the CMC/PAA hydrogel at different reaction time via two kinds of trigger. c) Proposed mechanism of hydrogel formation under visible light. d) The prepared hydrogel is transparent at the macroscale. e, f) The hydrogel surface and internal structure observed under an optical microscope.
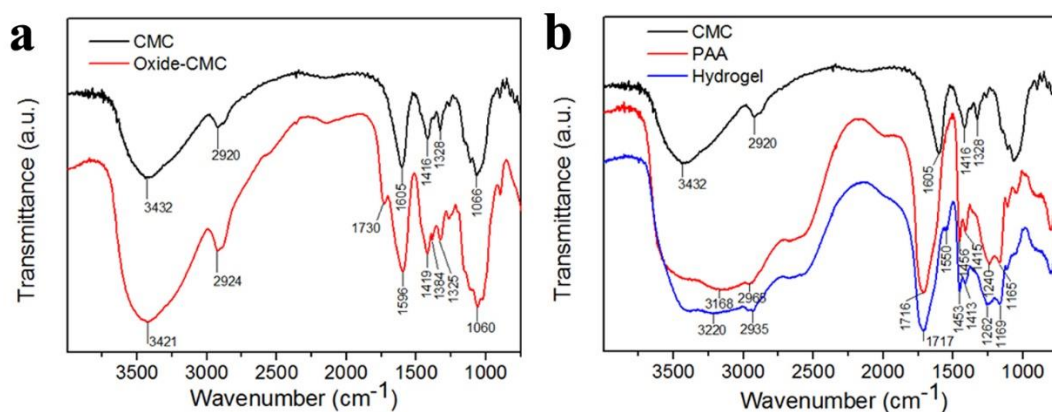
Fig. 3.2 a) FT-IR spectra of CMC and Oxide-CMC. The mixture consisted of 40 mg CAN, 0.40 g CMC and its water content was 20 mL, no monomer was added to this mixture. b) FT-IR spectra of CMC, PAA and CMC/PAA hydrogel. The hydrogel precursor consists of 40 mg CAN, 1.00 g AA, 0.40 g CMC and water content was fixed at 90.2 wt.%.

The CMC/PAA hydrogel was synthesized via a facile, one-pot, visible-light-triggered polymerization. This is in contrast to previously reported methods of hydrogel preparation that require multiple preparation steps and/or particular skills [10, 14]. The state of the hydrogel precursor depends on the solubility of carboxymethyl cellulose (CMC) in various pH and Ce^{4+} (ceric ammonium nitrate) ion concentration solutions. Parts of the CMC chains shrink into a coil structure in the presence of acid (provided by acrylic acid (AA) monomer) and highly charged ions (Fig. 3.1c). The remaining parts dissolve and result in a sticky mixture that prevents explosive polymerization. This mechanism makes the hydrogel precursor inhomogeneous and sticky. As described in the experimental section, the process of hydrogel formation only requires several minutes after the application of highly efficient visible light triggering. The prepared CMC/PAA hydrogel is transparent when observed by the naked eye (Fig. 3.1d). Nevertheless, it is found that the actual structure is inhomogeneous which consist of vast "microgel" when observed microscopically. In addition, the "microgel" is linked to other "microgel" by polymer chains at the edge of each "microgel", forming a super network with no obvious boundary observed (Fig. 3.1e, f). It should be noted that the structure of the hydrogel in this work is fundamentally different from the structure of

47

microgel reinforced hydrogels that have been reported [30].

In order to investigate the reaction mechanism of this visible-light-trigger polymerization, an additional experiment proceeded. In this experiment, the mixture consists of CMC and Ce^{4+} acetic acid aqueous was placed below a visible light. The color of the mixture changed from faint yellow to white and some undissolved matter (Oxide-CMC) was obtained during this process. FT-IR spectra of Oxide-CMC and CMC/PAA hydrogel are shown in Fig. 3.2. As shown in Fig. 3.2a, the CMC show a broad absorption peak at 3432 cm^{-1} which is due to the –OH stretching as well as intramolecular and intermolecular hydrogen bonds, the band at 2920 cm^{-1} is due to C-H stretching vibration, and one sharp peak at 1605 cm^{-1} show the presence of carboxymethyl ether group, the bands around 1416 cm^{-1} and 1328 cm^{-1} are assigned to –CH$_2$ scissoring and –OH bending vibration, respectively, and the band at 1066 cm^{-1} is due to –CH–O–CH$_2$ stretching. The FT-IR spectrum of Oxide-CMC show a new clearly sharp peak at 1730 cm^{-1} for –CHO stretching compared with that of CMC.
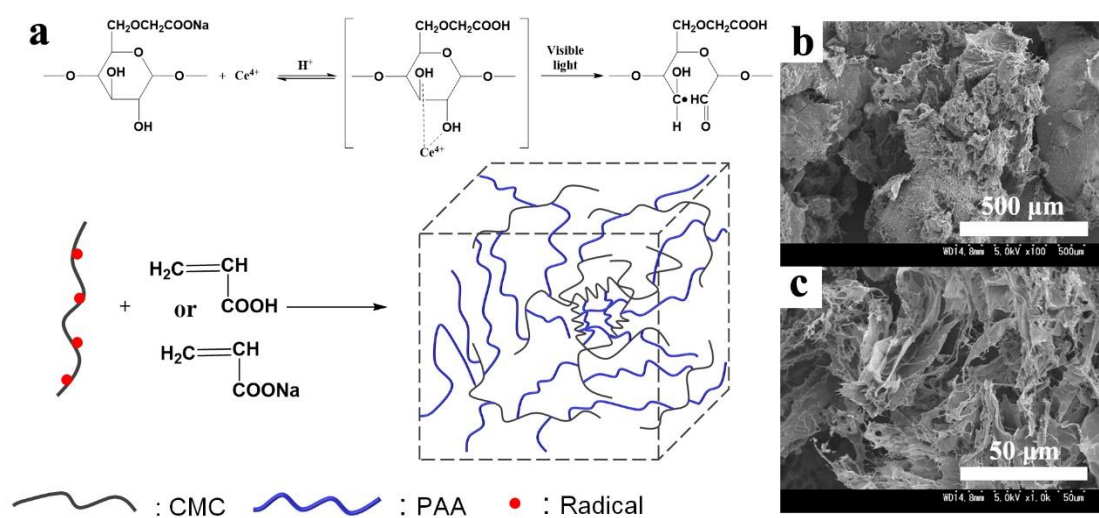
Fig. 3.3 a) The reaction mechanism of the visible-light-trigger polymerization. b, c) SEM images of CMC/PAA microgels after freeze-dried. The microgel precursor consisted of 80 mg CAN, 1.00 g AA, 0.40 g CMC and water content was fixed at 93.1 wt.%.

The new –CHO group confirms the reaction mechanism (Fig. 3.3a). The hydrogel consists of CMC and PAA show diverse FT-IR spectrum compare with that of CMC

and PAA. Different with the FT-IR spectrum of CMC, the FT-IR spectrum of the hydrogel is quite similar to that of PAA. However, it is evident that a new peak at 1550 cm^{-1} is due to –COONa group stretching of acrylate, and the peak at 1240 cm^{-1} and 1165 cm^{-1} shift to 1262 cm^{-1} and 1169 cm^{-1}, respectively, which due to the stretching vibration of –C–O group of acrylate (Fig. 3.2b). This result indicates the Na^+ in CMC has partly transferred into the PAA chains of the prepared hydrogel.

The mechanism of visible-light trigger polymerization, depending on the copolymerization mechanism of the vinyl monomer onto molecule with glucopyranose unit [31], is described as following: firstly, the ceric ion attacks the glucopyranose unit and forms a CMC-cerium complex. The Ce^{4+} ion is then reduced to a Ce^{3+} in the complex. Meanwhile a free radical and an aldehyde group are obtained by breaking the carbon 2 and 3 bonds of the glucopyranose unit. The free radical initiates the polymerization of the monomer, and a plenty of active PAA and CMC chains form a network via end-group termination (Fig. 3.3a) [29].

Table 3.1 the effect of molecular structure on gelation at different trigger conditions

Macromolecular cross-linker	The state of final product	
	Visible light trigger	Heat trigger
α-Cellulose	gel	viscous-gel
Carboxymethyl cellulose	gel	viscous-gel
Hydroxypropyl cellulose	no reaction	viscous
Chitosan	no reaction	viscous

In addition, it is interesting to find that cellulose or its derivatives with an integral D-glucose base ring (α-cellulose, carboxymethyl cellulose) can initiate the polymerization in the similar hydrogel system under visible light. In contrast, cellulose derivative without an integral D-glucose base ring (hydroxypropyl cellulose) or β-(1-4)-linked D-glucosamine (chitosan) can not be triggered by visible light in the same hydrogel system (Fig. 3.4 and Table 3.1). Moreover, hydroxypropyl cellulose and chitosan can get a viscous state via temperature trigger at 60 ℃, which is attributed to the oxidizability of

CAN at high temperature.
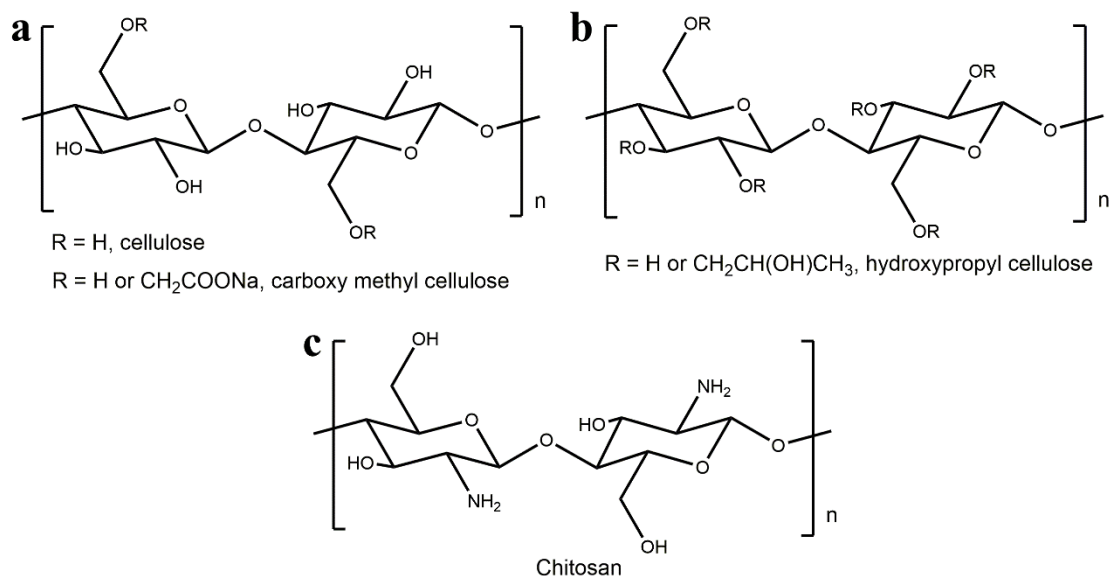
Fig. 3.4 Structure of biomaterials. a) The molecular structure of cellulose or carboxymethyl cellulose. b) The molecular structure of hydroxypropyl cellulose. c) The molecular structure of chitosan.

To investigate the microstructure of the hydrogel, a high feeding ratio of CMC: AA (0.4: 1, 40 wt.%) was selected. After polymerization, no hydrogel was obtained at this feeding ratio. However, the obtained product shows a flocculent microgel in an aqueous solution which can be observed by naked eye. Scanning electron microscopy (SEM) shows the size of the microgel is several hundred microns, which is the same as that of the "microgel" in original state with low feeding ratio. (Fig. 3.3b, c). The microgel shows an interconnected loose network structure, where original CMC and polymerized PAA completely combine with each other.

3.3.2 Tensile properties of hydrogels

The tensile properties of the hydrogel greatly depend on the photo-trigger reagent (CAN, in this case), which initiates the facile visible-light-triggered polymerization (Fig. 3.5). When the CAN concentration increases, the number of free radicals and potential cross-linking units increases [31]. As a result, we observed a gradual increase in elastic moduli from 65 kPa to 180 kPa with increasing CAN concentration. By

contrast, the fracture elongations decreased sharply from 730 % to 360 % with increasing the CAN concentration. The tensile strength reached a maximum 857 kPa at 1.25 wt.% CAN. The CMC/PAA hydrogels show much higher modulus and tensile strength than polyacryamide hydrogel (modulus < 10 kPa, tensile strength 35-106 kPa) with macromolecular micelle as cross-linker [32]. In contrast to the nanocomposite/polyacrylic acid hydrogel (modulus: tens kPa, tensile strength: 860 kPa [33]), the CMC/PAA hydrogel in the present work has a higher modulus at the same tensile strength.
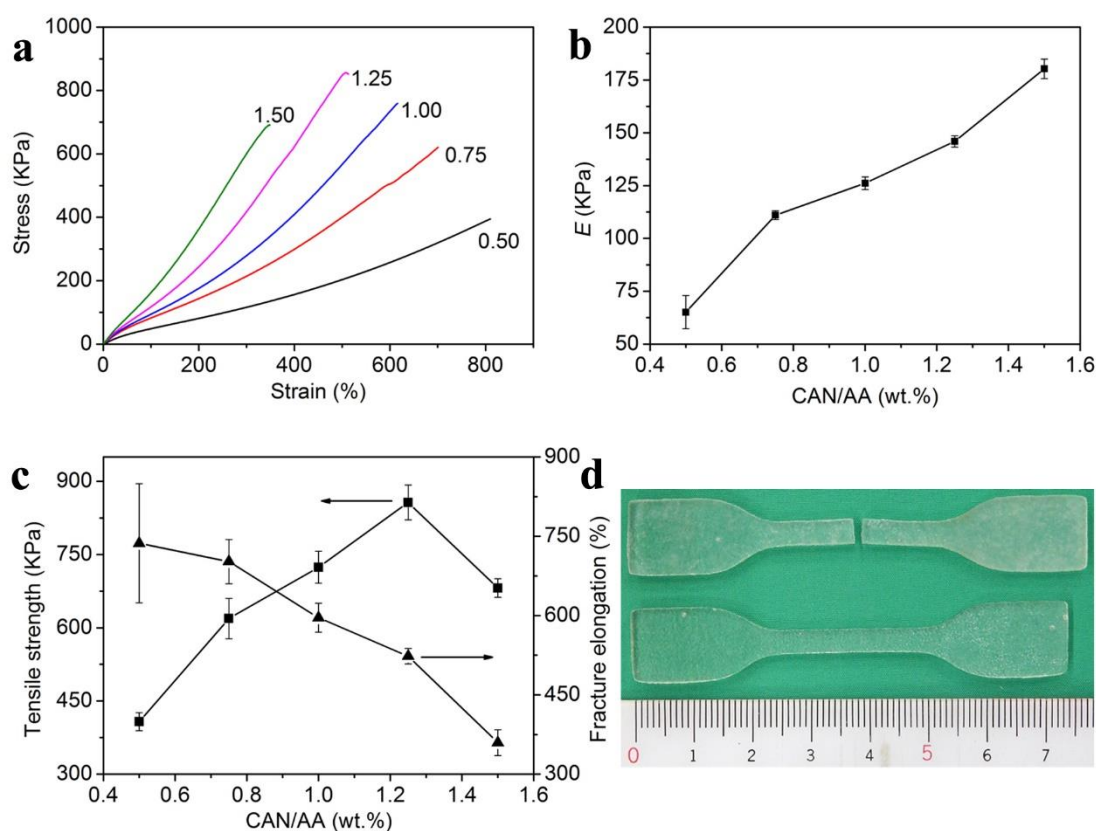
Fig. 3.5 The effect of photoinitiator content on the mechanical properties of CMC/PAA hydrogels. a) Tensile stress-strain curves of hydrogel with various CAN to AA weight ratios (wt.%). b) Elastic modulus (E) calculated from the slope within the initial linear region (less than 30% strain) of the stress-strain curves. c) The tensile strength and fracture elongation of hydrogels with various weight ratios. d) Photographs before and after fracture tensile test of dumbbell-shaped samples prepared with a 1.00 wt.% feeding ratio (CAN to AA). Error bars represent the standard deviation (n = 4).

51

In addition, the CMC/PAA hydrogel prepared with visible-light-trigger polymerization exhibits modulus and tensile strength ten times greater than the same hydrogel (modulus: 12.5 kPa, tensile strength: 42 kPa) prepared with heat radical polymerization (Fig. 3.6 and Table 3.2).
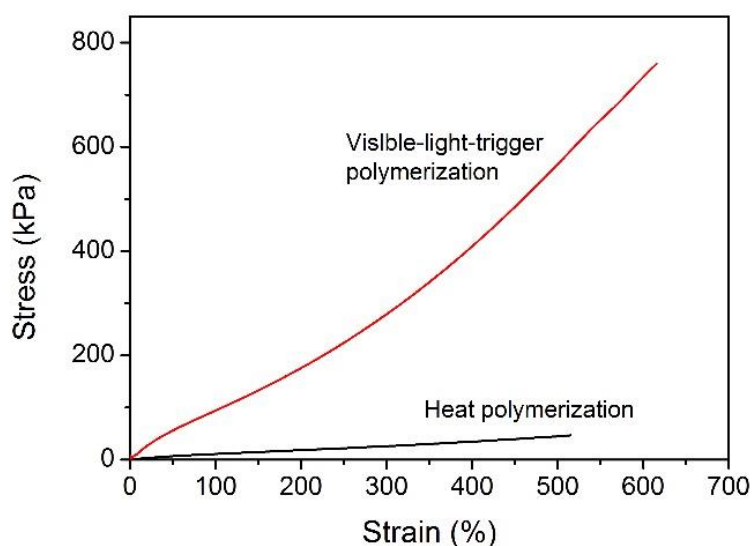
Fig. 3.6 Stress-strain curves of CMC/PAA hydrogels prepared by different methods.

Table 3.2 Components and tensile properties of CMC/PAA hydrogels prepared by different methods

Methods	AA	Water	CMC	CAN	MBA	Tensile strength	Elongation	Modulus
	(g)	(mL)	(g)	(mg)	(mg)	(kPa)	(%)	(kPa)
Visible-light-trigger	4	10	0.40	40	0	724.0 ± 32.6	596.0 ± 27.4	126.1 ± 3.0
Heat[a]	4	10	0.40	0	5	42.1 ± 5.7	500 ± 51.6	12.5 ± 0.9

[a] The hydrogel prepared with a conventional free radical polymerization at 80 °C, using APS instead of CAN as the initiator.

Different light sources are another crucial factor influencing the mechanical properties of hydrogels. The maximum stress and elastic modulus of the hydrogel prepared with metal halide lamp as the light source are higher than those of the hydrogel prepared with incandescent lamp (200 W, about 15% energy for visible light) as the

light source. However, the hydrogel with metal halide lamp as the light source has a lower fracture elongation than the hydrogel with an incandescent lamp as the light source. In addition, it is interesting to find that the hydrogel triggered by metal halide lamp with 100% output energy has a higher maximum stress and elastic modulus than the hydrogel triggered by metal halide lamp with 50% output energy. On the contrary, the fracture elongation decreases with increasing the visible light output. It indicates that the higher intensity of visible light can improve the density of cross-linking network which markedly affecting the mechanical properties. Moreover, the hydrogel also can be prepared even with sunlight as a trigger (Fig. 3.7).
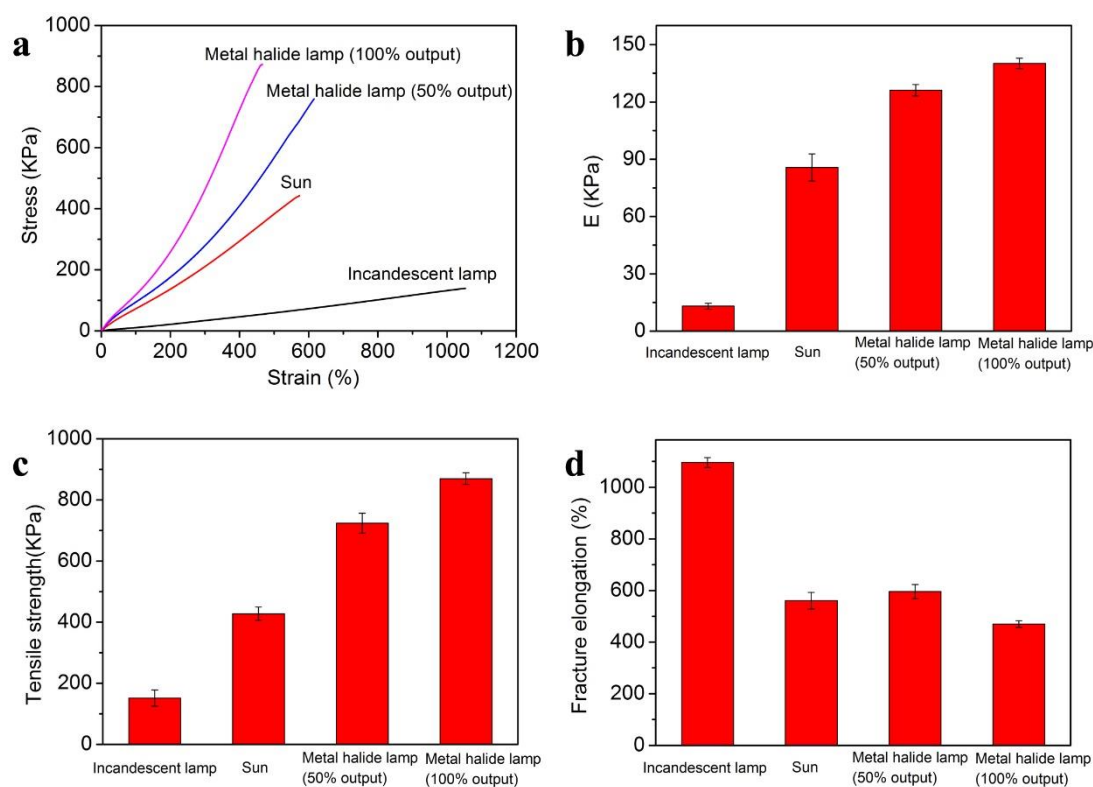
Fig. 3.7 The effect of light source on tensile properties of CMC/PAA hydrogels. a) Stress-strain curves of hydrogels prepared with various light resources. b) Elastic modulus (E) calculated from the slope within the initial linear region (less than 30% strain) of the stress-strain curves. c, d) The tensile strength and fracture elongation of hydrogels prepared with various light sources. (Error bar, S.D.; n=4).

The variation content of CMC and AA also strongly affected the mechanical behavior of the hydrogel. CMC is supposed to act as macromolecular cross-linker which is a key

player to form the CMC/PAA hydrogels with outstanding mechanical properties (Fig. 3.8). To confirm this, hydrogels with various CMC concentrations were prepared. It is found that the mixture has no viscous property when CMC content is below 5.00 wt.%. In this case, the mixture undergoes explosive polymerization, resulting in a great amount of bubble in the hydrogel. When the content of CMC is 12.50 wt.%, CMC cannot disperse well in the viscous system. Thus, an enhancement in tensile strength and elastic modulus are observed with increasing the CMC content from 2.50 wt.% to 10 wt.%, at 12.50 wt.% both tensile strength and elastic modulus decreases. The fracture elongation increases first and then decreases with increasing CMC content (Fig. 3.8d).
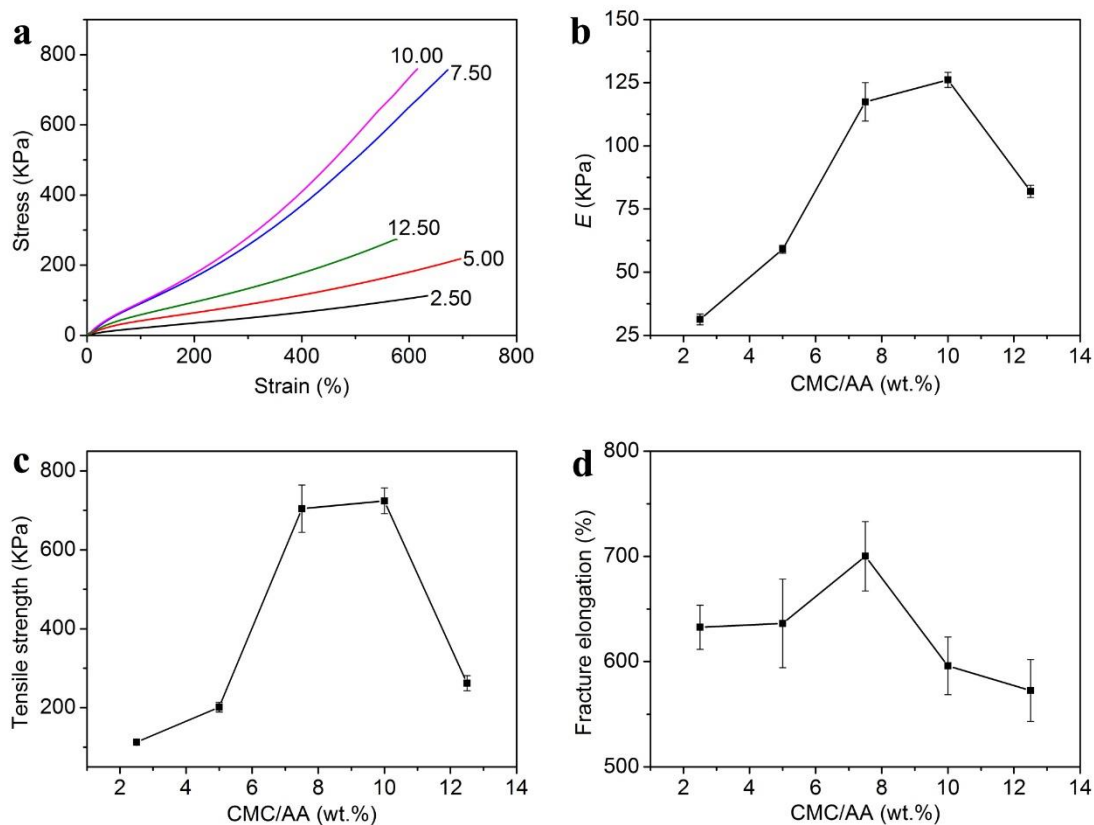
Fig. 3.8 Tensile properties of CMC/PAA hydrogels with different CMC contents. a) Stress-strain curves of hydrogels with various CMC to AA weight ratios (wt.%). b) Elastic modulus (E) calculated from the slope within the initial linear region (less than 30% strain) of the stress-strain curves. c, d) The tensile strength and fracture elongation of hydrogels with various CMC to AA weight ratios (wt.%). The hydrogel precursor

consisted of 4.00 g AA, 40 mg CAN, 10 mL water and various CMC feeding ratios as labelled. (Error bar, S.D.; n=4).
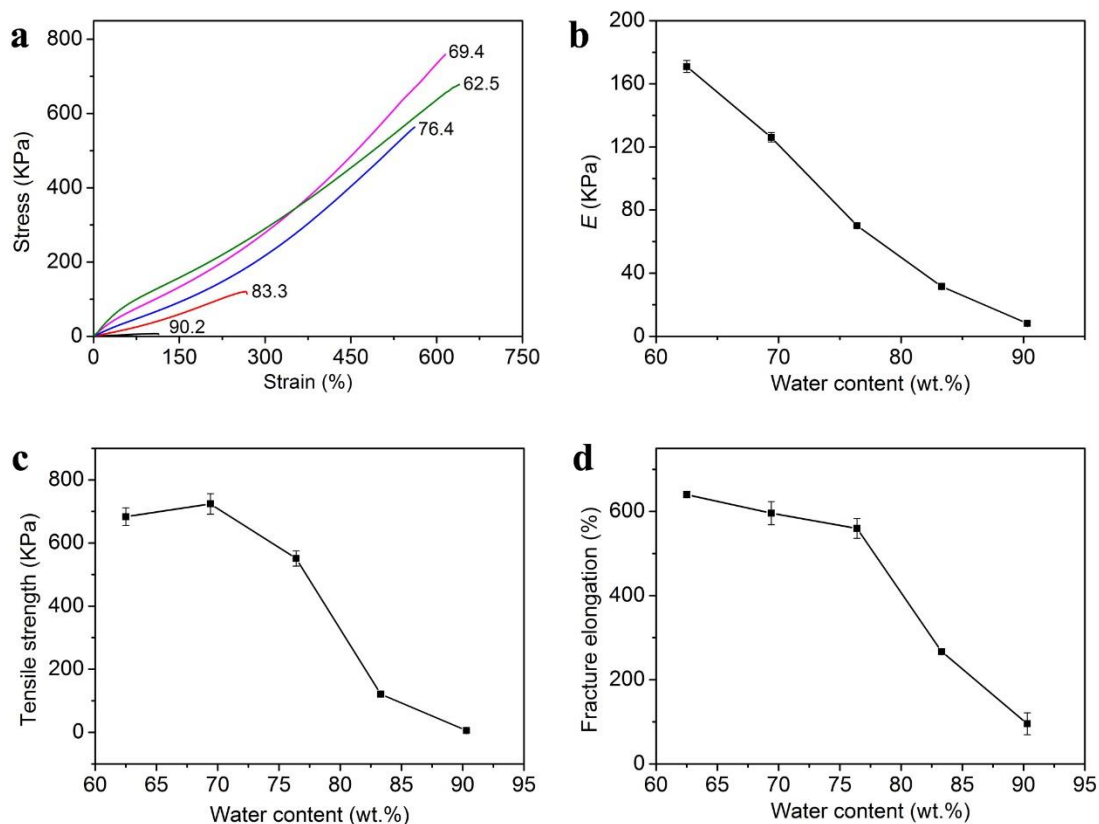
Fig. 3.9 Tensile properties of CMC/PAA hydrogels with different water content. a) Stress-strain curves of hydrogels with various water to hydrogel weight ratios (wt.%). b) Elastic modulus (E) calculated from the slope within the initial linear region (less than 30% strain) of the stress-strain curves. c, d) The tensile strength and fracture elongation of hydrogels with various water to hydrogel weight ratios (wt.%). The hydrogel precursor consisted of 40 mg CAN and 0.40 g CMC. Feeding ratio of AA to water were 1: 13, 2: 12, 3: 11, 4: 10 and 5: 9 (mL) which were calculated to corresponding water content as labelled. (Error bar, S.D.; n=4).

The polymer monomer concentration is also found to be important to the elastic modulus, tensile strength and fracture elongation of CMC/PAA hydrogels (Fig. 3.9). We transform it into a more common parameter (water content) for the following discussion. The elastic modulus and fracture elongation of CMC/PAA hydrogels decrease with increasing the water content. The tensile strength presents a decreasing

trend with the increase of water content. The maximum tensile strength is 724.03 ± 32.64 kPa at the water content of 69.4 wt. %. The higher monomer content (AA: water is 5: 9) provides excess acidity which declines the viscosity of the mixture. Thus, in this feeding ratio, the reaction also presents explosive polymerization with a little amount of bubble in the hydrogel. In contrast, hydrogel almost cannot be formed at lower monomer content (AA: water is 1: 13). It is indicated that lower polymer monomer concentration results in "microgel" link to each other difficulty (Fig. 3.3 b,c). In general, the "microgel" is easier to form huge crosslink network at higher monomer concentration (lower water content).

During the tensile tests, the hydrogel exhibited a uniform elongation even if the hydrogel structure is inhomogeneous [34]. The tensile fracture samples (with strain greater than 600%) exhibited an insignificant deformation of their original shapes. (Fig. 3.5d).

3.3.3 Energy dissipation of hydrogels in the first cycle

The tensile stress-strain curves of first cyclic experiments show a typical hysteresis under loading-unloading cycle, and a pronounced hysteresis loop is observed in the cyclic loading (Fig. 3.10a). The area between the loading-unloading curves represents the energy dissipated per unit volume [14]. The energy dissipation gradually increases as the maximum strain increases from 50% to 300%. A quantified data is demonstrated in Fig. 3.10b. It clearly shows that the as-prepared hydrogel could dissipate energy from 1.42 KJ/m^3 to 107.41 KJ/m^3. This phenomenon is interpreted as an energy dissipation mechanism in double-network hydrogels [35]. The polymer chains in the CMC/PAA hydrogel obtained via free-radical polymerization are generally nonuniform, speculative leading to the presence of several defects [36]. Parts of the chains in the defective domains rupture to dissipate the applied energy, resulting in the hysteresis loop in the first cycle. Moreover, due to the defects in the as-prepared hydrogel, we also observe softening in the hydrogel, that is specific to materials that exhibit the Mullins effect [37]. The softening increases progressively with increasing maximum strain of

the hydrogel (Fig. 3.10c).
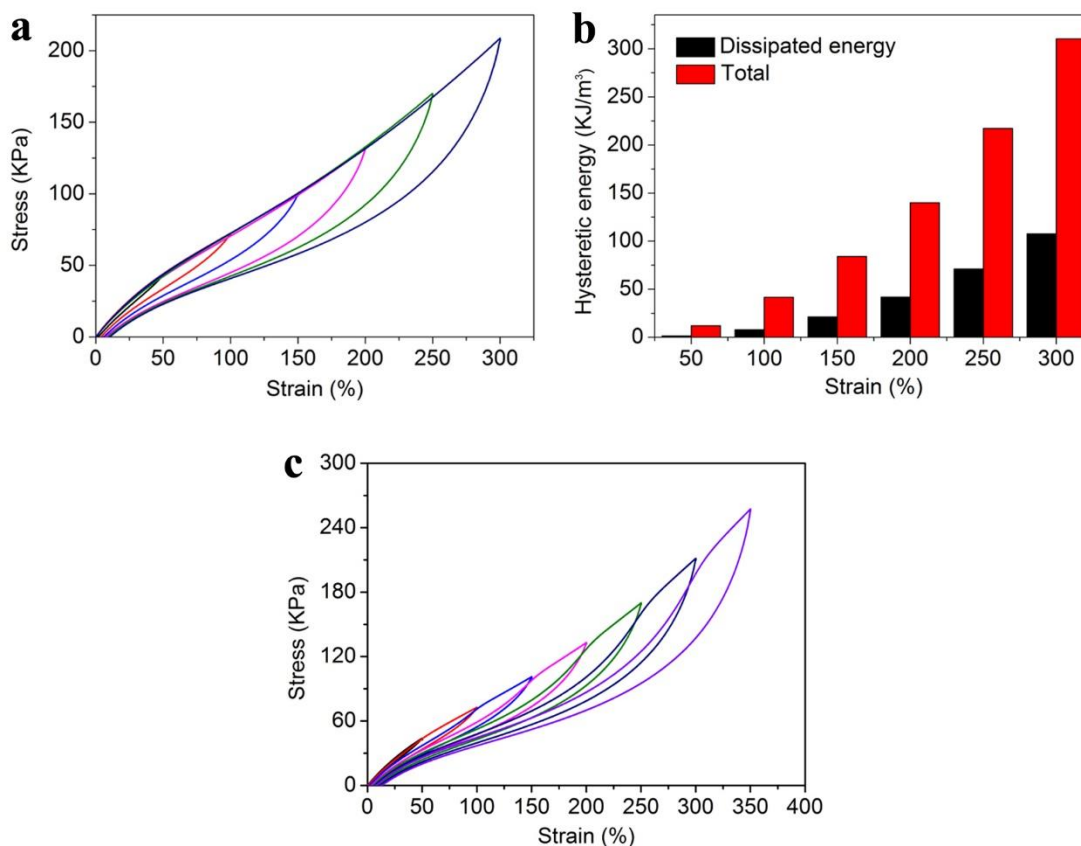
Fig. 3.10 a) Loading-unloading tensile test of the CMC/PAA hydrogel under various strains. b)The calculated hysteresis energy and dissipated energy of the CMC/PAA hydrogel during the loading-unloading tensile tests under different strains. c) Stress-strain response of hydrogels with a same sample subjected to a cyclic tensile test under different strains.

3.3.4 Anti-fatigue and rapid recovery properties of hydrogels

Although manufactured hydrogels with efficient energy dissipation mechanisms can bear a considerable applied force prior to fracture, the reversible brittle network re-formation process requires a suitable time scale, resulting an obvious residual strain (approximately 100%) and fatigue in cyclic tensile experiments [17]. This slow or limited recovery may be a major obstacle for practical applications [16].

In the present work, twenty successive cyclic tensile tests were applied to the CMC/PAA hydrogel at strains ranging from 50% to 300% (Fig. 3.11a and Fig. 3.12,

supporting information). All six samples show remarkably similar loading-unloading curves with slight hysteresis after an obviously hysteretic loop in the first cycle. To deeply understand the change of the internal network, we estimate the effective network chain density (N) based on the cyclic stress-strain curves of CMC/PAA hydrogel, following the equation in the literature [38, 39].

$$\tau = NRT[\alpha - (1/\alpha)^2] \quad (3\text{-}1)$$

Where, τ is the force per unit unstrained cross sectional area, R and T are the gas constant and absolute temperature, respectively, and the τ value at elongation of $\alpha = 2$ (strain 100%) is used in the calculation.
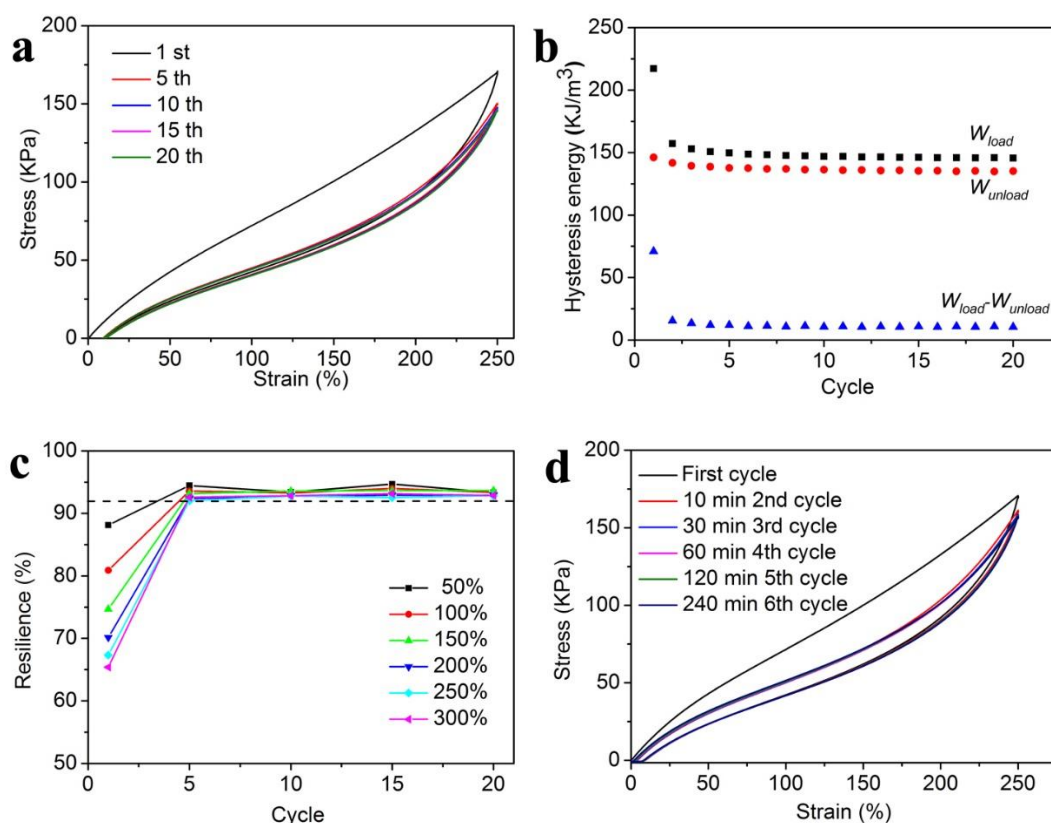
Fig. 3.11 a) Successive cyclic tensile tests of the hydrogel at a 250% strain for 20 cycles. b) Hysteresis energy change of hydrogels at a strain of 250% for 20 cycles, where W_{Load} is the area under the loading curve, W_{Unload} is the area under the unloading curve, and W_{Load} - W_{Unload} is the hysteresis energy dissipation (area between the loading and unloading). c) Resilience of the hydrogel ((W_{Load} - W_{Unload})/ W_{Load}) in each tensile cyclic test at various strains for 20 cycles. d) Recovery property of hydrogels for different

recovery times at zero stress.
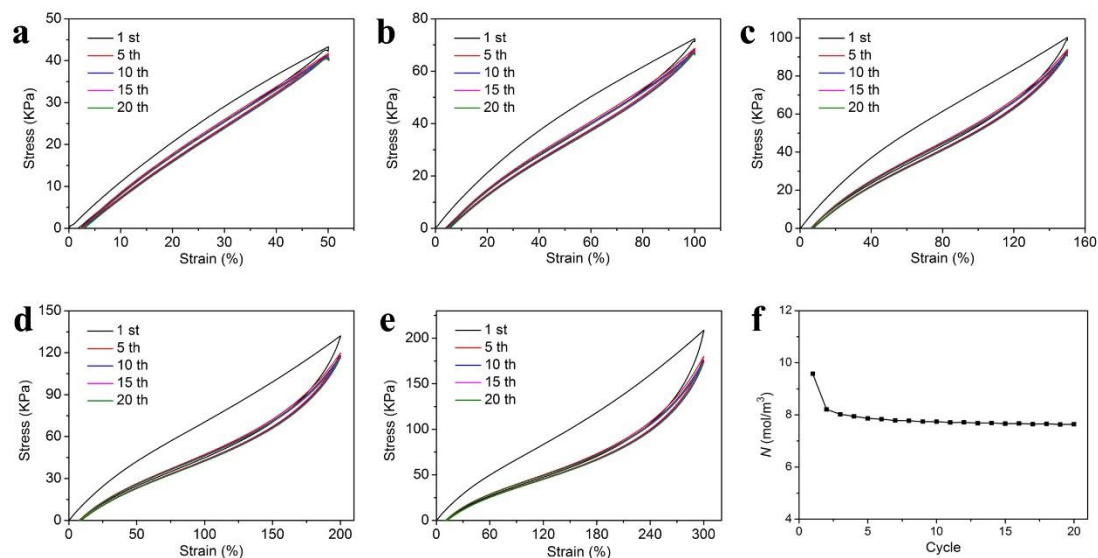
Fig. 3.12 Cyclic tensile test of CMC/PAA hydrogels at various strain. a) At a 50% strain for 20 cycles. b) At a 100% strain for 20 cycles. c) At a 150% strain for 20 cycles. d) At a 200% strain for 20 cycles. e) At a 300% strain for 20 cycles. f) The estimated effective network chain density (N) of CMC/PAA hydrogel.

The effective network chain density (N) decreases from 9.6 mol/m^3 to 8.0 mol/m^3 (Fig. 3.12f), indicates that the fracture of the internal structure in the hydrogel at the initial cycle process is irreversible. We define the initial cycle process in the hydrogel as "structure stabilizing" which results from the permanent covalent bond rupture. At a strain of 250%, the hysteresis becomes much smaller if the next cycle is conducted immediately after the conclusion of the previous cycle. In fact, with increasing the number of cycles, the hysteresis loops hardly change, resulting in plateauing of the hysteresis energy and especially the hysteresis energy dissipation (W_{Load}- W_{Unload}) (Fig. 3.11b). Resilience is a measure of materials to deform reversibly without loss of energy [40]. After the structure is stabilized, the hydrogel retains over 92% resilience in the cyclic tensile tests at various strain (Fig.3.11c). The resilience of the hydrogel is approximate to nature resilin (over 95% resilience), better than resilin biomaterials (over 100% strain, 75% resilience) at high strain [10, 41]. We calculated that 0.64-11.54 kJ/m^3 energy is dissipated through this stable reversible processing at a strain ranging from 50% to 300% which is lower than the energy dissipation in the first cycle (1.42-

107.41kJ/m^3). The residual strain remains constant on the experimental time scale (less than 1s) as the number of applied cycles increases, although an instantaneous residual strain (approximately 9%) is produced during structure stabilizing. The difference of resilience and residual strain before and after the structure stabilizing suggests that the hydrogel exhibits excellent rapid recovery and anti-fatigue characteristics through the energy dissipation mechanism after the structure is stabilized.
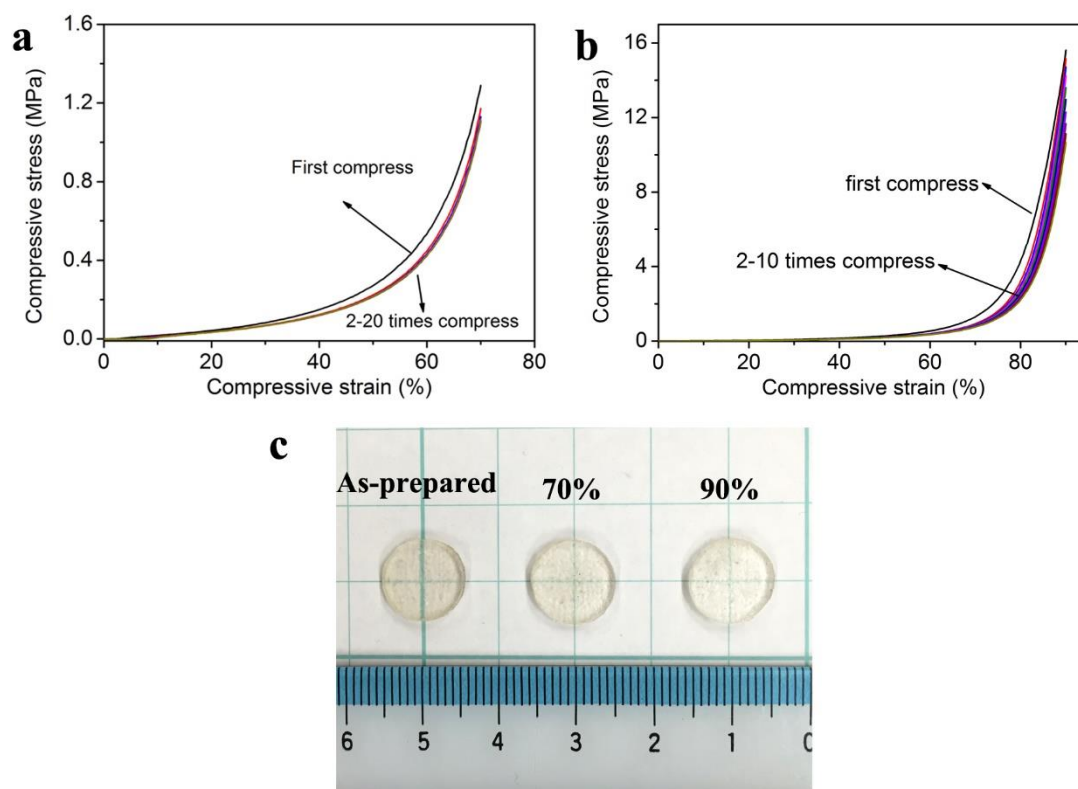
Fig. 3.13 a) Successive compressive tests of hydrogels at 70% strain for 20 cycles. b) Successive compressive test of hydrogel at 90% strain for 10 cycles. c) Image of hydrogels before and after compression.

To examine the time-dependent recovery properties of the CMC/PAA hydrogel at room temperature, the hydrogel was subjected to successive cyclic tensile tests at a prescribed time (Fig. 3.11d). After the cyclic tensile test under 250% strain of the hydrogel, the curve changed slightly relative to the curve obtained under successive 250% strain. In this case, the residual strain (approximately 3%) is negligible, which is lower than the residual strain (approximately 9%) under successive cyclic tensile test. The lower residual strain arises from the reforming of the hydrogen bonds and a small

number of ionic bonds [33]. For the irreversible residual strain (approximately 3%), it may result from the rupture of the hydrogel network and slight slip at the fixture and soft hydrogel [42]. Furthermore, the cyclic curve after the first cycle shows almost no variation although the rest time was varied.

Repeated compressive tests also reveal an anti-fatigue property at 70% compressive strain. The maximum compressive stress decreases from 1.29 MPa to approximately 1.10 MPa with the increase of compressive times. The curves of compression are almost coinciding, and the maximum compressive stress does no obviously decrease after the first compression (Fig. 3.13a). However, a higher compressive strain (90%) can gradually damage the internal structure, obviously decreasing the compressive strength, although there is no variation on the sample shape (Fig. 3.13b, c). Furthermore, the recovery time in the impact experiments was measured by a high-speed camera, only several milliseconds were required for the recovery process (Fig. 3.14).
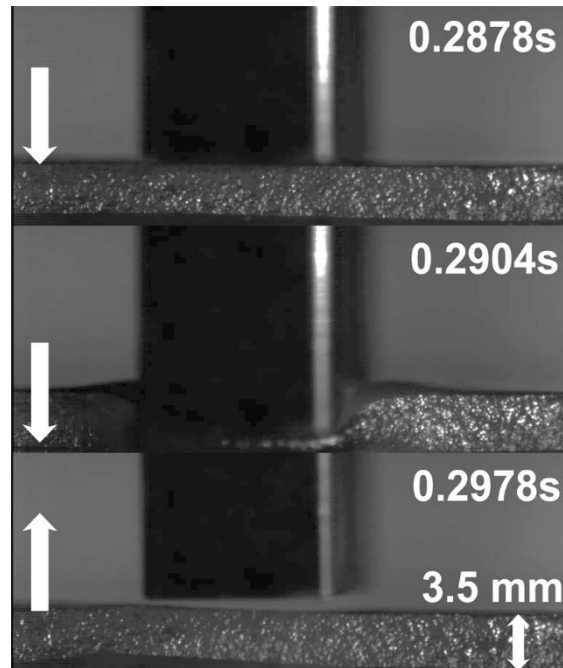

Fig. 3.14 Recovery time of hydrogel during an impact experiment.

3.3.5 Variation of hydrogel network under applied force

Our obtained data demonstrate that the rubbery hydrogel under deformation can effectively endure a tensile or compressive force. To visualize this mesoscopic structure

transformation, a thin hydrogel film (200 µm) was obtained by shock-frozen section. As shown in Fig. 3.15a, when the light source is a crossed polarizer, several bright optical spots are observed due to the liquid crystalline property of cellulose [43, 44]. The curling CMC act as the core of the "microgel" dispersed inhomogeneously in the hydrogel. When the hydrogel film was elongated to a strain of 150%, curling CMC domains deformed from an "island" to a "stream" along the straining direction. In the straining state, CMC domains are relatively homogeneously dispersed in the hydrogel. When the stress was removed the hydrogel film recovered to its original state. Furthermore, the location of curling CMC domains has no obvious variation; even the shape of curling CMC domains shows a negligible change under the polarized visible light. Therefore, it is confirmed that the rubbery hydrogel can effectively dissipate the applied energy through the curling CMC domain reversible deformation under the applied force (Fig. 3.15b).
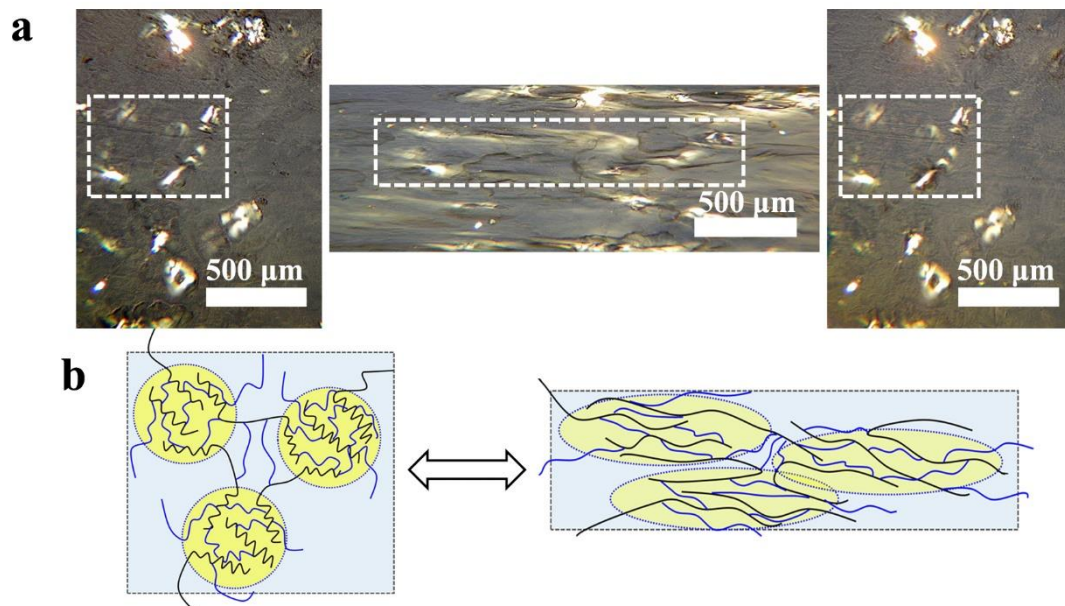

Fig. 3.15 The deformation mechanism and microstructure of the CMC/PAA hydrogel. a) The hydrogel film under polarized light: as-prepared (left), at 150% strain (middle), recovery to the original state (right). b) schematic of the reversible deformation mechanism of the hydrogel.

3.4 Conclusions

In conclusion, we have successfully designed a new strategy to fabricate a rubbery hydrogel with mesoscopic movable inhomogeneous structure using curling CMC as cross-linker and initiator. This facile, one-pot, visible-light-triggered polymerization method provides a fast, convenient and high efficiency strategy to synthesis rubbery hydrogel with instantaneous recovery and anti-fatigue properties. The novel rubbery hydrogels exhibit high tensile strength 400 kPa – 850 kPa, fracture elongation 350% – 700% and elastic modulus 65 kPa – 180 kPa. In addition, the hydrogel possesses some special properties such as negligible residual strain, instantaneous recovery, fatigue resistance and as high as 92% resilience after structure stabilizing, making the hydrogel an ideal candidate for further application in biomaterials. The cross-linking network consists of microgel aggregates with curling CMC as the core, which endows the excellent mechanical properties to the hydrogel by reversible deformation.

References

[1] Li Y, Rodrigues J, Tomas H. Injectable and biodegradable hydrogels: gelation, biodegradation and biomedical applications. Chemical Society reviews. 2012;41(6):2193-221.

[2] Capadona JR, Shanmuganathan K, Tyler DJ, Rowan SJ, Weder C. Stimuli-responsive polymer nanocomposites inspired by the sea cucumber dermis. Science. 2008;319(5868):1370-4.

[3] Van Vlierberghe S, Dubruel P, Schacht E. Biopolymer-based hydrogels as scaffolds for tissue engineering applications: a review. Biomacromolecules. 2011;12(5):1387-408.

[4] Thiele J, Ma Y, Bruekers SM, Ma S, Huck WT. 25th anniversary article: Designer hydrogels for cell cultures: a materials selection guide. Advanced materials. 2014;26(1):125-47.

[5] Calvert P. Hydrogels for Soft Machines. Advanced materials. 2009;21(7):743-56.

[6] Haque MA, Kurokawa T, Gong JP. Super tough double network hydrogels and their application as biomaterials. Polymer. 2012;53(9):1805-22.

[7] Webber RE, Creton C, Brown HR, Gong JP. Large strain hysteresis and mullins effect of tough double-network hydrogels. Macromolecules. 2007;40(8):2919-27.

[8] Gaharwar AK, Peppas NA, Khademhosseini A. Nanocomposite hydrogels for biomedical applications. Biotechnology and bioengineering. 2014;111(3):441-53.

[9] Bin Imran A, Esaki K, Gotoh H, Seki T, Ito K, Sakai Y, et al. Extremely stretchable thermosensitive hydrogels by introducing slide-ring polyrotaxane cross-linkers and ionic groups into the polymer network. Nature communications. 2014;5:5124.

[10] Lv S, Dudek DM, Cao Y, Balamurali MM, Gosline J, Li H. Designed biomaterials to mimic the mechanical properties of muscles. Nature. 2010;465(7294):69-73.

[11] He C, Zheng Z, Zhao D, Liu J, Ouyang J, Wang H. Tough and super-resilient hydrogels synthesized by using peroxidized polymer chains as polyfunctional initiating and cross-linking centers. Soft Matter. 2013;9(10):2837.

[12] Gong JP. Why are double network hydrogels so tough? Soft Matter. 2010;6(12):2583.

[13] Shull KR. Materials science: a hard concept in soft matter. Nature. 2012;489(7414):36-7.

[14] Sun JY, Zhao X, Illeperuma WR, Chaudhuri O, Oh KH, Mooney DJ, et al. Highly stretchable and tough hydrogels. Nature. 2012;489(7414):133-6.

[15] Zhao X. Multi-scale multi-mechanism design of tough hydrogels: building dissipation into stretchy networks. Soft Matter. 2014;10(5):672-87.

[16] Naficy S, Spinks GM, Wallace GG. Thin, tough, pH-sensitive hydrogel films with rapid load recovery. ACS applied materials & interfaces. 2014;6(6):4109-14.

[17] Lin P, Ma S, Wang X, Zhou F. Molecularly engineered dual-crosslinked hydrogel with ultrahigh mechanical strength, toughness, and good self-recovery. Advanced materials. 2015;27(12):2054-9.

[18] Cui Z, Wang W, Obeng M, Chen M, Wu S, Kinloch I, et al. Using intra-microgel crosslinking to control the mechanical properties of doubly crosslinked microgels. Soft Matter. 2016;12(33):6985-94.

[19] Zhao F, Qin X, Feng S. Microstructure, mechanical and swelling properties of microgel composite hydrogels with high microgel content and a microgel cluster crosslinker. RSC Adv. 2015;5(56):45113-21.

[20] Milani AH, Bramhill J, Freemont AJ, Saunders BR. Swelling and mechanical properties of hydrogels composed of binary blends of inter-linked pH-responsive microgel particles. Soft Matter. 2015;11(13):2586-95.

[21] Huang T, Xu HG, Jiao KX, Zhu LP, Brown HR, Wang HL. A Novel Hydrogel with High Mechanical Strength: A Macromolecular Microsphere Composite Hydrogel. Advanced materials. 2007;19(12):1622-6.

[22] Yang J, Han CR, Xu F, Sun RC. Simple approach to reinforce hydrogels with cellulose nanocrystals. Nanoscale. 2014;6(11):5934-43.

[23] Tan M, Zhao T, Huang H, Guo M. Highly stretchable and resilient hydrogels from the copolymerization of acrylamide and a polymerizable macromolecular surfactant. Polymer Chemistry. 2013;4(22):5570.

[24] Nair V, Deepthi A. Cerium(IV) ammonium nitrate--a versatile single-electron oxidant. Chemical reviews. 2007;107(5):1862-91.

[25] Zhu L, Guo J, Liu P, Zhao S. Novel strategy for palygorskite/poly(acrylic acid) nanocomposite hydrogels from bi-functionalized palygorskite nanorods as easily separable adsorbent for cationic basic dye. Applied Clay Science. 2016;121-122:29-35.

[26] McDowall D, Gupta B, Stannett V. Grafting of vinyl monomers to cellulose by ceric ion initiation. Progress in Polymer Science. 1984;10(1):1-50.

[27] Rahman L, Silong S, Zin WM, Rahman M, Ahmad M, Haron J. Graft copolymerization of methyl acrylate onto sago starch using ceric ammonium nitrate as an initiator. Journal of applied polymer science. 2000;76(4):516-23.

[28] Joshi JM, Sinha VK. Ceric ammonium nitrate induced grafting of polyacrylamide onto carboxymethyl chitosan. Carbohydrate Polymers. 2007;67(3):427-35.

[29] Fakhru L, Razi A, Qudsieh IY, Yunus WMZW, Ahmad MB, Rahman MZA. Graft copolymerization of methyl methacrylate onto sago starch using ceric ammonium nitrate and potassium persulfate as redox initiator systems. Journal of applied polymer science. 2001;82(6):1375-81.

[30] Hu J, Hiwatashi K, Kurokawa T, Liang SM, Wu ZL, Gong JP. Microgel-Reinforced Hydrogel Films with High Mechanical Strength and Their Visible Mesoscale Fracture Structure. Macromolecules. 2011;44(19):7775-81.

[31] Wu S, Jin Z, Kim JM, Tong Q, Chen H. Graft copolymerization of methyl acrylate onto pullulan using ceric ammonium nitrate as initiator. Carbohydrate Polymers. 2009;76(1):129-32.

[32] Zhao T, Tan M, Cui Y, Deng C, Huang H, Guo M. Reactive macromolecular micelle crosslinked highly elastic hydrogel with water-triggered shape-memory behaviour. Polymer Chemistry. 2014;5(17):4965.

[33] Zhong M, Liu XY, Shi FK, Zhang LQ, Wang XP, Cheetham AG, et al. Self-healable, tough and highly stretchable ionic nanocomposite physical hydrogels. Soft Matter. 2015;11(21):4235-41.

[34] Chen Q, Zhu L, Zhao C, Wang Q, Zheng J. A robust, one-pot synthesis of highly mechanical and recoverable double network hydrogels using thermoreversible sol-gel polysaccharide. Advanced materials. 2013;25(30):4171-6.

[35] Luo F, Sun TL, Nakajima T, Kurokawa T, Zhao Y, Sato K, et al. Oppositely charged polyelectrolytes form tough, self-healing, and rebuildable hydrogels. Advanced materials. 2015;27(17):2722-7.

[36] Malkoch M, Vestberg R, Gupta N, Mespouille L, Dubois P, Mason AF, et al. Synthesis of well-defined hydrogel networks using Click chemistry. Chemical communications. 2006(26):2774.

[37] Diani J, Fayolle B, Gilormini P. A review on the Mullins effect. European Polymer Journal. 2009;45(3):601-12.

[38] Yang J, Han CR, Duan JF, Xu F, Sun RC. Mechanical and viscoelastic properties of cellulose nanocrystals reinforced poly(ethylene glycol) nanocomposite hydrogels. ACS applied materials & interfaces. 2013;5(8):3199-207.

[39] Haraguchi K, Farnworth R, Ohbayashi A, Takehisa T. Compositional Effects on Mechanical Properties of Nanocomposite Hydrogels Composed of Poly(N,N-dimethylacrylamide) and Clay. Macromolecules. 2003;36(15):5732-41.

[40] Gosline J, Lillie M, Carrington E, Guerette P, Ortlepp C, Savage K. Elastic proteins: biological roles and mechanical properties. Philosophical transactions of the Royal Society of London Series B, Biological sciences. 2002;357(1418):121-32.

[41] Fang J, Mehlich A, Koga N, Huang J, Koga R, Gao X, et al. Forced protein unfolding leads to highly elastic and tough protein hydrogels. Nature communications. 2013;4:2974.

[42] Lillie M, Chalmers G, Gosline J. The effects of heating on the mechanical properties of arterial elastin. Connective tissue research. 1994;31(1):23-35.

[43] Moon RJ, Martini A, Nairn J, Simonsen J, Youngblood J. Cellulose nanomaterials review: structure, properties and nanocomposites. Chemical Society reviews. 2011;40(7):3941-94.

[44] Klemm D, Heublein B, Fink HP, Bohn A. Cellulose: fascinating biopolymer and sustainable raw material. Angewandte Chemie. 2005;44(22):3358-93.

Chapter 4 Rapid Recovery Double Cross-linking Hydrogel with Stable Mechanical Properties and High Resilience Triggered by Visible Light

4.1 Introduction

Hydrogels are wet and soft materials with biocompatibility and/or stimuli-responsiveness; they have been widely used in the field of biology, tissue engineering, and soft machines [1-6]. However, most reported hydrogels exhibit poor mechanical strength and toughness, severely limiting their application [7]. In recent years, the hydrogel designed according to the energy dissipation mechanism has overcome this shortcoming and greatly expanded the application of hydrogels. Researchers have intensively investigated different mechanisms for dissipating energy in various hydrogels, including double-network hydrogel [8, 9], nanocomposite hydrogel [10, 11], topological hydrogel [12, 13], resilin-based hydrogel [14], macromolecular cross-linking hydrogel [15, 16] and other hydrogels. These reported tough hydrogels exhibit remarkable comprehensive mechanical properties: high strength, large strain, high rigidity, and toughness [17].

Many tough hydrogels with excellent mechanical properties are expected to be used in more specialized fields (such as artificial muscle, sensors, and actuators). However, some of these hydrogels lack fatigue resistance and instantaneous recovery, which seriously limits their application in the above-mentioned fields [18]. Mechanical parts (e.g., soft robot) or artificial organs (e.g., artificial muscles) made of hydrogels generally should be able to withstand repeated deformation at different rates and sustain them for a long time. To meet these demands, the designed hydrogels must have instantaneous recovery and high resilience. Ten years ago, Elvin *et al.* developed a protein hydrogel by cloning resilin from the wing tendon of an adult dragonfly; the

resulting hydrogel exhibited high resilience (recovery after deformation).[19] In recent years, Lv *et al.* synthesized an artificial elastomeric protein hydrogel which mimicked the molecular architecture of titin through the combination of protein domains GB1 and resilin. The hydrogel exhibits high resilience and behaves as rubber-like materials at low strain and as shock-absorber-like materials at high strain [14].

Although the hydrogel exhibits considerably rapid recovery and resilience, the strategy for preparing these hydrogels generally require multiple steps, particular skills, and high costs. Because of these limitations, the goal of the current study is to explore a simple and inexpensive method to prepare hydrogels with instantaneous recovery and high resilience. Liu et al. designed a graphene peroxide/polyacrylamide nanocomposite hydrogel by in situ free radical polymerization [20]. The hydrogel without *N,N'*-methylene bisacrylamide (MBA) as a second cross-linker has a significant residual strain during the cyclic tensile process. However, after adding MBA, the residual strain almost disappears, and the resilience is improved. In addition, He et al. had attempted to synthesize a macromolecule cross-linking hydrogel using peroxidized polymer chains as cross-linker and initiator [16]. When a small amount of MBA is added, the resilience of the hydrogels is also dramatically improved. Although these hydrogels have rapid recovery and high resilience, their tensile modulus is below 60 kPa, and the biocompatibility of the hydrogel is unclear.

Cellulose/polyacrylic acid hydrogels have been widely reported for the application of drug delivery [21] and adsorbent [22]. The good biocompatibility and stimuli-responsiveness make it an excellent candidate for biomaterials [23]. However, the mechanical properties of the hydrogels cannot meet the needs of functional materials. In this study, we synthesized a double cross-linking polyacrylic acid (PAA) hydrogel by a facile, one-pot, visible-light-trigger polymerization. In this polymerization, carboxymethyl cellulose (CMC) acts as an initiator as well as the first cross-linker, and MBA acts as the second cross-linker. The effect of MBA on the mechanical properties and the swelling ratios were investigated. The results of DMA suggested that MBA had a significant effect on the movement of polymer chains within the hydrogel. It was observed that the hydrogel had a softening effect similar to that of rubber materials. In

addition, after the structure stabilized, the hydrogel showed a remarkably rapid recovery (high resilience and low residual strain) in both successive and intermittent cyclic tensile tests. We anticipate that the simple preparation method and the special performance of the hydrogel can open up new potential applications for both soft machines and biomaterials, such as soft robots and tissue engineering, etc.

4.2 Experimental

4.2.1 Materials

Carboxymethyl cellulose sodium salt (CMC, EP), acrylic acid (AA, EP), ceric ammonium nitrate ($(NH_4)_2Ce(NO_3)_4$, CAN, GR), *N,N'*-methylene bisacrylamide (MBA, GR), and sodium chloride (NaCl, GR) were purchased from Nacalai Tesque, Inc.. All of the chemical reagents were used as-received. Distilled water was used for all experiments.

4.2.2 Synthesis of hydrogels

The hydrogels were prepared as follows: 40 mg CAN, 4.00 g AA, and 10.0 mL of a series MBA aqueous solutions were added to a vial step by step, and mixed by magnetic stirring in ice bath. After that, 0.40 g CMC was slowly added to the mixture with strongly magnetic stirring (as shown in Table 1). The precursor hydrogel was stably dispersed for 1 h with vigorous stirring. The viscous precursor hydrogel was transferred into a transparent glass mold, and covered with a glass plate. Finally, the glass mold was placed 20 cm below a visible light (LS-M210, Sumita, 50% output) for 5 min. The obtained hydrogels were cut into different sizes for further testing.

4.2.3 Swelling experiments

Swelling experiments were performed by immersing as-prepared hydrogels in conical flasks filled with distilled water or NaCl aqueous solution. The flasks were set in a temperature controlled bath at 25 °C for 50 h. The swelling ratio (SR) was

calculated as follows in equation:

$$SR = W_s/W_a \qquad (4\text{-}1)$$

where W_s was the weight of swollen hydrogel, and W_a was the weight of the as-prepared hydrogel. All of the samples for swelling experiment were measured 3 times.

4.2.4 Characterizations

The uniaxial elongation properties were carried out according to JIS K6251 on a universal testing machine (Instron 3300 series, 50 N load cell, Instron Co., Ltd., Canton, America) and the measurement conditions were as follows: hydrogels were cut into the dumbbell-shape with the size length of 75 mm (L), gauge length of 25 mm (L_o), width of 4 mm (w) and height of 2 mm (h). The tests were conducted at a cross-head speed of 500 mm/min.

The storage modulus and loss modulus of the hydrogel specimens were measured as a function of frequency using a dynamic mechanical analysis (DMA, RSA-G2, TA Instrument, New Castle, DE, U.S.A.). Hydrogels were cut into disc shapes with diameters of 9 mm and heights of 2 mm. Before measurement, the specimens were applied an axial force (0.981 N). The frequency sweeping experiments were performed under constant strain amplitude (1%) at a frequency range of $100 - 0.1$ Hz.

For the cyclic tensile test, loading–unloading measurements were performed using the same universal testing machine at constant velocity of 100 mm/min. The gels sizes: 60 mm length, 10 mm width (w), 2 mm height (h), and 30 mm gauge length (l_o). The samples were covered with oil to prevent water from evaporating. Tensile stress (σ) was calculated as $\sigma = F/wh$, tensile strain (ε) was defined $\varepsilon = (l - l_o)/l_o \times 100\%$, where F is the load, and l is current length. The hysteresis energy loss (ΔU) was defined as the area of hysteresis loop encompassed by the loading–unloading curve, equation (4-2).

$$\Delta U = \int_{Loading} \sigma d\varepsilon - \int_{unLoading} \sigma d\varepsilon \quad (4-2)$$

In addition, resilience (R) was calculated as follows in equation (4-3):

$$R\,(\%) = \frac{\int_{unLoading} \sigma d\varepsilon}{\int_{Loading} \sigma d\varepsilon} \times 100\% \quad (4-3)$$

All of the hydrogel performance tests were performed at room temperature.

4.3 Results and discussion

4.3.1 Synthesis of double cross-linking PAA hydrogel
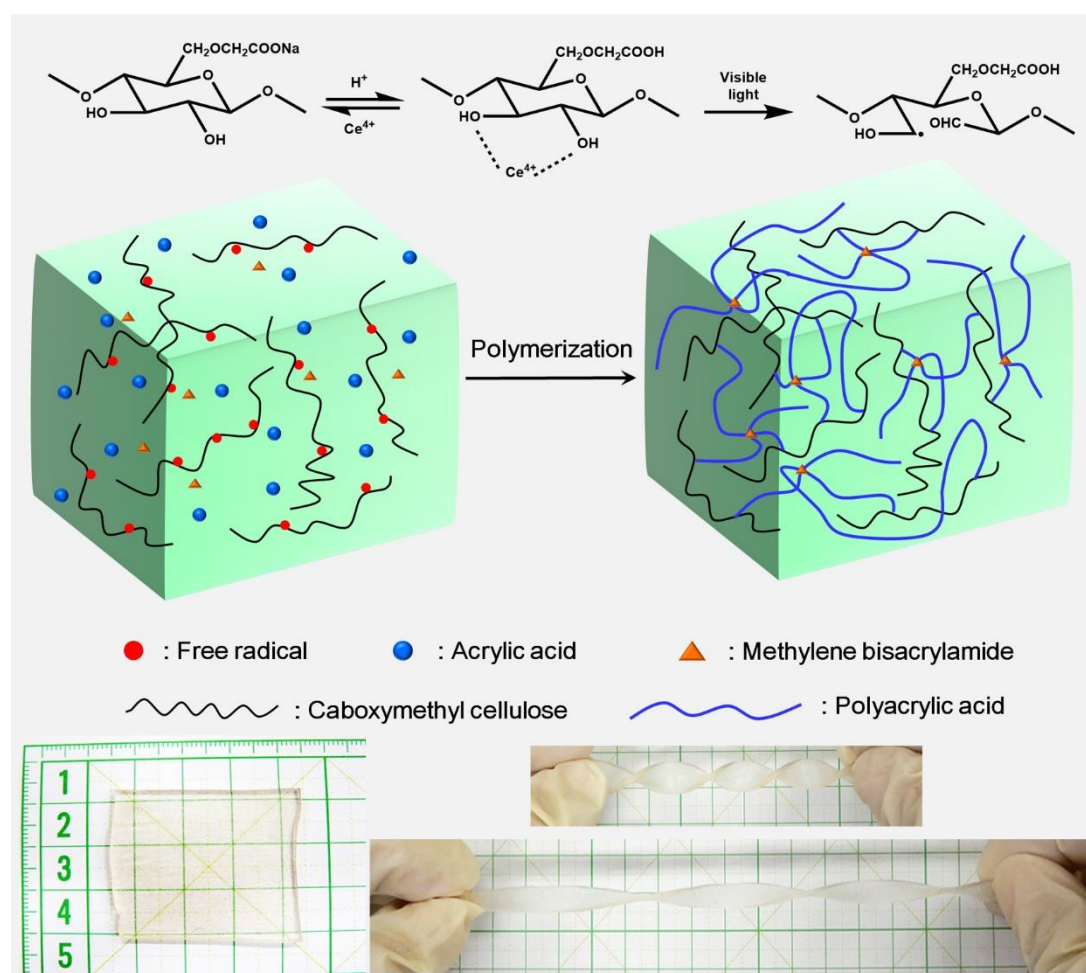
Schematic 4.1 Proposed mechanism of hydrogel formation under visible light. Grating, 1 cm.

Due to its large reduction potential value (+1.61 V vs normal hydrogen electrode), low toxicity, ease of handling, and experimental simplicity, cerium (IV) ammonium nitrate (CAN) is generally accepted as an oxidizing agent.[24] In a large number of polymerization reactions, particularly for the modification of biomass (such as cellulose, starch, chitosan, etc.), cerium (IV) acts as an initiator [25-28]. So far, temperature has been considered to be a triggering factor for these polymerizations. However, we have

dramatically found that visible light (wavelength: 380-760 nm) is a more effective trigger than temperature. The hydrogel precursor rapidly becomes a tough hydrogel via the visible-light-trigger polymerization. Due to the copolymerization mechanism of the vinyl monomer on the glucopyranose unit [29], the mechanism of visible-light trigger polymerization is described as follows: first, the ceric ion attacks the glucopyranose unit to form a CMC-cerium complex; then the Ce^{4+} ion is reduced to Ce^{3+} in the complex, while a free radical and aldehyde are obtained by the rupture of the carbon 2 and 3 bonds of the glucopyranose unit [30]; and last, the free radical initiates the polymerization, and a network is formed via end-group termination of active polymer chains. During the polymerization, CMC acts as an initiator as well as the first cross-linker, and MBA acts as the second cross-linker. The formation process of the hydrogel is illustrated in Schematic 1, the prepared hydrogel was transparent with excellent mechanical properties.
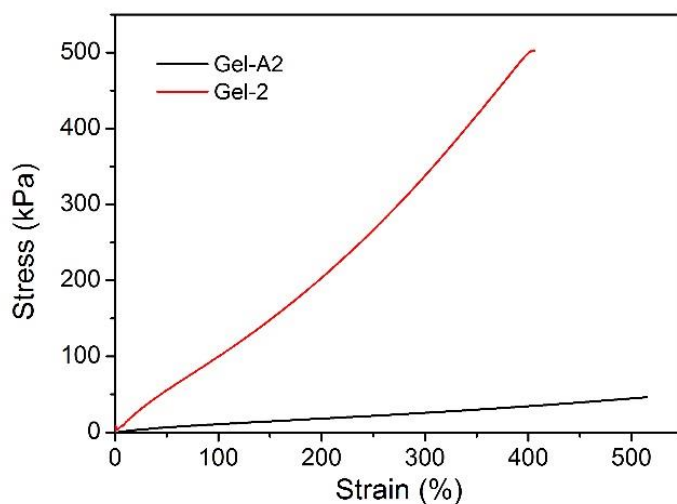

Fig. 4.1 Stress-strain curves of hydrogels with different triggering conditions; Gel-2 and Gel-A2 triggered with visible light and heat, respectively.

As a comparison, Gel-A2 having the same components as Gel-2 except that the trigger condition was prepared. The Gel-A2 with MBA as the cross-linker and CMC as the filler was prepared by conventional free radical polymerization, showing a lower mechanical properties than Gel-2 (Fig. 4.1). Gel-2 showed ten times higher tensile strength and elastic modulus than Gel-A2 (Table 4.1). This indicates that visible-light-

trigger polymerization is an efficient method for manufacturing cellulose-containing hydrogels.

**4.3.2 Mechanical properties of double cross-linking PAA hydrogel**
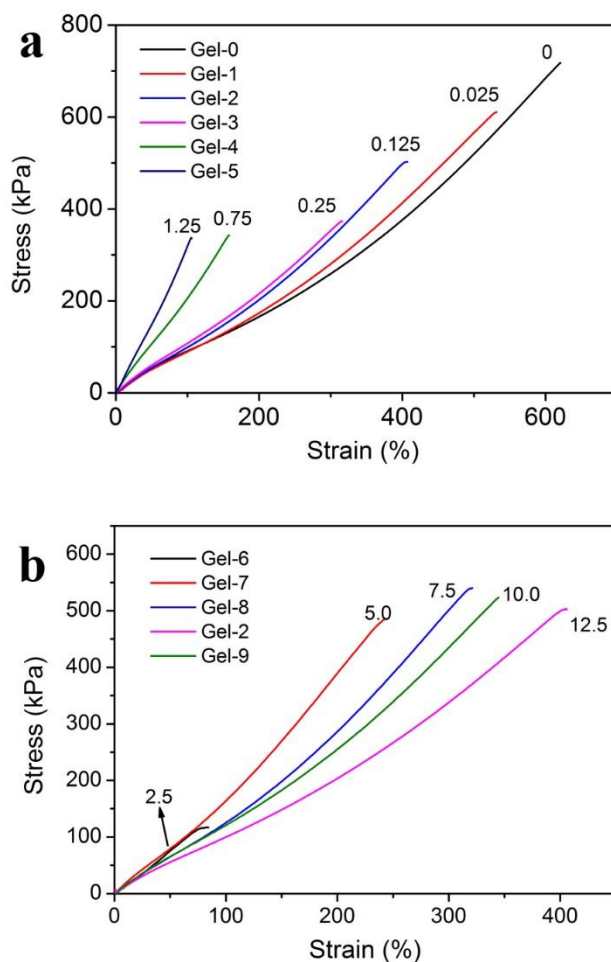
Fig. 4.2 Stress-strain curves of double cross-linking PAA hydrogels a) With various weight ratios of MBA to AA (wt.%), as labeled. b) With various weight ratios of CMC to AA (wt.%), as labeled.

Conventional hydrogels consisting of polymer and molecule cross-linker generally show negative mechanical properties (i.e., low tensile strength and low modulus) due to the heterogeneity of the network structure caused by molecular cross-linker during the gelation [7]. The molecule cross-linker as a component can greatly affect the performance of the hydrogels. Fig. 4.2a displays the stress–strain curves of double cross-linking hydrogels (Gel-0 to Gel-5) with MBA as the second cross-linker. It is

observed that the tensile strength of double cross-linking hydrogels gradually decreased from 724 to 352 kPa as the MBA content increased from 0 to 1.25 wt.%. In the same manner as the tensile strength, the fracture elongation decreases from 596% to 109% as the MBA content increases (Fig. 4.2a and Table 4.1).

Table 4.1 The composition of double cross-linking PAA hydrogels, and the mechanical properties of the hydrogels.

Hydrogel	AA (g)	Water (mL)	CMC (g)	CAN (mg)	MBA (mg)	Tensile strength (kPa)	Elongation (%)	Modulus (kPa)
Gel-0	4	10	0.4	40	0	724.0 ± 32.6	596.0 ± 27.4	126.1 ± 3.0
Gel-1	4	10	0.4	40	1	603.6 ± 67.1	549.1 ± 26.9	114.5 ± 2.6
Gel-2	4	10	0.4	40	5	493.5 ± 31.2	428.0 ± 37.3	116.0 ± 5.8
Gel-3	4	10	0.4	40	10	383.6 ± 13.3	318.4 ± 7.0	127.4 ± 6.7
Gel-4	4	10	0.4	40	30	329.0 ± 19.9	151.2 ± 9.9	224.2 ± 2.9
Gel-5	4	10	0.4	40	50	352.7 ± 21.3	108.9 ± 3.7	307.5 ± 3.8
Gel-6	4	10	0.1	40	5	105.5 ± 16.0	77.1 ± 12.6	146.5 ± 4.4
Gel-7	4	10	0.2	40	5	210.6 ± 47.8	244.8 ± 14.8	172.4 ± 5.0
Gel-8	4	10	0.3	40	5	545.0 ± 6.4	322.4 ± 8.1	140.4 ± 2.5
Gel-9	4	10	0.5	40	5	512.0 ± 63.7	339.5 ± 25.3	149.6 ± 20.9
Gel-A2[a]	4	10	0.4	0	5	42.1 ± 5.7	500.0 ± 51.6	12.5 ± 0.9

[a] The hydrogel prepared with a conventional free radical polymerization at 80 °C, using APS (0.10g, 2.5 wt.% of APS:AA) instead of CAN as initiator.

It is well-known that mechanical properties of three-dimensional cross-linking network hydrogels are highly dependent on the cross-linking density [31]. When the hydrogel does not contain MBA as the second cross-linker, the prepared hydrogel (Gel-0) has a low cross-linking density, which can endure great deformation under applied force through the stretching and movement of the polymer chains. Therefore, Gel-0 shows high tensile strength and fracture elongation. The stretching and movement of polymer chains is limited due to the improved cross-linking density after the

introduction of the MBA into the hydrogel. The molecule cross-linker easily forms plenty of stress concentration points, leading to hydrogel fracture at low applied force. However, the stiffness of the hydrogel increases considerably with increasing the cross-linking density, resulting in a high elastic modulus of the hydrogel. The elastic modulus is approximately constant and then increases to 307 kPa with increasing the MBA contents (Table 4.1).

CMC is also considered to be a key role in the formation of the double cross-linking hydrogel. To confirm this, hydrogels with various CMC concentrations were prepared (Fig. 4.2b and Table 4.1). It is found that the polymerization is not complete in the presence of a small amount of CMC (Gel-6). Therefore, the tensile strength and fracture elongation of Gel-6 are only105 kPa and 77%, respectively. When a higher content of CMC is added to the hydrogel precursors (Gel-7, Gel-8, Gel-2 and Gel-9), the tensile strength of these Gels is about 500 kPa. The fracture elongation of the Gels increases first and then decreases due to the synergistic effect of the two cross-linkers. In addition, the elastic modulus of the Gels are maintained between 116 – 172 kPa.

4.3.3 Swelling properties of double cross-linking PAA hydrogels

Hydrogels, as soft and wet materials, consisting of a cross-linking network and a large amount of water (50-90%), have been used in aqueous environments, such as drug delivery [32], tissue engineering [33] and contact lenses [34]. The swelling behavior of hydrogels is the key point for final application. Hydrogels generally exhibit excellent mechanical performance in their as-prepared state. However, most of the hydrogels typically show a high swelling ratio for low cross-linking density, which may pose a huge volume increase in the aqueous environment, resulting in a significant decline in the mechanical properties [35]. The swelling ratio of the double cross-linking hydrogel can be obviously decreased by introducing MBA to increase the cross-linking density.
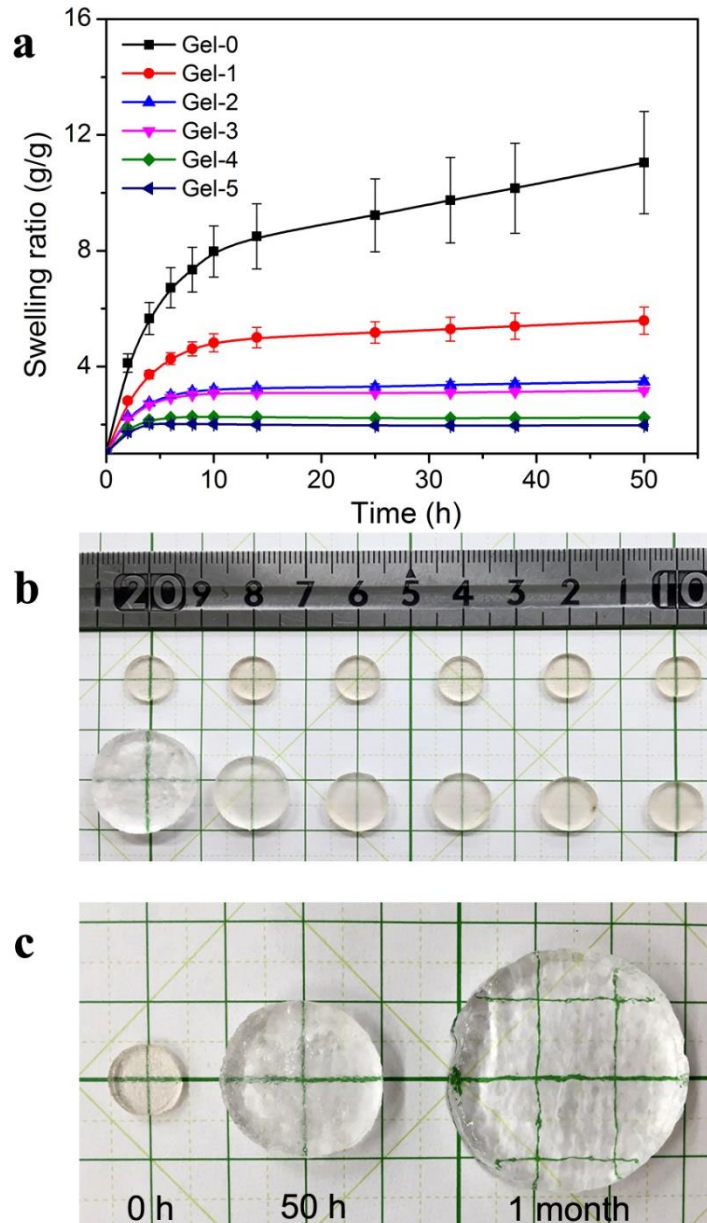
Fig. 4.3 a) Swelling ratio – time curves of double cross-linking PAA hydrogels with various MBA contents. (Error bars, S.D.; n=3) b) The image of double cross-linking PAA hydrogels before and after swelling. c) The swollen state of Gel-0 after 50 h and 1 month. Grating, 1 cm.

To investigate the swelling behavior of double cross-linking hydrogels, the hydrogel samples were measured in distilled water to evaluate the effect of MBA on the swelling behavior. As shown in Fig. 4.3a, the SR of Gel-0 increases with increasing time, and the swelling equilibrium is not obtained in the experimental time scale. However, it can be noticed that the SRs of other hydrogels decrease drastically with the introduction of

MBA. Fig.4.3b depicts that the volume change of the hydrogels gradually decrease with the increase of MBA content after swelling. The hydrogels (Gel-2, Gel-3, Gel-4, and Gel-5) exhibit a swelling equilibrium within about 10 h when higher MBA content is selected. The swelling properties of the hydrogel are mainly dependent on the hydrophilic ability of functional groups and the cross-linking density of hydrogels [36]. Therefore, Gel-0 has a high hydrophilic polymer chain, and a low cross-linking density has a higher SR. Moreover, Gel-0 consisting of CMC and PAA can be disentangled and slid during the swelling process which leads to a further reduction of the cross-linking density, resulting in an enlarged SR in 1 month (Fig. 4.3c). In contrast, the cross-linking density of other hydrogels increases with the introduction of MBA, where MBA acts as an additional cross-linking site, resulting in the restrained movement of the polymer chains during the swelling process.

4.3.4 Dynamic mechanical analysis

To deepen understanding of the role of MBA in double cross-linking hydrogels, the viscoelastic response of the prepared hydrogel was determined by using a RSA-G2 solids analyzer. The compressive storage modulus E' (a measure of elastic response of a material) and the loss modulus E'' (a measure of viscous response of a material) of the double cross-linking hydrogels were determined as the frequency changes. Fig. 4.4a, b depict that E' is always higher than E'' in the frequency range $0.1 - 100$ Hz. The value of E' has a slightly linear increasing trend with increasing the frequency. The E´ values of each hydrogel increase as the MBA contents increase from $0 - 1.00$ wt.%, for example, the E' value at 5 Hz increases from 300 to 800 kPa. The effect of MBA on the elasticity of the hydrogel is achieved by changing the effective network chain density. It is reported that the storage modulus in the low frequency range is related to the effective network chain density (N) [37, 38]. It can be depicted as the follows equation (4-4):

$$E' = \lambda N \text{RT} \qquad (4\text{-}4)$$

Where, E' is taken from the storage modulus, λ is the hydrogel-based constant, R and

T are the gas constant and absolute temperature, respectively.

The effective network chain density can be significantly improved by introducing a moderate amount of MBA into the double cross-linking hydrogel. Therefore, the storage modulus increases with increasing the cross-linker concentration [38]. However, an excess of MBA (Gel-5, 1.25 wt.% MBA) does not further increase the E' of the hydrogel. This result may be due to the fact that high MBA content cannot improve the effective network chain density (at a 1% compress strain), according to equation (4).
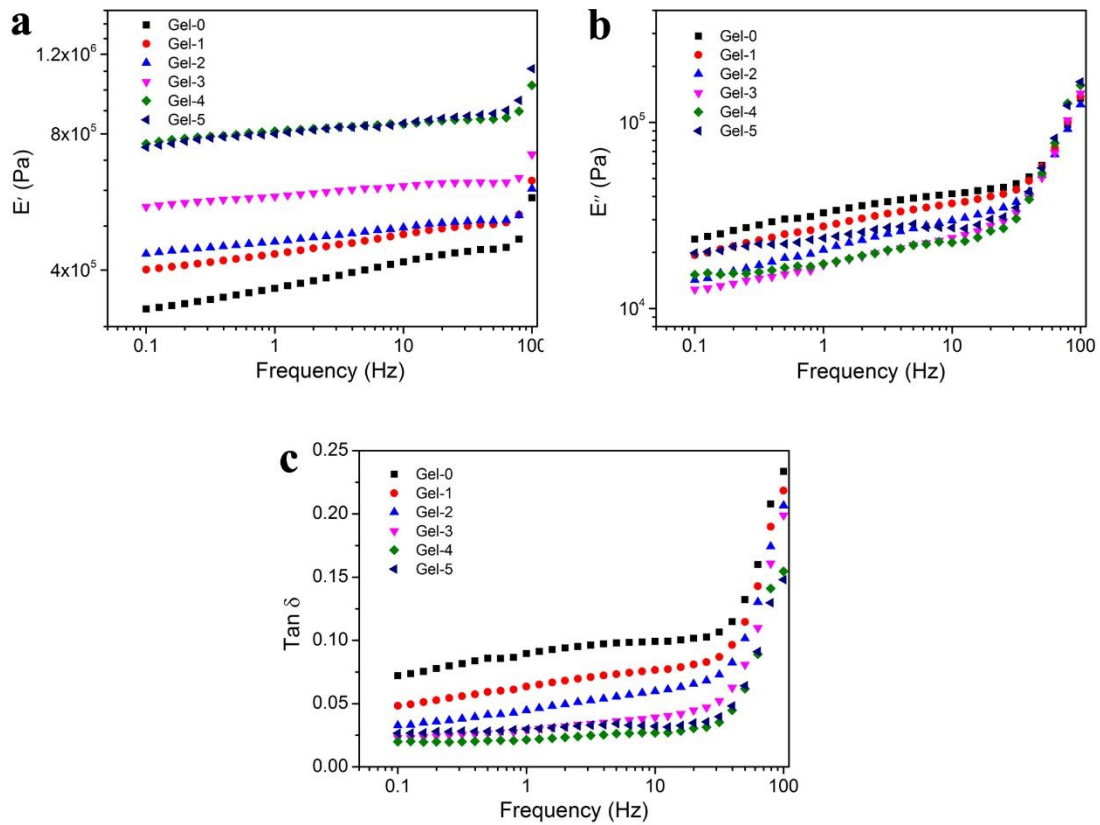

Fig. 4.4 Viscoelasticity of double cross-linking PAA hydrogels. a) Storage modulus.

b) Loss modulus. c) Tan δ.

Tan δ (calculated from E''/E') is considered as applied energy dissipation ratio (Fig. 4.4c). The tan δ value of the hydrogels is gradually decreased with increasing the MBA content (0 − 1.0 wt.%) at each frequency (for example, the tan δ value of the hydrogels decreases from 0.10 to 0.03 at 5 Hz with increasing MBA content from 0 − 1.0 wt.%). Moreover, the trend of tan δ and the storage modulus is similar, the value of tan δ increases with the addition of excess MBA content (1.25 wt.%). Adding a certain amount of MBA can increase the cross-linking density of the three-dimensional

network of the hydrogel, which limits the movement of the polymer chains, reduces the internal friction between the polymers, and reduces the tan δ value. In contrast, redundant cross-linking units formed by an excessive amount of MBA increases the internal friction between polymers, resulting in an increase in the value of tan δ.
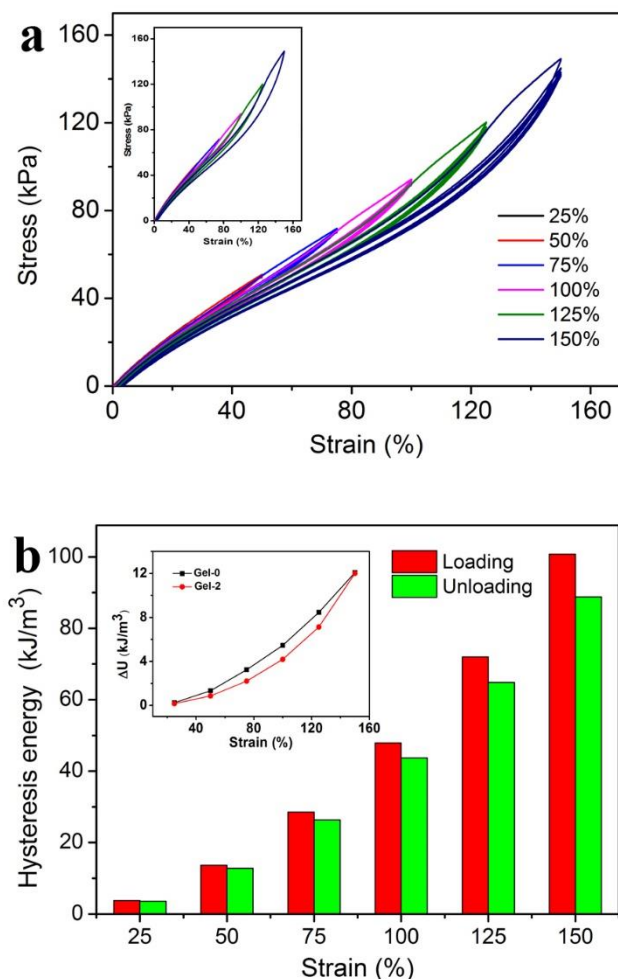

Fig. 4.5 a) Stress-strain responses of Gel-2 submitted to a cyclic tensile with increasing maximum strain every 5 cycles. b) The calculated hysteresis energy of Gel-2 during the first cyclic of softening process.

4.3.5 Softening effect

The prepared hydrogel (Gel-2) was submitted to a cyclic uniaxial tensile test with the maximum strain increasing every 5 cycles. Fig. 4.5a presents the stress-strain responses of Gel-2. In Fig. 4.5a, a softening which is specific to materials exhibiting the Mullins effect is observed.
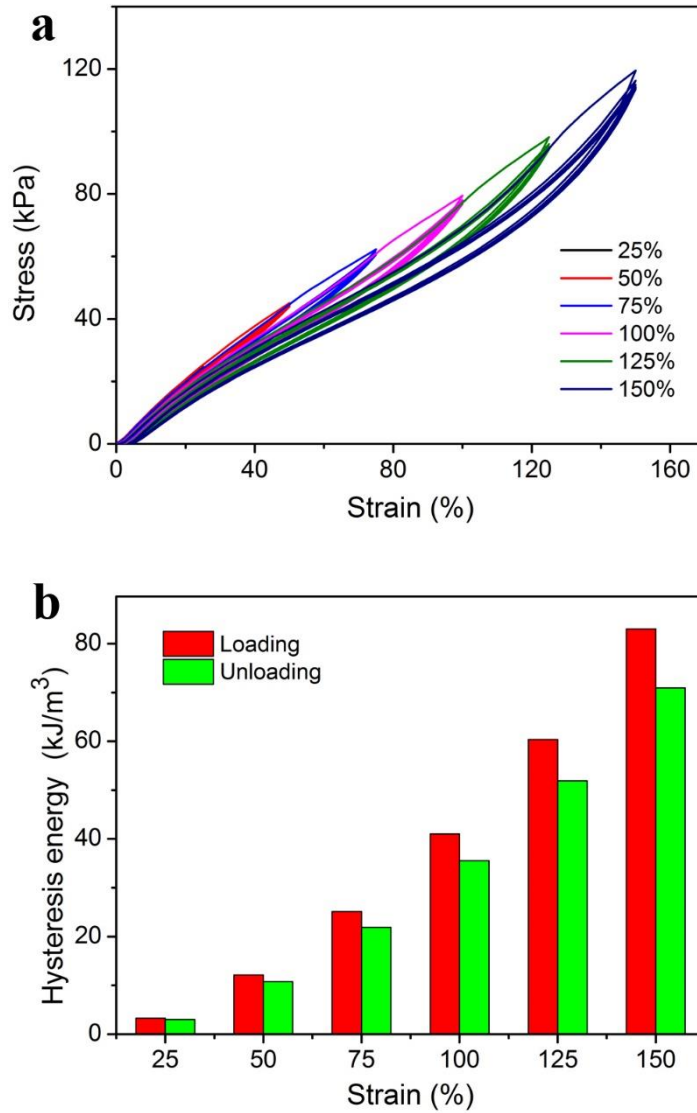
Fig. 4.6 a) Stress-strain responses of Gel-0 submitted to a cyclic tensile with increasing maximum strain every 5 cycles. b) The calculated hysteresis energy of Gel-0 during the first cyclic of softening process.

It is noted that for the same applied strain, a lower resulting stress appears after the first load, and the hydrogel response curves coincide during the following cycles. When the extension exceeds the previously applied maximum extension, the hydrogel stress-strain response curve continues to increase along the initial loading curve after returning from the same path in the previous tensile test (Fig. 4.5a, inset). Moreover, the softening increases progressively with increasing the maximum strain (Fig. 4.5b). Gel-0 without molecule cross-linker also has a similar softening effect (Fig. 4.6). By comparing the hysteresis energy loss of Gel-0 and Gel-2 during the softening process, it is found that

the addition of the molecule cross-linker (MBA) could alleviate this softening effect (Fig. 4.5b, inset). These special properties are usually characteristic of rubber materials, indicating that the hydrogel may have some rubber-like properties.

4.3.6 Internal network variation
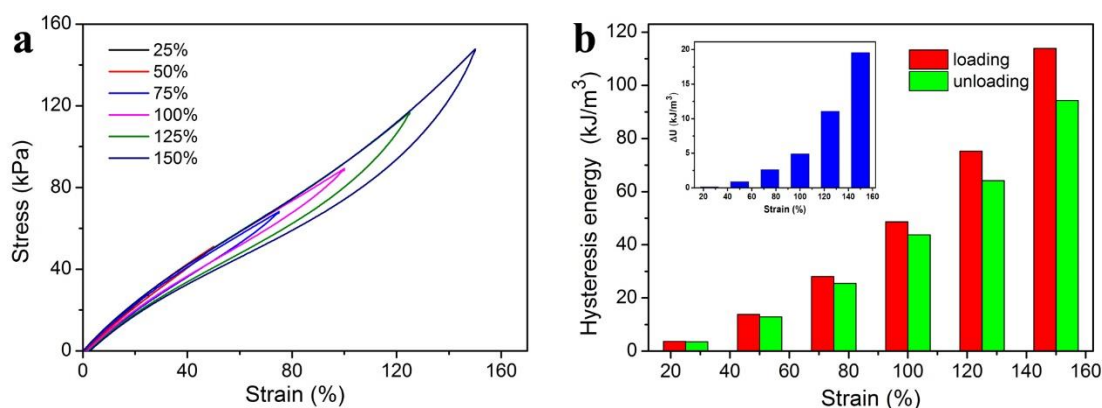
Fig. 4.7 a) Cyclic tensile tests of Gel-2 with various strain. b) The calculated hysteresis energy of Gel-2 during the cyclic tensile tests.

The presence of the Mullins effect indicated that the internal network of the hydrogel may have changed during the stretching process. The tensile stress-strain curve of Gel-2 shows an obvious hysteresis loop in the first cyclic test at various strains (Fig. 4.7a). This phenomenon has been reported in typical double-network hydrogels and filled rubbers, which is further elucidated by the energy dissipation mechanism [39, 40]. It suggests that there are some microstructure changes, including the disentanglement and sliding of polymer chains as well as the rupture of network, which result in the hysteresis loop in the first cycle. The calculated hysteresis energy shows that the magnitude of the hysteresis loop increases with increasing maximum strain of the hydrogel (Fig. 4.7b). ΔU (hysteresis energy loss or energy dissipation) exhibits a nonlinear increase with increasing maximum strain (Fig. 4.7b, inset).

4.3.7 Recovery properties in successive cyclic test

The double cross-linking hydrogel is different from most artificial hydrogel or filled rubber, the hysteresis becomes much smaller if the next cycle is conducted immediately

after the conclusion of the previous cycle (for example: at a strain of 125%, Fig. 4.8a). In fact, with increasing the number of cycles, the hysteresis loops hardly change. To understand the change in the internal network within the double cross-linking hydrogel during the stretching process, we estimate the effective network chain density (N) based on the stress-strain cyclic curve data of Gel-2, following the equation (4-5) reported in the literature [41, 42].

$$\tau = N\text{RT}[\alpha - (1/\alpha)^2] \quad (4\text{-}5)$$

where, τ is the force per unit unstrained cross sectional area, R and T are the gas constant and absolute temperature, respectively, and the τ value at elongation of $\alpha = 2$ (strain 100%) is used in the calculation. The estimated N values are shown in Fig. 4.8b. From Fig. 4.8b, it is noted that the disentanglement and sliding of the polymer chains, and the rupture of the network lead to the decrease of the effective network chain density. The cross-linking network structure variation in the first cycle is defined as "structure stabilizing".

Resilience is a measure of the ability of a material to deform reversibly without loss of energy, which is often used to represent the properties of highly elastic materials (for example, resilin-based materials) [43]. Gel-2 exhibits excellent elastic properties after the structure stabilizes (initial cycle), in this case, the performance of the hydrogel is more suitably represented by resilience instead of hysteresis energy loss [14]. It is observed that the resilience of Gel-2 remained over 95% at various strains, after the initial cycle (Fig. 4.8c). In addition, Gel-2 shows an insignificant residual strain (less than 3%) under various strains, which results from the rupture of the hydrogel network and a slight slip at the fixture and soft hydrogel (Fig. 4.8d) [44]. The resilience and residual strain (at a strain of 125%) of Gel-0 without MBA as the second cross-linker are 92.9% and 5.85%, respectively (Fig. 4.13). It indicates that the addition of MBA increases the resilience and the stability of the hydrogel during the deformation process. Although the hydrogel was covered with oil during the tests, the evaporation of water during the large deformation was unavoidable as the cycle increased, resulting in a slight decrease in residual strain. These results indicate that the double cross-linking hydrogel possesses stable mechanical properties in the successive cyclic tensile system.
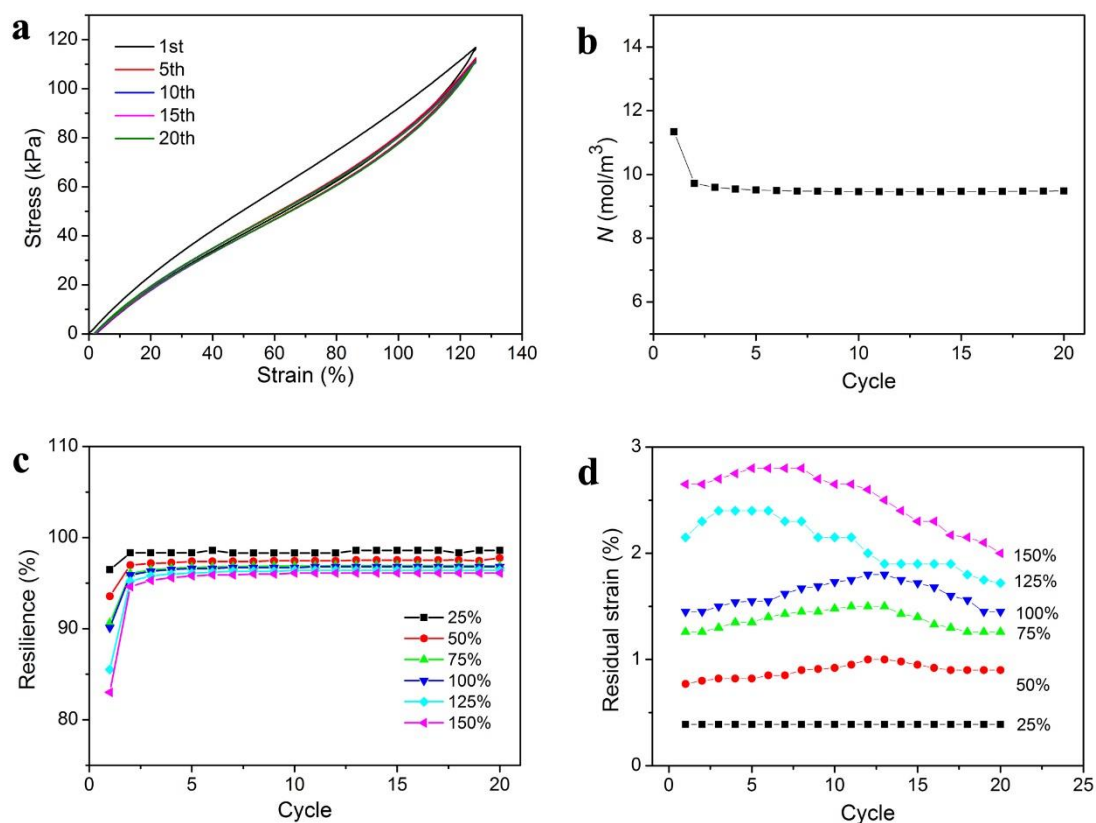
Fig. 4.8 a) Successive cyclic tensile tests of Gel-2 at a 125% strain for 20 cycles. b) The estimated effective network chain density (*N*) of Gel-2. c) Resilience of Gel-2 at various strains for 20 cycles. d) Residual strain of Gel-2 at various strains for 20 cycles.
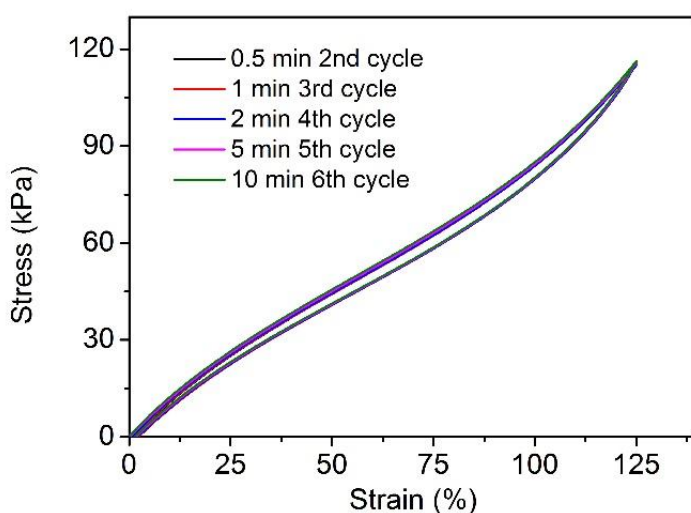

Fig. 4.9 Intermittent cyclic tensile tests of Gel-2 at a 125% strain with different rest time.

4.3.8 Recovery properties in intermittent cyclic test

The application of hydrogels in biomedical and soft machines actually require them to have stable mechanical properties, such as: resilience, tensile strength, residual strain, etc. Such stable mechanical properties ensure that the material (e.g., artificial muscles, soft robots) prepared from the hydrogel has reliable performance in all cases.
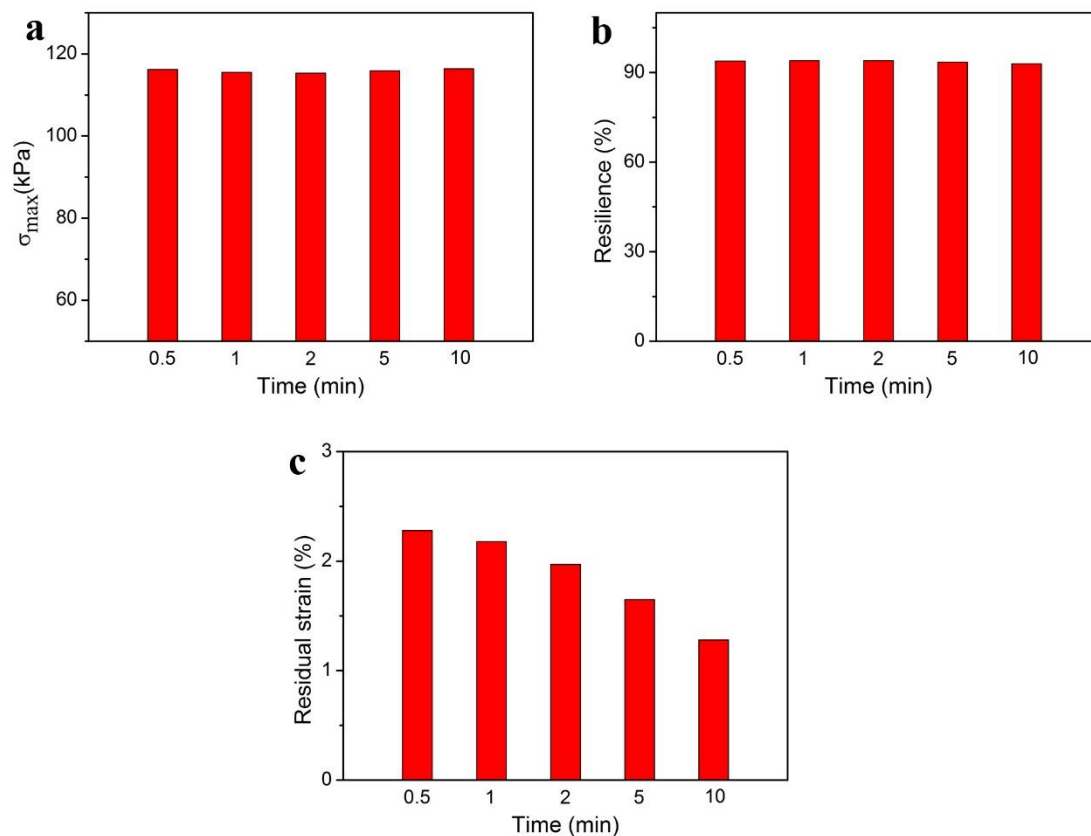

Fig. 4.10 Intermittent cyclic tensile tests of Gel-2 at a 125% strain with different rest time. a) Maximum stress. b) Resilience. c) Residual strain.

Most of reported hydrogels possess obviously time-dependent recovery properties which significantly increase with increasing rest time, resulting in hydrogels with changing properties of during the time of use, for example, a reported tough protein hydrogel, whose recovery performance (resilience, residual strain and maximum stress) seriously depends on time. The hysteresis recovery rate rapidly increases within 20 min, and the mechanical properties are constantly changing during this time [45]. In contrast, the mechanical properties of the double cross-linking hydrogel are independent of the

rest time. It is observed that the curves of Gel-2 almost remain constant with the rest time and cyclic increase (Fig. 4.9). The resilience, residual strain, and maximum stress of Gel-2 were stabilized at 93%, less than 3% and 115 kPa, respectively, with the increase of rest time and cyclic times (Fig. 4.10). The stable mechanical properties give the hydrogel potential applications in the field of sensors (needing a certain accuracy).

**4.3.9 Effect of swelling on recovery properties**
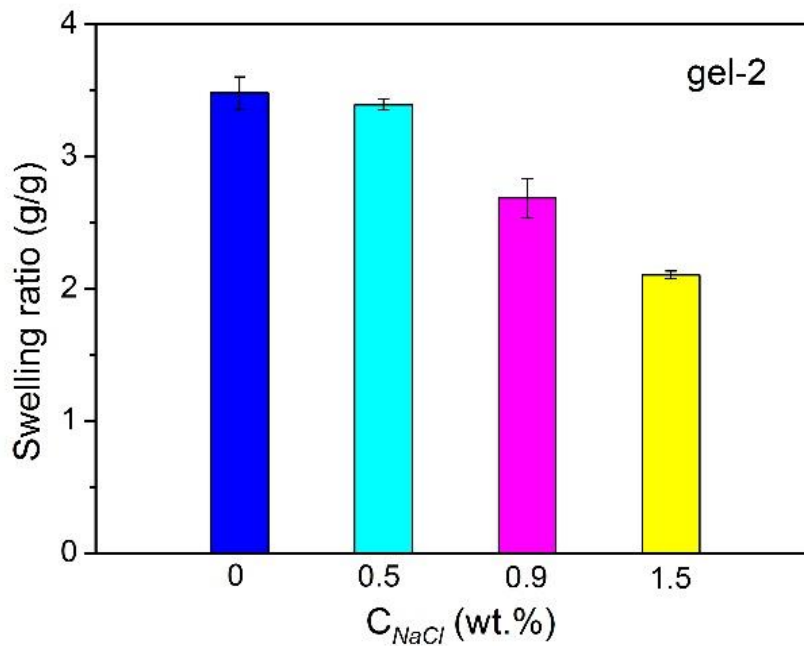
Fig. 4.11 Swelling ratios of Gel-2 at various NaCl concentrations.

The application of hydrogels in the field of biomaterials are usually exposed to low concentrations of salt solution environment. Polyelectrolyte hydrogels usually perform a lower SR in salt solutions than in distilled water. For example, Fig. 4.11 represents the equilibrium SR of Gel-2 in NaCl solution at different concentrations. The SR of Gel-2 is observed to be 2.67 in normal saline (0.9 wt. % NaCl) aqueous. The swollen Gel-2 (S-Gel-2) with a water content of 88.5% has a stress-strain curve similar to Gel-2 (Fig. 4.12a). It can be seen that the resilience of Gel-2 and S-Gel-2 increase from 85.3% and 87.0% to 96.0% and 97.5%, respectively, after the initial cycle (Fig. 4.12b).
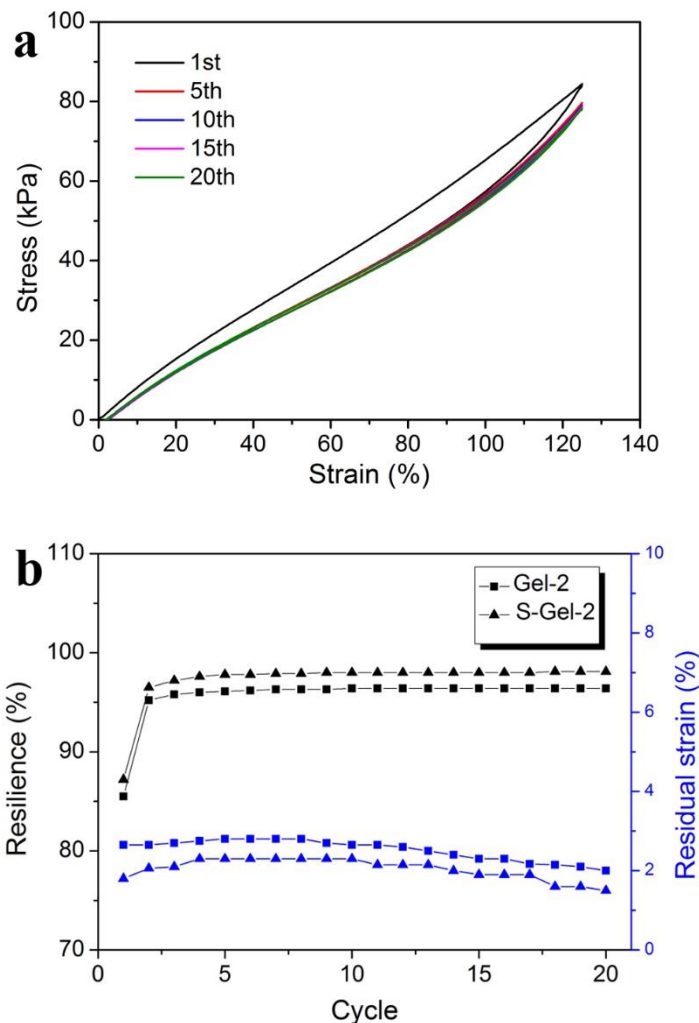
Fig. 4.12 a) Cyclic tensile test of S-Gel-2 at a 125% strain for 20 cycles. b) Resilience and residual strain of Gel-2 and S-Gel-2 at a strain of 125%.

The residual strain of S-Gel-2 is lower than that of Gel-2 in cyclic tensile tests (Fig. 4.12b). This fact confirms that the network structure of Gel-2 has been changed after swelling in normal saline solution. In addition, the swelling equilibrium also has a significant effect on the hydrogel without molecule cross-linker. The resilience of swollen Gel-0 (S-Gel-0) is increased from 92.9% to 96.9% compared to Gel-0, and the residual strain is reduced from 5.85% to about 2% (Fig. 4.13). The disentanglement and sliding of the polymer chains during the swelling process results in a smaller internal friction between the polymer chains in the cyclic tensile test. Thus, the hydrogel that achieved swelling equilibrium has higher resilience and lower residual strain than that of the as-prepared state.
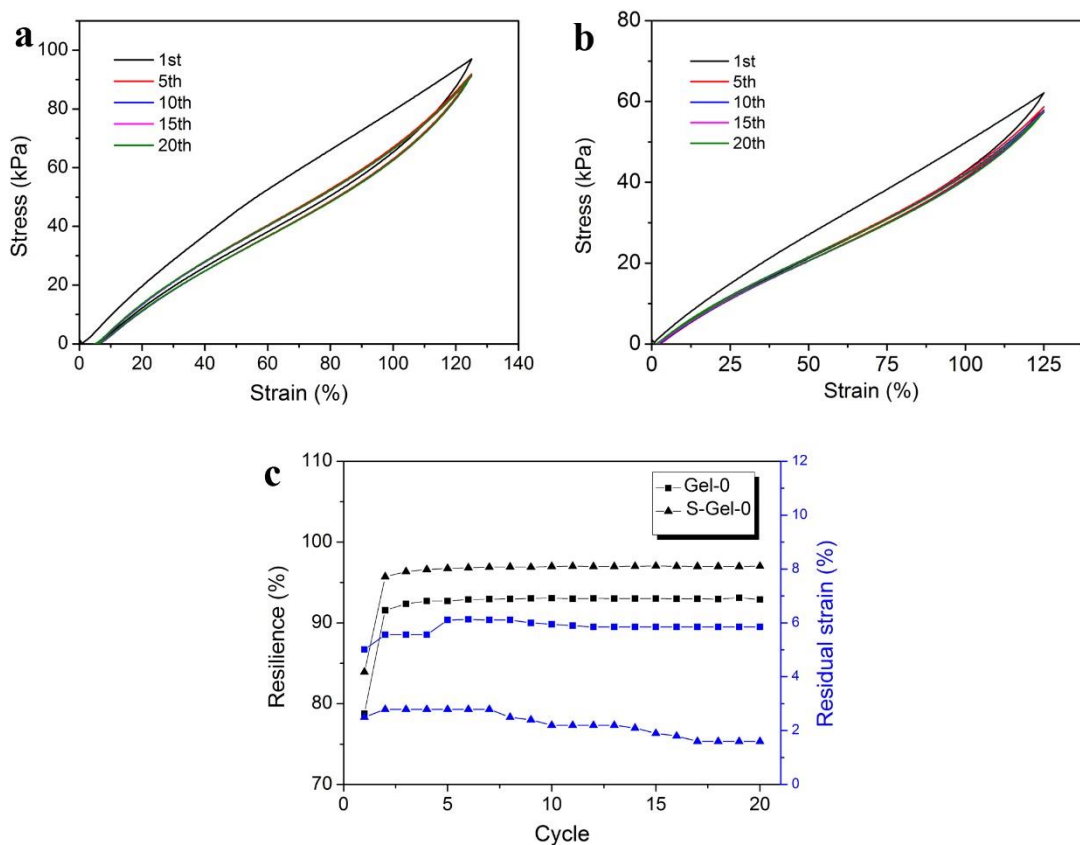
Fig. 4.13 a) Cyclic tensile test of Gel-0 at a 125% strain for 20 cycles. b) Cyclic tensile test of S-Gel-0 at a 125% strain for 20 cycles. c) Resilience and residual strain of Gel-0 and S-Gel-0 at a strain of 125%.

4.4 Conclusions

In this study, a novel design strategy was developed to fabricate a double cross-linking PAA hydrogel. The facile polymerization was triggered by visible light, where active CMC as initiator and the first cross-linker, MBA as the second cross-linker. The tensile strength and the swelling ratio were reduced with increasing the MBA contents, while the elastic modulus showed an increased trend in the same conditions. DMA suggested that the addition of MBA reduced the internal friction between the macromolecules in the hydrogel, which increased the elasticity and decreased the viscosity of the hydrogel. The hydrogel exhibited a softening effect similar to conventional rubber materials, and further studies showed that the disentanglement and sliding of polymer chains as well as the rupture of network led to this effect. After the

structure stabilized, the hydrogel exhibited remarkable recovery properties (resilience over 93% and 95% for successive and intermittent cyclic tensile tests, respectively, and residual strain less than 3%). It was noted that the recovery properties were almost constant in various conditions and independent of time, which could extend the application of the hydrogel in the field where high accuracy is required. In addition, the hydrogel presented a higher resilience and lower residual strain after the hydrogel reached the swelling equilibrium. The hydrogel has potential applications in soft machines and biomaterials.

References

[1] Li Y, Rodrigues J, Tomas H. Injectable and biodegradable hydrogels: gelation, biodegradation and biomedical applications. Chemical Society reviews. 2012;41(6):2193-221.

[2] Capadona JR, Shanmuganathan K, Tyler DJ, Rowan SJ, Weder C. Stimuli-responsive polymer nanocomposites inspired by the sea cucumber dermis. Science. 2008;319(5868):1370-4.

[3] Van Vlierberghe S, Dubruel P, Schacht E. Biopolymer-based hydrogels as scaffolds for tissue engineering applications: a review. Biomacromolecules. 2011;12(5):1387-408.

[4] Thiele J, Ma Y, Bruekers SM, Ma S, Huck WT. 25th anniversary article: Designer hydrogels for cell cultures: a materials selection guide. Advanced materials. 2014;26(1):125-47.

[5] Zheng WJ, An N, Yang JH, Zhou J, Chen YM. Tough Al-alginate/poly(N-isopropylacrylamide) hydrogel with tunable LCST for soft robotics. ACS applied materials & interfaces. 2015;7(3):1758-64.

[6] Calvert P. Hydrogels for Soft Machines. Advanced materials. 2009;21(7):743-56.

[7] Haque MA, Kurokawa T, Gong JP. Super tough double network hydrogels and their application as biomaterials. Polymer. 2012;53(9):1805-22.

[8] Webber RE, Creton C, Brown HR, Gong JP. Large strain hysteresis and mullins effect of tough double-network hydrogels. Macromolecules. 2007;40(8):2919-27.

[9] Liu S, Li L. Recoverable and Self-Healing Double Network Hydrogel Based on kappa-Carrageenan. ACS applied materials & interfaces. 2016;8(43):29749-58.

[10] Gao G, Du G, Sun Y, Fu J. Self-healable, tough, and ultrastretchable nanocomposite hydrogels based on reversible polyacrylamide/montmorillonite adsorption. ACS applied materials & interfaces. 2015;7(8):5029-37.

[11] Jaiswal MK, Xavier JR, Carrow JK, Desai P, Alge D, Gaharwar AK. Mechanically Stiff Nanocomposite Hydrogels at Ultralow Nanoparticle Content. ACS Nano. 2016;10(1):246-56.

[12] Bin Imran A, Esaki K, Gotoh H, Seki T, Ito K, Sakai Y, et al. Extremely stretchable thermosensitive hydrogels by introducing slide-ring polyrotaxane cross-linkers and ionic groups into the polymer network. Nature communications. 2014;5:5124.

[13] Kamata H, Akagi Y, Kayasuga-Kariya Y, Chung UI, Sakai T. "Nonswellable" hydrogel without mechanical hysteresis. Science. 2014;343(6173):873-5.

[14] Lv S, Dudek DM, Cao Y, Balamurali MM, Gosline J, Li H. Designed biomaterials to mimic the mechanical properties of muscles. Nature. 2010;465(7294):69-73.

[15] Falabella CA, Melendez MM, Weng L, Chen W. Novel macromolecular crosslinking hydrogel to reduce intra-abdominal adhesions. The Journal of surgical research. 2010;159(2):772-8.

[16] He C, Zheng Z, Zhao D, Liu J, Ouyang J, Wang H. Tough and super-resilient hydrogels synthesized by using peroxidized polymer chains as polyfunctional initiating and cross-linking centers. Soft Matter. 2013;9(10):2837.

[17] Gong JP. Why are double network hydrogels so tough? Soft Matter. 2010;6(12):2583.

[18] Naficy S, Spinks GM, Wallace GG. Thin, tough, pH-sensitive hydrogel films with rapid load recovery. ACS applied materials & interfaces. 2014;6(6):4109-14.

[19] Elvin CM, Carr AG, Huson MG, Maxwell JM, Pearson RD, Vuocolo T, et al. Synthesis and properties of crosslinked recombinant pro-resilin. Nature. 2005;437(7061):999-1002.

[20] Liu J, Chen C, He C, Zhao J, Yang X, Wang H. Synthesis of graphene peroxide and its application in fabricating super extensible and highly resilient nanocomposite hydrogels. ACS Nano. 2012;6(9):8194-202.

[21] Maeda S, Hara Y, Yoshida R, Hashimoto S. Active polymer gel actuators. International journal of molecular sciences. 2010;11(1):52-66.

[22] COMPOSITES PART B: ENGINEERING.

[23] Gao X, Cao Y, Song X, Zhang Z, Zhuang X, He C, et al. Biodegradable, pH-responsive carboxymethyl cellulose/poly(acrylic acid) hydrogels for oral insulin delivery. Macromolecular bioscience. 2014;14(4):565-75.

[24] Nair V, Deepthi A. Cerium(IV) ammonium nitrate--a versatile single-electron oxidant. Chemical reviews. 2007;107(5):1862-91.

[25] Zhu L, Guo J, Liu P, Zhao S. Novel strategy for palygorskite/poly(acrylic acid) nanocomposite hydrogels from bi-functionalized palygorskite nanorods as easily separable adsorbent for cationic basic dye. Applied Clay Science. 2016;121-122:29-35.

[26] McDowall D, Gupta B, Stannett V. Grafting of vinyl monomers to cellulose by ceric ion initiation. Progress in Polymer Science. 1984;10(1):1-50.

[27] Rahman L, Silong S, Zin WM, Rahman M, Ahmad M, Haron J. Graft copolymerization of methyl acrylate onto sago starch using ceric ammonium nitrate as an initiator. Journal of applied polymer science. 2000;76(4):516-23.

[28] Joshi JM, Sinha VK. Ceric ammonium nitrate induced grafting of polyacrylamide onto carboxymethyl chitosan. Carbohydrate Polymers. 2007;67(3):427-35.

[29] Wu S, Jin Z, Kim JM, Tong Q, Chen H. Graft copolymerization of methyl acrylate onto pullulan using ceric ammonium nitrate as initiator. Carbohydrate Polymers. 2009;76(1):129-32.

[30] Fakhru L, Razi A, Qudsieh IY, Yunus WMZW, Ahmad MB, Rahman MZA. Graft copolymerization of methyl methacrylate onto sago starch using ceric ammonium nitrate and potassium persulfate as redox initiator systems. Journal of applied polymer science. 2001;82(6):1375-81.

[31] Jeon O, Song SJ, Lee K-J, Park MH, Lee S-H, Hahn SK, et al. Mechanical properties and degradation behaviors of hyaluronic acid hydrogels cross-linked at various cross-linking densities. Carbohydrate Polymers. 2007;70(3):251-7.

[32] Xia XX, Wang M, Lin Y, Xu Q, Kaplan DL. Hydrophobic drug-triggered self-assembly of nanoparticles from silk-elastin-like protein polymers for drug delivery. Biomacromolecules. 2014;15(3):908-14.

[33] Pina S, Oliveira JM, Reis RL. Natural-based nanocomposites for bone tissue engineering and regenerative medicine: a review. Advanced materials. 2015;27(7):1143-69.

[34] Kim J, Conway A, Chauhan A. Extended delivery of ophthalmic drugs by silicone hydrogel contact lenses. Biomaterials. 2008;29(14):2259-69.

[35] Johnson BD, Beebe DJ, Crone WC. Effects of swelling on the mechanical properties of a pH-sensitive hydrogel for use in microfluidic devices. Materials Science and Engineering: C. 2004;24(4):575-81.

[36] Akar E, Altinisik A, Seki Y. Preparation of pH- and ionic-strength responsive biodegradable fumaric acid crosslinked carboxymethyl cellulose. Carbohydr Polym. 2012;90(4):1634-41.

[37] Okay O, Oppermann W. Polyacrylamide−Clay Nanocomposite Hydrogels: Rheological and Light Scattering Characterization. Macromolecules. 2007;40(9):3378-87.

[38] Xiong L, Hu X, Liu X, Tong Z. Network chain density and relaxation of in situ synthesized polyacrylamide/hectorite clay nanocomposite hydrogels with ultrahigh tensibility. Polymer. 2008;49(23):5064-71.

[39] Li H, Yang L, Weng G, Xing W, Wu J, Huang G. Toughening rubbers with a hybrid filler network of graphene and carbon nanotubes. J Mater Chem A. 2015;3(44):22385-92.

[40] Gong JP. Materials science. Materials both tough and soft. Science. 2014;344(6180):161-2.

[41] Yang J, Han CR, Duan JF, Xu F, Sun RC. Mechanical and viscoelastic properties of cellulose nanocrystals reinforced poly(ethylene glycol) nanocomposite hydrogels. ACS applied materials & interfaces. 2013;5(8):3199-207.

[42] Haraguchi K, Farnworth R, Ohbayashi A, Takehisa T. Compositional Effects on Mechanical Properties of Nanocomposite Hydrogels Composed of Poly(N,N-dimethylacrylamide) and Clay. Macromolecules. 2003;36(15):5732-41.

[43] Gosline J, Lillie M, Carrington E, Guerette P, Ortlepp C, Savage K. Elastic proteins: biological roles and mechanical properties. Philosophical transactions of the Royal Society of London Series B, Biological sciences. 2002;357(1418):121-32.

[44] Lillie M, Chalmers G, Gosline J. The effects of heating on the mechanical properties of arterial elastin. Connective tissue research. 1994;31(1):23-35.

[45] Fang J, Mehlich A, Koga N, Huang J, Koga R, Gao X, et al. Forced protein unfolding leads to highly elastic and tough protein hydrogels. Nature communications. 2013;4:2974.

Chapter 5 High Modulus Hydrogel Obtained from Hydrogen Bond Reconstruction and Application in Vibration Damper

5.1 Introduction

Hydrogels are engineering materials with a high water content and exhibit a three-dimensional network structure [1,2]. Due to their inherently excellent biocompatibility and stimuli-responsiveness, hydrogels have been applied in the field of tissue engineering [3-5]. In recent years, hydrogels incorporating effective energy dissipation mechanisms or presenting distinctive structures exhibit remarkable overall mechanical properties (tensile strength of 0.2–10 MPa; fracture elongation of 100–6000%, and toughness of 100–15 000 J m^{-2}) [6]. These hydrogels, which exhibit similar properties to conventional rubbers, are excellent candidates for vibration control materials in tissue engineering [7]. The vibration absorption material must have sufficient rigidity (to reduce the amplitude during vibration); therefore, this material must have a high modulus (*e.g.*, cartilage, a natural vibration absorption material, has a modulus greater than 1 MPa) [8]. However, the modulus of most hydrogels is of the order of 0.1 MPa [9,10], which greatly limits their use as a vibration absorption material.

In recent years, researchers have developed a number of high-modulus hydrogels through novel design concepts and special structures [11]. Gong *et al.* have designed an oppositely charged polyelectrolyte PMPTC/PNaSS hydrogel [12]. In the preparation process, a uniformly dispersed polyelectrolyte hydrogel was obtained by a two-step polymerization reaction. The resulting hydrogel was dialyzed to ensure that the ionic bonds in the hydrogel were sufficiently strong. The highest modulus of the PMPTC/PNaSS hydrogel can reach 7.9 MPa. In addition, Lin *et al.* improved a dual-crosslinked hydrogel consisting of covalent and ionic bonds [13]. In this hydrogel, the

initial PAM–PAA network was synthesized using a covalent cross-linker, and then, the coordination bonds were formed after immersing the single network hydrogel in a highly concentrated Fe^{3+} solution. The modulus of the PAM/PAA hydrogel can reach 3.5 MPa. Moreover, optimization of the network structure in the as-prepared hydrogel is an effective way to increase the modulus. For instance, increasing the crystallinity of the polymer chains within the hydrogel by the addition of a salt or base solution at high concentration can enhance the modulus of the hydrogel. Thus, the modulus of the PAM-CS hydrogel can reach 0.3–0.4 MPa through crystallization enhancement; however, the use of a strong base may cause potential problems in applications [14]. Therefore, it is a big challenge to produce a hydrogel with high modulus through a convenient, efficient, and green synthesis method. Most hydrogels contain a variety of complex hydrogen bond networks across polymer chains; these hydrogen bond interactions between polymer chains can be leveraged to achieve a reconstruction of the hydrogel network to improve the modulus of the hydrogel.

In our previous study, we prepared a carboxymethyl cellulose/polyacrylic acid hydrogel with excellent mechanical properties (tensile strength of 0.85 MPa, fracture elongation of 700%, and modulus of 0.18 MPa) by a facile, visible-light-triggered, one-pot polymerization method [15,16]. Herein, an aluminum ion cross-linked hydrogel (Gel) was synthesized by the same method, and then, the as-prepared Gel was reinforced *via* the evaporation-swelling method (E-S method) to obtain the high-modulus hydrogels (HM-Gel), with a tensile strength of 1.26–1.74 MPa and an elastic modulus of 0.59–1.94 MPa. In addition, both Gel and HM-Gel exhibited improved damping performance due to the presence of aluminum ion as a reinforcement cross-linking site; thus, the applicability of the hydrogel as a vibration control material is greatly improved. This E-S method provides a way for increasing the modulus of many reported hydrogels and can broaden their application as a vibration control material.

5.2 Experimental

5.2.1 Materials

Carboxymethyl cellulose sodium salt (CMC, EP), acrylic acid (AA, EP), ceric ammonium nitrate ($(NH_4)_2Ce(NO_3)_4$, CAN, GR), and aluminium chloride hexahydrate ($AlCl_3 \cdot 6H_2O$, GR) were purchased from Nacalai Tesque, Inc. All chemical reagents were used as received. Distilled water was used in all experiments.

5.2.2 Sample preparation

The HM-Gels were prepared *via* two steps consisting of visible-light-triggered polymerization and evaporation-swelling. Briefly, 40 mg of CAN, 3.60 g of AA, and 10.0 mL of distilled water were added to a vial stepwise and mixed under magnetic stirring in an ice bath. Subsequently, 0.40 g of CMC was slowly added to the mixture under vigorous magnetic stirring. The precursor hydrogel was stably dispersed for 40 min under vigorous stirring. A range of concentrations of $AlCl_3 \cdot 6H_2O$ (0–1.5 mol%, Al^{3+} to AA) was added to a series of vials, and the mixtures were stirred for 20 min. The viscous precursor hydrogels were transferred to transparent glass molds and covered with glass plates. Finally, the glass molds were immersed in water at 20 °C and placed 20 cm below a visible light source (LS-M210, Sumita) for 5 min. The prepared carboxymethyl cellulose/polyacrylic acid hydrogels were named Gel-*X*, where *X* denoted the Al^{3+}concentration (mol %) relative to that of monomer (AA). The obtained Gels were placed in a dry oven and dried at various temperatures for 24 h (for 25 °C, the hydrogel was dried at room temperature for 3 days). The dried Gels were immersed in distilled water for 50 h to obtain a swelling equilibrium. The swollen hydrogels at equilibrium with a high modulus were named HM-Gel. All hydrogels were dried in air at 60 °C.

5.2.3 Characterization

The phase transition time of the hydrogels was determined by dynamic mechanical analysis (DMA, RSA-G2, TA Instrument, New Castle, DE, USA). We used a stress

relaxation modulus program for the hydrogel gelation time tests using a disc model at 25 °C, 1 Hz, and 1% strain. The program and light were turned on at the same time.

The uniaxial elongation properties were measured using the JIS K6251 (a Japanese industrial rubber) as a standard *via* a universal testing machine (Instron 3300 series, 50 N load cell, Instron Co., Ltd., Canton, America); the procedure for the measurements was as follows: hydrogels were cut in a dumbbell shape with a 75 mm length (L), 25 mm gauge length (L_o), 4 mm width (w), and 2 mm height (h), and tests were conducted at a cross-head speed of 500 mm min^{-1}. The compression properties were measured using the same universal testing machine at a cross-head speed of 1 mm min^{-1}. Hydrogels were cut in a disc shape with 9 mm diameter and 2 mm height.

The storage modulus and loss modulus of the hydrogel specimens were measured as a function of frequency using dynamic mechanical analysis (DMA, RSA-G2, TA Instrument). Hydrogels were cut into a disc shape with 9 mm diameter and 2 mm height. Before measurements, an axial force of 0.981 N was applied on the specimens. The frequency sweeping experiments were performed under a constant strain amplitude (1%) in the frequency range from 100 to 0.1 Hz.

For the cyclic tensile tests, loading–unloading measurements were performed using the same universal testing machine at a constant velocity of 100 mm min^{-1}. The Gels were cut into pieces with the following size: 60 mm length (l), 10 mm width (w), 2 mm height (h), and 30 mm gauge length (l_o). The samples were covered with oil to prevent water evaporation. Tensile stress (σ) was calculated as $\sigma = F/wh$, where F is the load.

Swelling experiments were performed by immersing the Gels and dried-Gels in conical flasks filled with distilled water. The flasks were placed in a temperature-controlled bath at 25 °C for 50 hours. For the swelling experiment, all samples were measured 3 times.

The changes of the CMC crystalline network structure in Gel and HM-Gel were investigated using an optical microscope (Eclipse model ME 600D, Nikon, Japan). The thin hydrogel films were obtained by shock-freezing using a microtome (RM2145, Leica Microsystems, Japan). The length, width, and thickness of the hydrogel films were 15 mm, 2 mm, and 200 µm, respectively.

Differential thermal analysis (DTA) of the samples was performed using a TG instrument (DTG-60, Shimadzu Co., Ltd., Kyoto, Japan) at a scan rate of 10 °C min^{-1} from room temperature to 400 °C under a N$_2$ atmosphere (flow rate of 50 mL min^{-1}). Samples of 4–6 mg were placed in aluminum crucibles using an empty aluminum crucible as a reference.

To fully understand the changes in the internal network, we estimated the effective network chain density (N) based on the cyclic stress–strain curves of HM-Gel (dried in air at 60 °C), according to the following equation reported in the literature:

$$\tau = NRT[\alpha - (1/\alpha)^2] \quad (5\text{-}1)$$

Where τ is the force per unit of unstrained cross-sectional area, R and T are the gas constant and absolute temperature, respectively, and a τ value at elongation of $\alpha = 2$ (strain 100%) is used in the calculation.

For the experiments evaluating the damping performance, a commercially available test tube mixer was used as the vibration source; the vibration machine was equipped with a hydrogel vibration damper, a support plate, and a force sensor. The sampling frequency was set at 20 points per second.

All the hydrogel performance tests were performed at room temperature.

5.3 Results and discussions

5.3.1 Visible-light intensity for hydrogel formation

Light as an efficient and easily acquired trigger has been extensively used for radical-initiated polymerization [17]. Visible light, which is safe, low cost, and easy to use, is favored in synthetic polymerization applications [18]. In our previous study, visible light was found to be an efficient trigger for the synthesis of cellulose-containing hydrogels [15]. In this polymerization, ceric ions attack the glucopyranose units to form a CMC–cerium complex. Then, Ce^{4+} ions are reduced to Ce^{3+} within the complex, and a free radical and aldehyde are obtained by the rupture of the carbon 2 and 3 bonds of the glucopyranose unit [19]. Finally, the free radical initiates the monomer

polymerization and a network is formed through end-group termination of the active polymer chains (Schematic 5.1). This polymerization can even be performed under sunlight, and the gelation process is completed within only 1 minute (Fig. 5.1, inset).
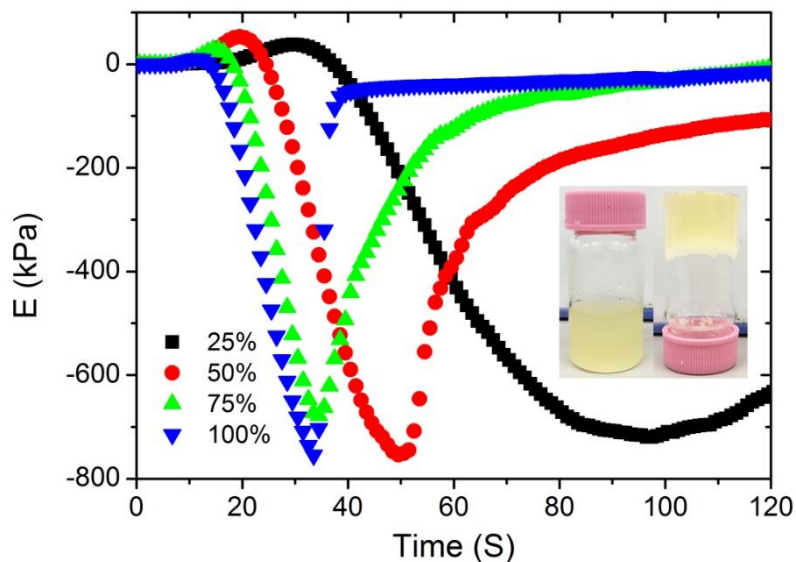

Fig. 5.1 Effect of various light intensity on the time of hydrogel state transformation: pseudo relaxation modulus – time curves of Gel-1.0.
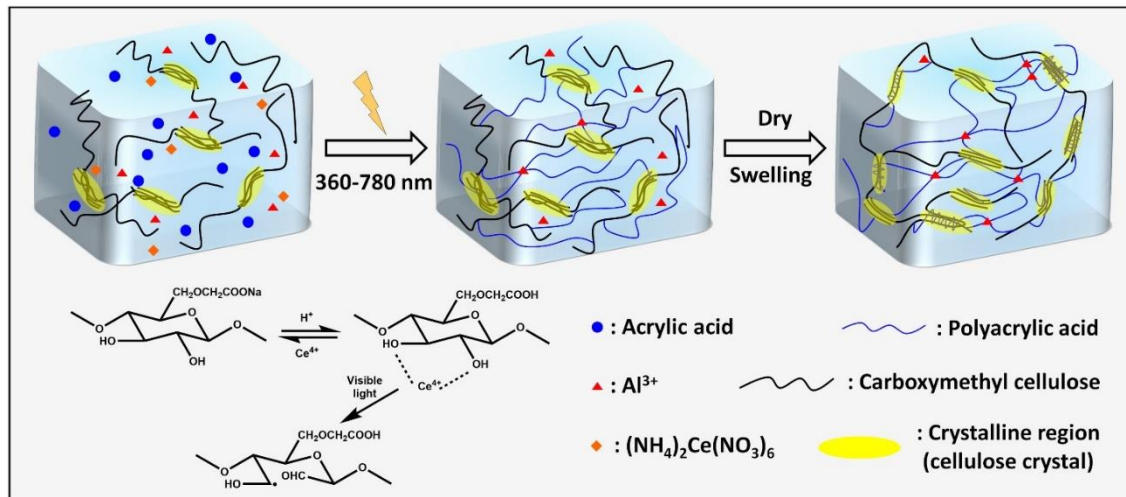
Schematic 5.1 Proposed mechanism of hydrogel formation under visible light and the reinforced process by evaporation-swelling method.

To study the effect of light intensity on hydrogel performance, a metal halide lamp (LS-M210, Sumita) was selected as a stable visible light source. The luminous emittance is proportional to the output energy.
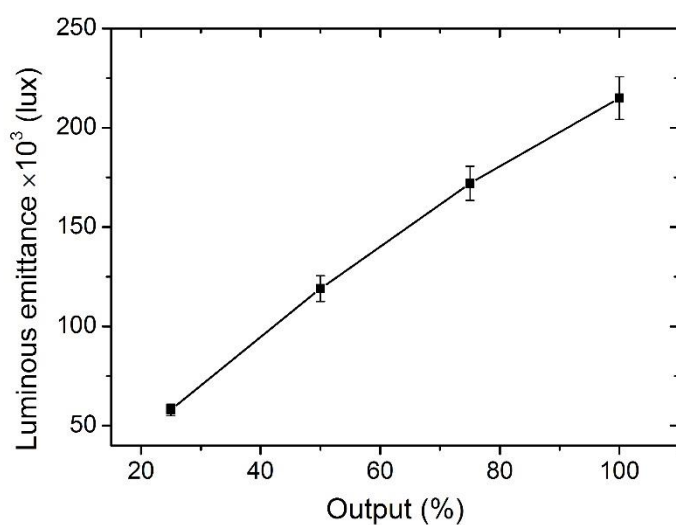
Fig. 5.2 Relationship between output energy and luminous emittance.
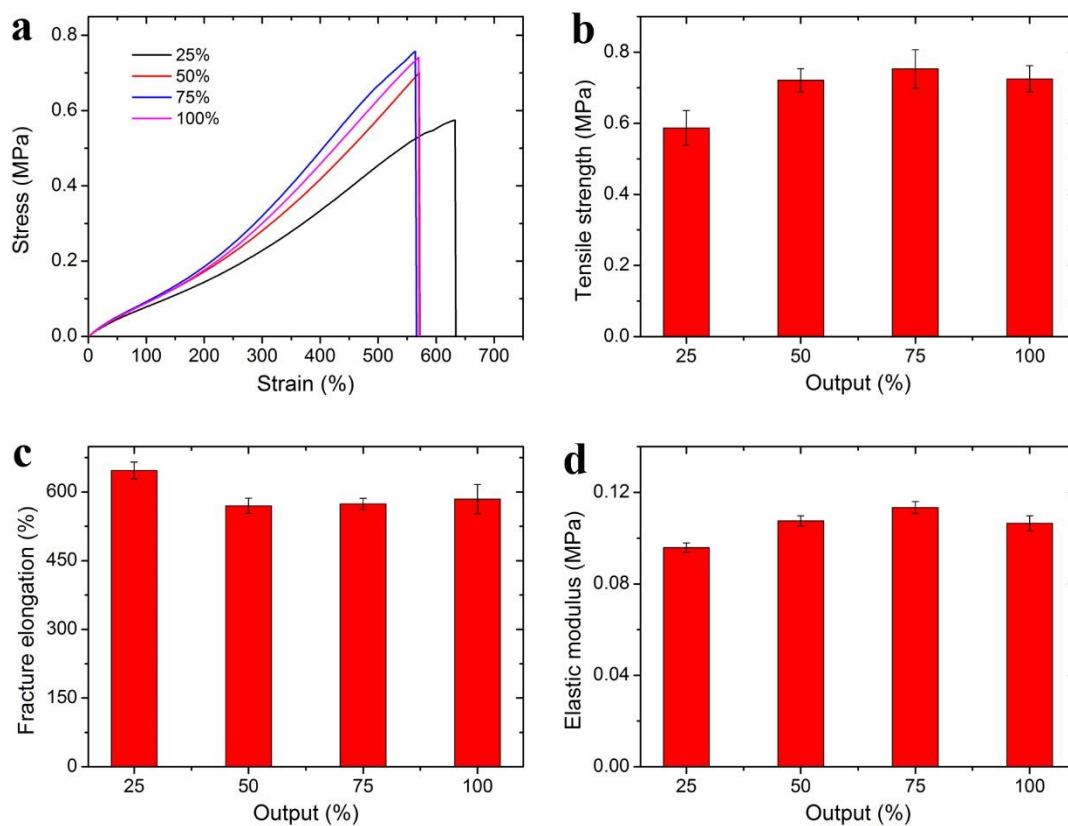
Fig. 5.3 Effect of output energy on mechanical properties of Gel-1.0. a) stress-strain curves; b) tensile strength; c) fracture elongation; d) elastic modulus of Gel-1.0 prepared with various output energy.

Fig. 5.2 shows that the luminous emittance was in the range of 58–215 kLux depending on the output energy (from 25% to 100%). Since the generated radicals are

highly dependent on the induction of visible light, the gelation time is closely related to the visible light intensity. The pseudo relaxation modulus showed that the hydrogel precursors from the viscous state to the just-formed solid state require 68 s, 30 s, 20 s, and 22 s at the visible light output energy of 25%, 50%, 75%, and 100%, respectively (Fig. 5.1). This suggests that high light intensity helps to shorten the gelation time, but higher light intensity has a limited effect on the gelation time. Moreover, the visible light intensity greatly affects the mechanical properties of the hydrogel. At a lower output energy (25%), the tensile strength, fracture elongation, and elastic modulus of Gel-1.0 were 0.59 MPa, 640%, and 0.096 MPa, respectively. When a higher output energy of 50%, 75%, and 100% was applied, the tensile strength and elastic modulus of Gel-1.0 clearly improved (Fig. 5.3). However, the fracture elongation slightly decreased with the increasing output energy.

5.3.2 Improvement of mechanical properties

To improve the mechanical performance of hydrogels, researchers have intensively investigated different reinforced networks including double networks [3], topological networks [20], polyampholyte based networks [21], hydrogen bond cross-linked networks [22], or ionic cross-linked networks [23]. Among them, the ionic cross-linking is one of the most deeply investigated. Metal cations play an important role in hydrogels containing anionic polymer chains as they can form coordination bonds with the negatively charged polymer chains to increase the cross-linking density of hydrogels [24,25]. When an external loading is applied, these coordination bonds act as reversible sacrificial bonds and rupture to dissipate the applied energy. An improvement in tensile strength, elastic modulus, and fracture elongation was observed by adding 0.1 mol% Al^{3+} (Fig. 5.4). However, the mechanical properties of the hydrogels tend to remain stable with the addition of more than 0.5 mol% Al^{3+}; in particular, within the 500% elongation, the stress–strain curves of Gel-0.5, Gel-1.0, and Gel-1.5 were almost coinciding. This phenomenon indicates that an excess of

Al^{3+} concentration has little effect on the mechanical properties of the hydrogel since most of the carboxyl groups in the PAA chain are maintain in the acid form (–COOH).
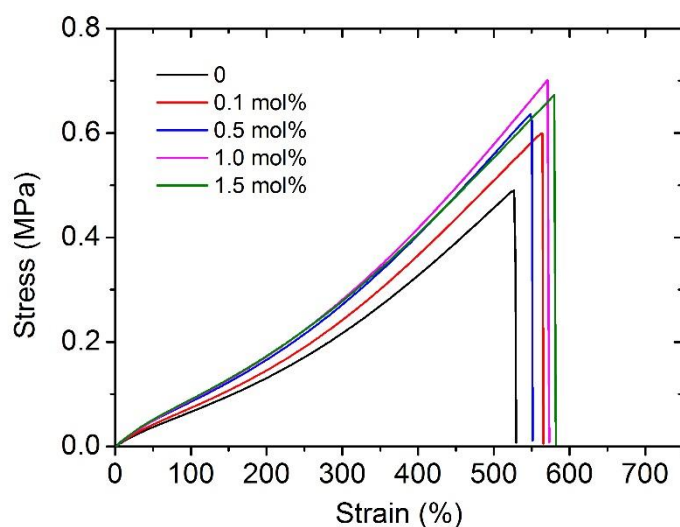

Fig. 5.4 Stress-strain curves of Gels with various Al^{3+} content.

The hydrogels prepared by visible-light-triggered polymerization possessed remarkable mechanical properties (*e.g.*, Gel-0.5, tensile strength of 0.66 MPa, strain of 550%, and elastic modulus of 0.106 MPa). However, Gel-0.5, as well as many reported hydrogels [26,27], showed a lower elastic modulus as compared to some synthetic hydrogels (*e.g.*, polyelectrolyte hydrogels) [28] or natural tissues (*e.g.*, cartilage) [29,30]. In this study, we applied the evaporation-swelling (E-S) method on the as-prepared Gel to achieve an approximately 10-fold increase in the elastic modulus of the hydrogel (Schematic 5.1). The mechanical properties of the as-prepared Gel underwent fundamental changes as a result of the restructuring of the hydrogel internal network. Fig. 5.5a shows that the E-S method-treated Gel (HM-Gel-0.5, air) reaches a high tensile strength and elastic modulus of 1.50 MPa and 0.96 MPa, respectively, which are 2.27 and 9 times higher than those of Gel-0.5. When the evaporation operation was conducted in vacuum, the HM-Gel-0.5 (vacuum) exhibited tensile strength (1.78 MPa) and elastic modulus (1.29 MPa) that were 2.70 and 12.2 times higher than those of Gel-0.5, respectively (Fig. 5.5a). Apparently, the HM-Gels dried in vacuum displayed a higher tensile strength and elastic modulus than the HM-Gels dried in air, whereas a lower fracture elongation was found in the HM-Gels dried in vacuum. (Table 5.1).

Table 5.1 Mechanical properties of HM-Gel at different evaporation conditions.

Hydrogel	Tensile strength (MPa)		Fracture elongation (%)		Elastic modulus (MPa)	
	Air	Vacuum	Air	Vacuum	Air	Vacuum
D-Gel-0	1.21±0.01	1.26±0.06	159.7±4.12	119.3±6.7	0.751±0.028	0.987±0.075
D-Gel-0.1	1.39±0.01	1.70±0.06	153.4±1.1	144±2.2	0.903±0.010	1.138±0.097
D-Gel-0.5	1.55±0.06	1.74±0.04	150.2±10.8	129.0±2.7	1.017±0.141	1.267±0.049
D-Gel-1.0	1.50±0.12	1.73±0.05	122.7±4.9	107.6±3.5	1.222±0.056	1.450±0.046
D-Gel-1.5	1.06±0.13	1.35±0.12	107.8±12.2	91.4±5.6	0.886±0.169	1.257±0.015

As shown in Fig. 5.5b, the evaporation temperature is a decisive factor for the mechanical performance of HM-Gels. When the evaporation proceeds at room temperature, the tensile strength and elastic modulus of HM-Gel-0.5 were only 1.24-fold and 1.83-fold, respectively, as compared to those of Gel-0.5. The tensile strength and elastic modulus of HM-Gel-0.5 dramatically increased with the increasing evaporation temperature, whereas the fracture elongation gradually decreased. This indicates that the evaporation temperature during the evaporation-swelling process is critical for the reconstruction of an internal network of the hydrogel. However, when Gel-0.5 was dried at 100 °C for 24 h, the degeneration of the CMC network resulted in a substantial impairment of the mechanical properties. In addition, the evaporation temperature in the E-S method has a substantial effect on the water content of the hydrogel after the swelling equilibrium is reached. The water content of the hydrogel decreased from 83.3 wt% to 66.5 wt% as the evaporation temperature increased (Fig. 5.5b, inset labels).

Although the concentration of Al^{3+} has a limited effect on the mechanical properties of the as-prepared hydrogels, it is noted that the mechanical properties of HM-Gels can be greatly changed *via* the introduction of Al^{3+}. The tensile strength increased to about 1.70 MPa upon increasing the Al^{3+} content from 0.1 mol% to 1.0 mol%, whereas the fracture elongation gradually decreased. However, a higher Al^{3+} content (1.5 mol%) could reduce the comprehensive mechanical properties of the HM-Gel (Fig. 5.5c). The

elastic modulus was calculated from the derivative of the stress–strain curves of the HM-Gels. At a strain of 30%, the elastic modulus of HM-Gels was in the range of 1.11–1.45 MPa, depending on the Al^{3+} content, which was higher than 0.91 MPa of HM-Gel without the reinforced cross-linking site (Al^{3+}). The elastic modulus of HM-Gel-1.0 was as high as 1.92 MPa at a strain of 60% (Fig. 5.5d). The results indicate that an increase in Al^{3+}content can improve the tensile strength and elastic modulus of the hydrogels, whereas the fracture elongation first increased and then decreased. However, the addition of excess Al^{3+} reduces the mechanical properties of the hydrogel.
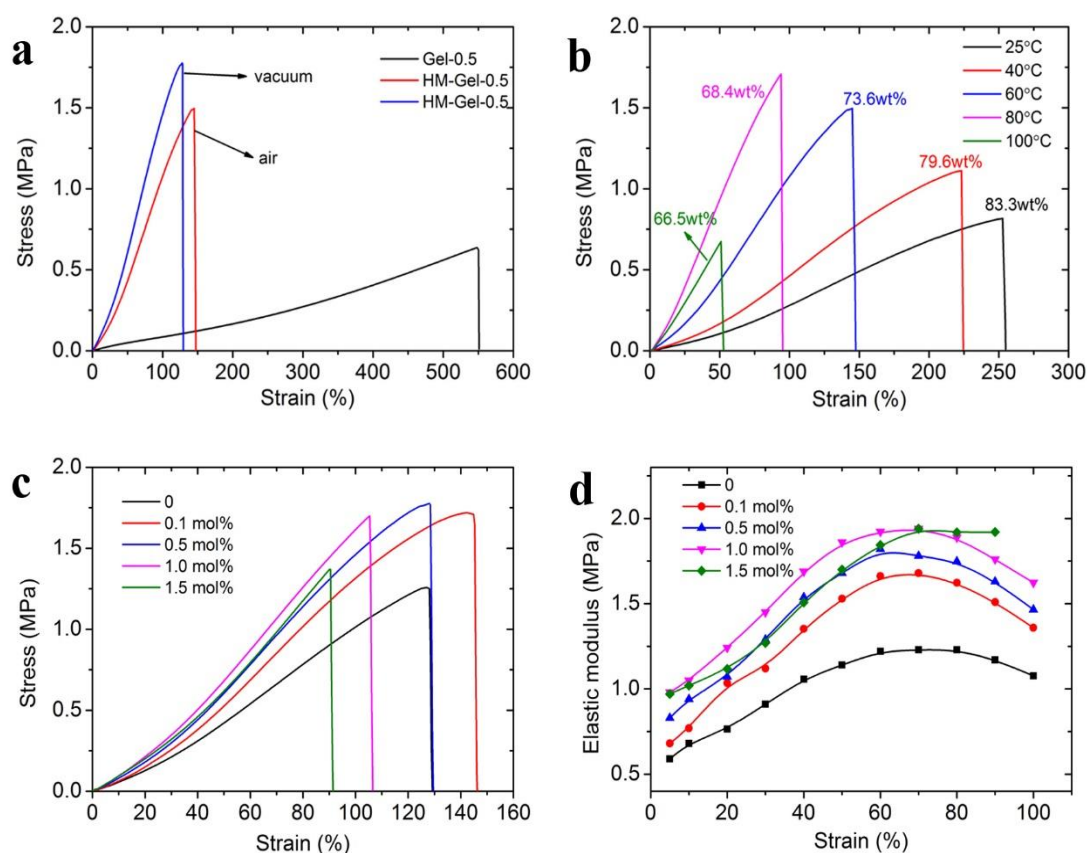
Fig. 5.5 a) Stress-strain curves of Gel-0.5, HM-Gel-0.5 (evaporation in air, 60 °C, red line; and evaporation in vacuum, 60 °C, blue line). b) Stress-strain curves of HM-Gel-0.5 under various evaporation temperature, the water content of equilibrium swelling hydrogel as labelled. c) Stress-strain curves of HM-Gels (evaporation in vacuum) with various Al^{3+} content. d) The elastic modulus of HM-Gels calculated from the derivative of the stress-strain curves of Fig. 5.5c.
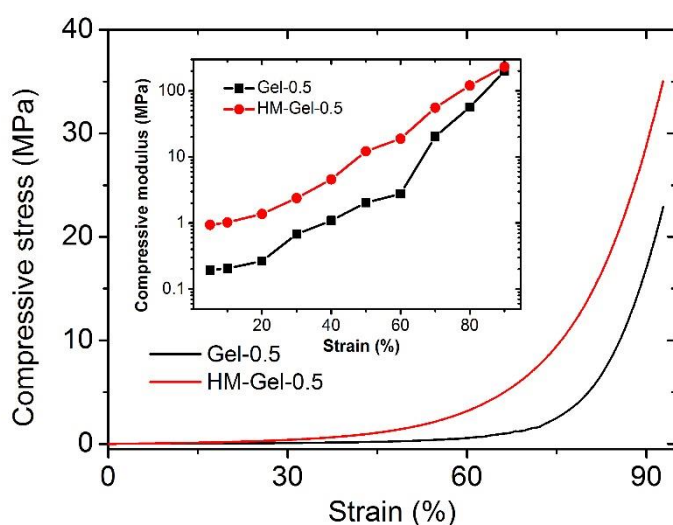
Fig. 5.6 Compressive stress-strain curves of Gel-0.5 and HM-Gel-0.5, the calculated compressive modulus is inserted in the Figure.

Both Gel and HM-Gel, like most tough hydrogels, are capable of withstanding large compressive stress [31]. Fig. 5.6 shows that the compressive stress of Gel-0.5 and HM-Gel-0.5 can reach 17.1 MPa and 28.8 MPa, respectively, at a compressive strain of 90%. HM-Gel-0.5 exhibited a higher compressive stress than other reported hydrogels under the same strain condition [26,32]. In the present study, the compressive modulus of HM-Gel-0.5 was always several times that of Gel-0.5, which should also be attributed to the recombination of the internal network structure of the hydrogel during the evaporation-swelling process.

5.3.3 Internal structure evolution

The conventional method for studying a hydrogel structure is to freeze-dry the hydrogel and then observe the pore structure of the hydrogel by an SEM [33]. Although the basic skeleton structure of the hydrogel after freeze-drying is retained, its fine structure changes (*e.g.* the hydrogel changes from transparent to white). To investigate the actual changes occurring in the internal network of the hydrogel during the evaporation-swelling process, thin films (200 μm) of these two kinds of hydrogel (Gel and HM-Gel) were obtained by shock-frozen section and observed using a polarized

106

optical microscope in the wet state. In this hydrogel, some of the CMC are present in the aggregated state (crystalline cellulose) rather than completely in the form of molecules. Therefore, although the hydrogel is transparent, the internal network is heterogeneous. Due to the polarization property of crystalline cellulose [34], we observed that a large amount of CMC was present in the form of crystals in the hydrogel (Fig. 5.7).
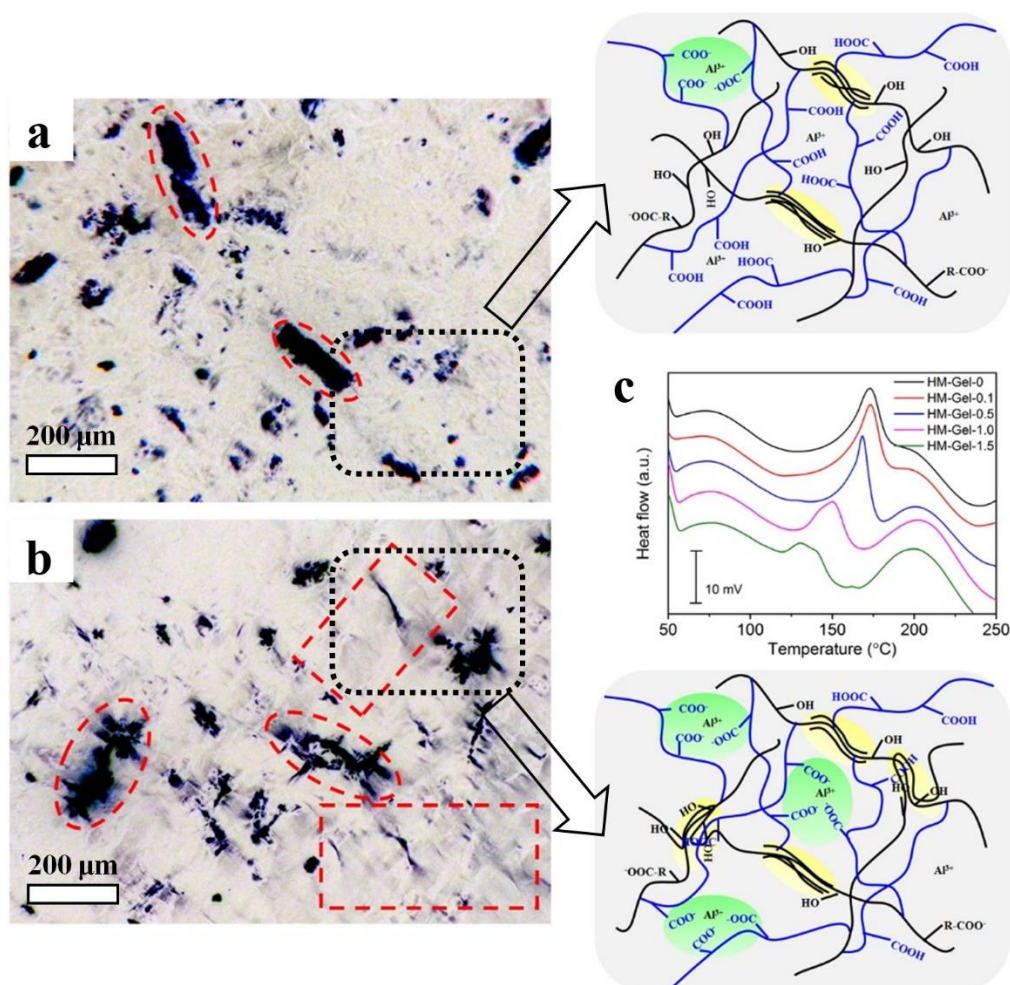

Fig. 5.7 a, b) Images of Gel-0.5 and HM-Gel-0.5 film in "wet" state under polarized light. The images are in negative mode for easy viewing. c) Effect of Al^{3+} content on DTA curves of HM-Gels.

In the as-prepared Gel (Fig. 5.7a), in addition to undissolved CMC chains exhibiting polarization property (black regions), the isolated CMC molecules involved in the polymerization reaction were not polarized (light-colored regions); this indicated that this CMC fraction was present in the non-crystalline form in the hydrogel. After the as-

prepared Gel was treated through the E-S method (Fig. 5.7b), the edges of the crystalline CMC became irregular and many shadows (crystalline) filled in the light-colored regions as compared to the image shown in Fig. 5.7a. This indicated that the CMC crystal morphology and crystallinity had undergone tremendous changes. The images show that the E-S method greatly changes the hydrogel internal network of the hydrogel and increases the network's cross-linking density. The FT-IR spectra (Fig. 5.8) showed that the absorption peaks of –COO–H in HM-Gel-0.5 were much stronger than those of PAA at 3000–3600 cm^{-1}, indicating both PAA chains and CMC chains were involved in this reinforcement crystallization. In addition, the attenuation of the absorption peak of 1240 cm^{-1} (–CO–OH) suggested that part of the carboxyl group and aluminum ion form more stable coordination compounds during this treatment process.
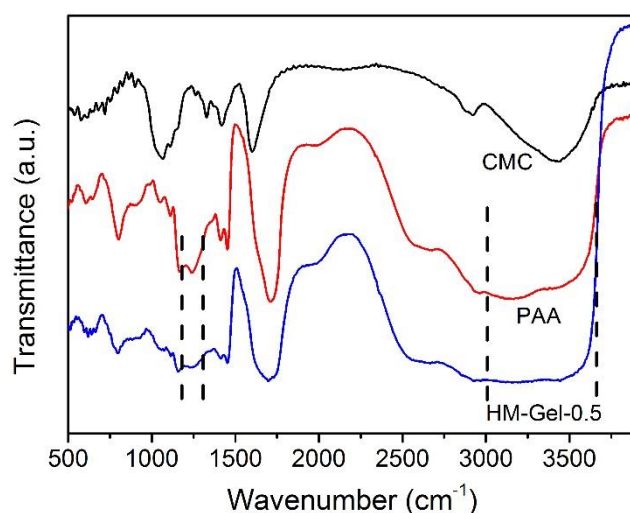

Fig. 5.8 FT-IR spectra of CMC, PAA and HM-Gel-0.5.

On the other hand, although the coordination bond could enhance the mechanical properties of the HM-Gel, the crystallinity of the HM-Gel was reduced. For example, an excessively high content of aluminum ions (as in HM-Gel-1.5) resulted in a very low crystallinity (the secondary crystallization region at only 75–130 °C), which led to a decrease in mechanical properties (Fig. 5.7c). The calculated effective network chain density (N) definitely confirmed that with the increase of Al^{3+} from 0 to 1 mol%, the N increased from 82 mol m^{-3} to 130 mol m^{-3}, whereas the excessively high amount of Al^{3+} led to the decrease of the N (Fig. 5.9) [35]. Therefore, by adjusting the content

of aluminum ions to control the crystallinity of the HM-Gel, the required mechanical properties can be achieved.
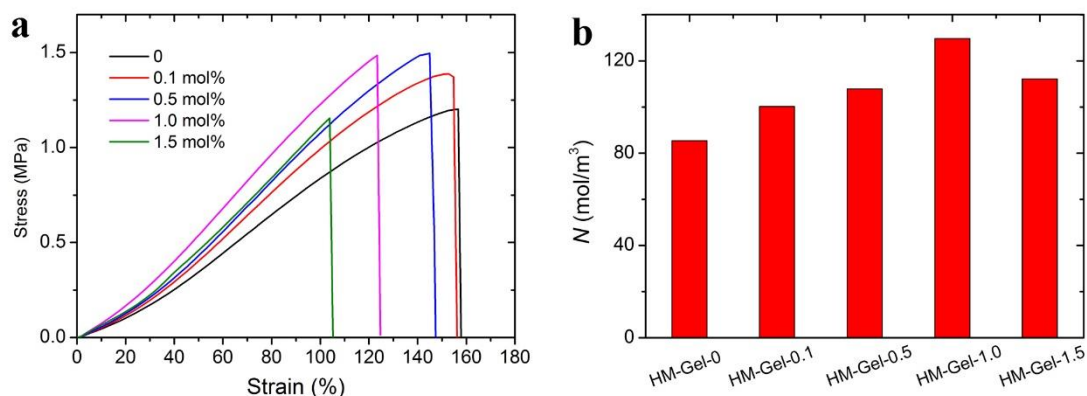

Fig. 5.9 a) Stress-strain curves of HM-Gels (evaporation in air) with various Al^{3+} content. b) Effective network chain density (N) of HM-Gel with various Al^{3+} content.

5.3.4 Swelling property
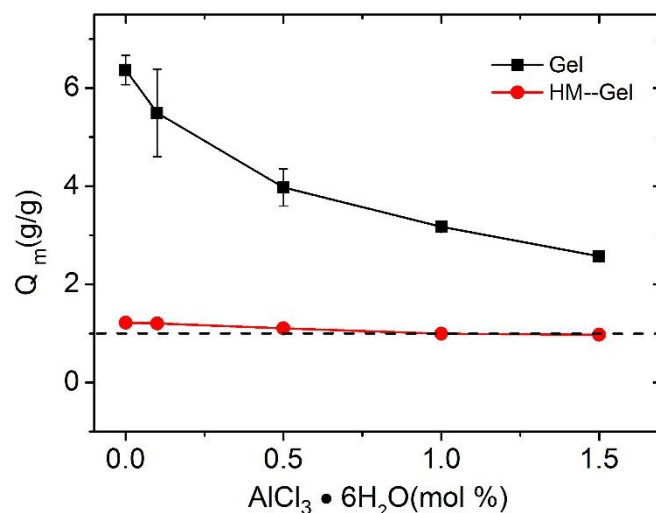
Fig. 5.10 Equilibrium swelling ratio (Q_m) of Gels and HM-Gels with various Al^{3+} contents.

Hydrogels, as soft and wet materials, consist of a cross-linked network and plenty of water (50–90%) and have been commonly used in aqueous environments [36,37]. The swelling behavior of hydrogels is very important for their practical applications [20]. The swelling ratio (Q_m) of Gels decreased from 6.37 to 2.57 with the increase of Al^{3+} content. In sharp contrast, the Q_m of HM-Gels slightly changed from 1.22 to 0.97

in the same composition (Fig. 5.10). This large difference in the swelling ratios indicates that the crystallization induced by the E-S method severely hinders the swelling of the hydrophilic polymer network in distilled water.

5.3.5 Viscoelasticity of the hydrogels

In Fig. 5.11, the storage modulus E' and $\tan \delta$ are shown for the as-prepared Gels and HM-Gels as functions of frequency at a strain of 1.0%.
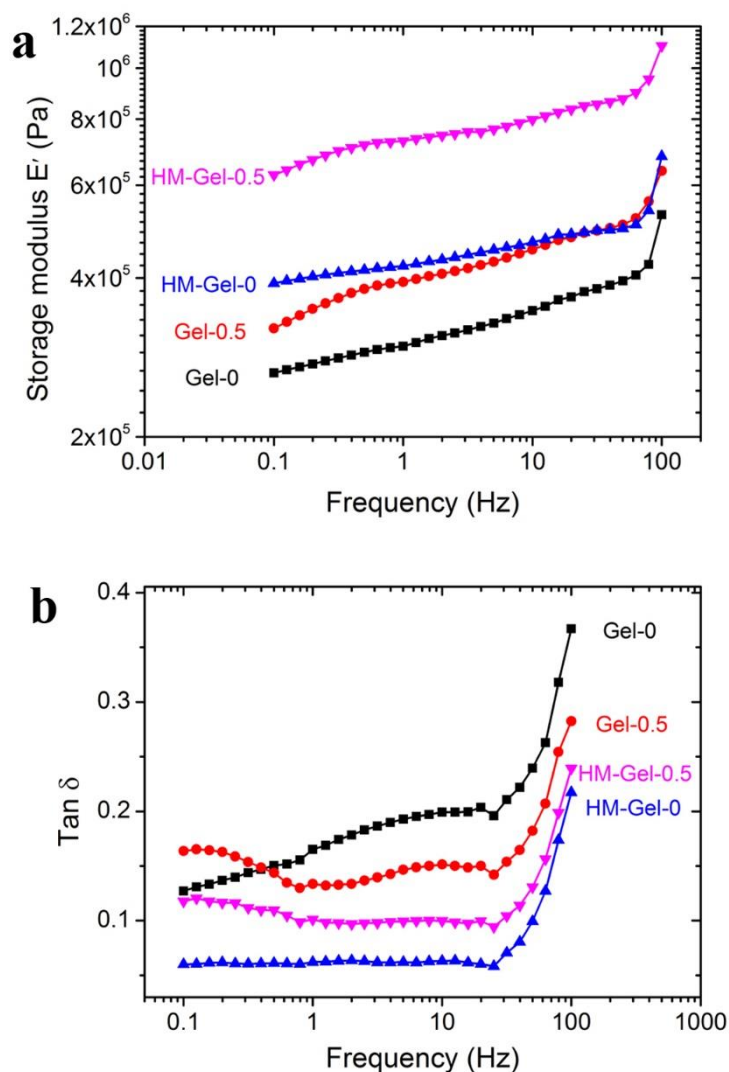

Fig. 5.11 Dynamic mechanical analysis of hydrogels. a) Storage modulus (E'), b) Tan δ (damping factor) of Gel-0, HM-Gel-0 and Gel-0.5, HM-Gel-0.5.

The E' of all hydrogels increased as the frequency increased. Gel-0.5 had a higher E' than Gel-0 in the experimental frequency range; this suggested that the newly

formed cross-linking site could increase the cross-linking network density by introducing Al^{3+} [38]. The enhanced effect of Al^{3+} also occurred in HM-Gel, and the $\Delta E'$ ($E'_{Gel-0.5} - E'_{Gel-0}$, and $E'_{HM-Gel-0.5} - E'_{HM-Gel-0}$) increased from 100 kPa of Gel to more than 200 kPa of HM-Gel at the frequency of 0.1–100 Hz. These results confirm that the ions generated more coordination compounds, which increased the density of the cross-linked network during the evaporation-swelling process. The E' of the hydrogels with the same components (*i.e.*, Gel-0 and HM-Gel-0 and Gel-0.5 and HM-Gel-0.5) were also different before and after the evaporation-swelling treatment. The increased E' indicates that the hydrogen bond recombination inside the hydrogel not only changes the structure of the cross-linked network, but also increases the cross-linking density of the network. The damping factor (tan δ) is determined by the storage modulus and loss modulus ratio [39].

Unlike the storage modulus, the tan δ value of hydrogels with the same composition was reduced before and after treatment *via* the E-S method; this may be because the increased cross-linking density limited the movement of partial polymer chains. The tan δ value of all hydrogels showed a clear critical frequency at approximately 25 Hz (Fig. 5.11b and Fig. 5.12) and increased rapidly as the frequency increased; this indicated that the energy dissipation caused by intermolecular friction was proportional to the frequency. For the hydrogel without Al^{3+}, the tan δ value of HM-Gel-0 was significantly lower than that of Gel-0 after evaporation-swelling treatment. However, with the introduction of a certain amount of Al^{3+} into the hydrogel, the decrease in tan δ value of the hydrogel containing Al^{3+} before and after the evaporation-swelling treatment was significantly smaller than that of the aluminum-free hydrogel. Interestingly, the tan δ of Gel-0.5 and HM-Gel-0.5 had another critical frequency (approximately 1 Hz); this phenomenon could also be observed in the hydrogel with a higher Al^{3+} content (over 0.5 mol% Al^{3+}, Fig. 5.12). This change in the frequency response may be due to the rupture of ionic bonds within the hydrogel containing Al^{3+}. Therefore, the damping characteristic of hydrogels contributes to their potential application in the field of vibration absorption.
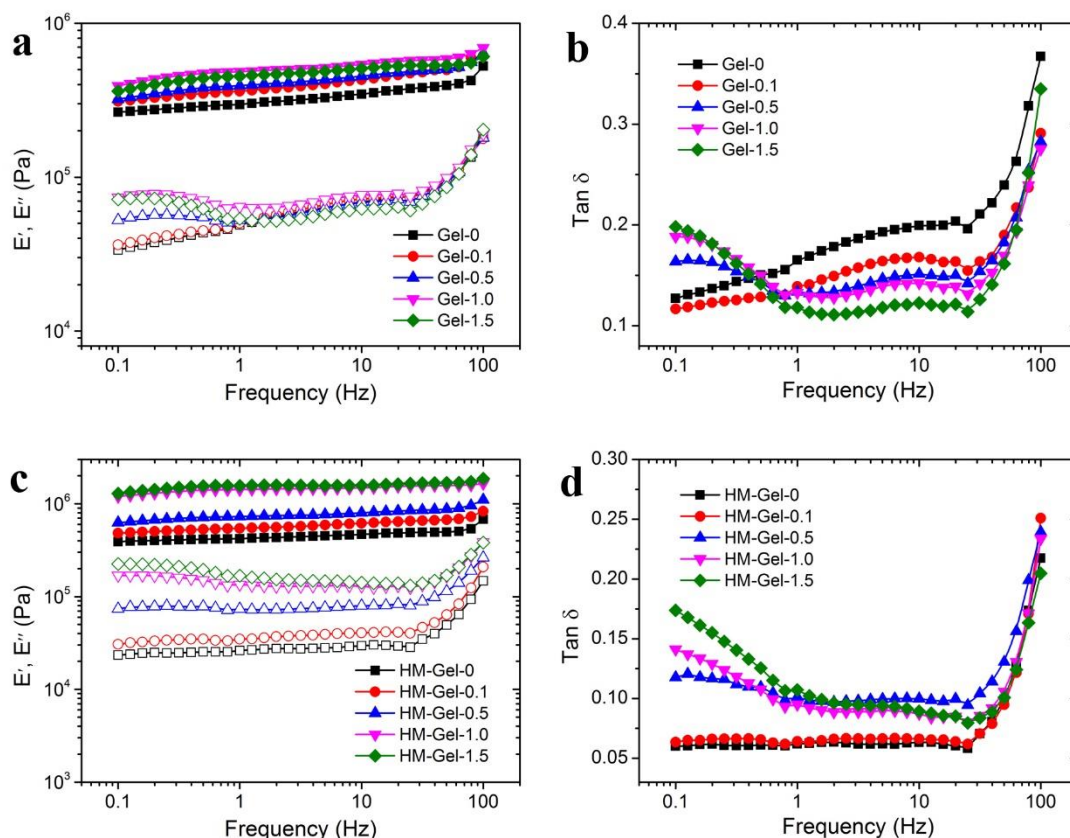
Fig. 5.12 Dynamic mechanical analysis of Gel and HM-Gel. a) Storage modulus (E') and loss modulus (E''); b) Tan δ of Gel with various Al^{3+} content. c) Storage modulus (E') and loss modulus (E''); d) Tan δ of HM-Gel with various Al^{3+} content.

5.3.6 Cyclic mechanical property

The HM-Gel exhibited excellent tensile and compressive properties during successive cyclic process. Fig. 5.13a shows that the HM-Gel-0.5 has basic stable stress–time curves. However, it should be noted that the maximum stress for HM-Gel-0.5 slightly decreased from 0.56 MPa at an initial time and then trended to remain unchanged at 0.50 MPa. This may be due to the fact that during the stretching process, the hydrogel network obtained by free radical polymerization generally undergoes rupture and sliding of the polymer chains as well as rupture of ionic and hydrogen bonds, according to a previous study [16]. In addition, the slight sliding between the hydrogel and the fixture also contributes to decreasing the maximum stress [40]. After the stretched hydrogel was stored at room temperature for 24 hours in a sealed and humid

environment, the sample exhibited very similar stress–time curves to the previous curves. The similarity between the curves indicated that the ionic and hydrogen bonds in the Gel were substantially healed [41]. The only non-coincident part was the curve of the first loading process, confirming that the irreversible rupture and permanent sliding of the partial polymer chains only occurred during the first stretching process [16].
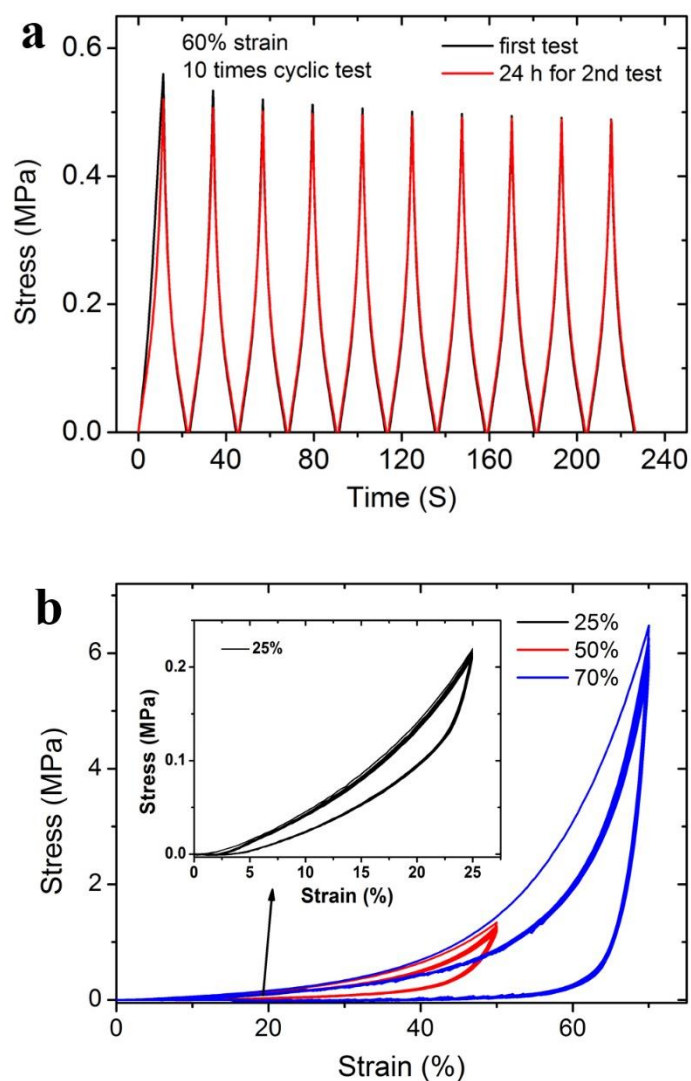

Fig. 5.13 a) Cyclic tensile tests of HM-Gel-0.5 for 10 times at a strain of 60%, and perform the same operation after 24 h. b) Cyclic compressive tests of HM-Gel-0.5 for 10 times at various strain.

Fig. 5.13b shows the cyclic compression curves obtained after 10 successive tests at various strains. At a lower strain (less than 25%), the compression loading–unloading

curves were always consistent; this indicated that the internal network structure of HM-Gel-0.5 was retained. However, as the compressive strain increases, the network structure of HM-Gel-0.5 changes. At a strain of 50% and 70%, the curves of the second cycle were inconsistent with those of the first cycle; this suggested that a large deformation may cause irreversible damage to the network structure. At a strain of 25%, 50%, and 70% (from the second cycle), the hydrogels displayed a stable hysteresis energy dissipation, which resulted from the rupture of ionic and hydrogen bonds and the friction between polymer chains. Thus, the HM-Gel is a suitable candidate for vibration absorption materials.

5.3.7 Vibration absorption of the hydrogel

To verify the actual vibration absorption effect of the hydrogel, we tested the vibrational absorption of the hydrogel (HM-Gel-0.5) using the commercial test tube mixer (Present Mixer 2013, remove the spring bracket, Fig. 5.14). The test tube mixer was vigorously vibrated on a metal plate and submitted to a large displacement without any cushioning. When the test tube mixer was placed on the hydrogel, the machine was able to operate stably on the hydrogel after it experienced a partial initial displacement (caused by resonance). Thus, the hydrogel was able to efficiently absorb the vibration and stabilize the test tube mixer. The detected vibration forces of Gel and HM-Gel were 1.4 N and 0.6 N, respectively, which were lower than the vibration force of the machine without a vibration damper (8.5 N). In a vibration absorption material, stiffness is an important performance index, and a high stiffness can improve the material's vibration absorption performance [8,42].

The stiffness is defined as

$$k = \frac{F}{\delta} \quad \text{or} \quad k = \frac{AE}{L} \tag{5-2}$$

Where F is the force on the body, δ is the displacement along the force, A is the cross-sectional area, E is the elastic modulus, and L is the length of the element.
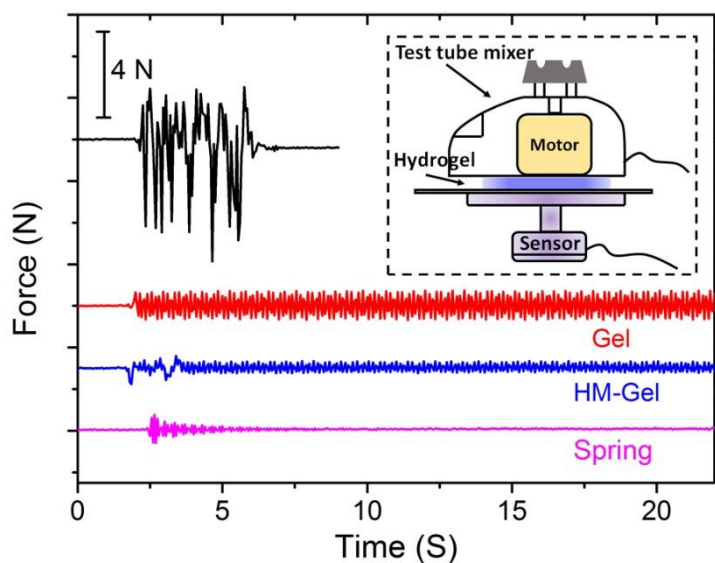
Fig. 5.14 Comparison of vibration absorption effect obtained with different vibration damper in free mode.

For the specific case of an unconstrained uniaxial tension or compression, the elastic modulus can be thought of as a measure of the stiffness of a structure. Thus, the high-modulus hydrogel (HM-Gel-0.5, with an elastic modulus of approximately 1 MPa), obtained by the E-S method, can withstand a greater load under the unit strain than the low-modulus hydrogel (Gel-0.5, with an elastic modulus of approximately 0.1 MPa) and showed a better vibration absorption performance (Fig. 5.14). Of course, the metal spring bracket displayed the best vibration absorption.

5.4 Conclusions

In summary, we first synthesized a hydrogel (Gel) with good mechanical properties *via* a visible-light-trigger polymerization. To increase the modulus of the hydrogel, such that this can be applied as vibration absorption material, we leveraged the hydrogen bonds in the hydrogel to induce a CMC crystallization to alter the network structure within the hydrogel *via* the E-S method. The obtained optimal HM-Gel possessed an excellent mechanical properties with tensile strength and elastic modulus of 1.55 MPa and 1.02 MPa, respectively. Furthermore, different evaporation temperatures and the added various aluminum ion concentration have an extremely

important effect on the tensile strength, modulus, and swelling ratio of the hydrogel. The coordination bonds formed by aluminum ions and anionic polymers increased the damping in the hydrogel during vibration, thus improving the vibration absorption performance of the hydrogel. In addition, HM-Gel-0.5 exhibited stable mechanical properties in both the cyclic tensile and compression tests. The preliminary application experiment shows that the high-modulus hydrogel has a better vibration absorption effect than the low-modulus hydrogel. We hope that this design concept can enhance the modulus of more hydrogels containing hydrogen bonds, such that these hydrogels can be used not only as machinery vibration absorbers but also as biological vibration absorbers (for example: articular cartilage).

References

[1] Dragan ES. Design and applications of interpenetrating polymer network hydrogels. A review. Chemical Engineering Journal. 2014;243:572-90.

[2] Zhao X. Multi-scale multi-mechanism design of tough hydrogels: building dissipation into stretchy networks. Soft Matter. 2014;10(5):672-87.

[3] Nonoyama T, Wada S, Kiyama R, Kitamura N, Mredha MT, Zhang X, et al. Double-Network Hydrogels Strongly Bondable to Bones by Spontaneous Osteogenesis Penetration. Advanced materials. 2016;28(31):6740-5.

[4] Hopkins AM, De Laporte L, Tortelli F, Spedden E, Staii C, Atherton TJ, et al. Silk Hydrogels as Soft Substrates for Neural Tissue Engineering. Advanced Functional Materials. 2013;23(41):5140-9.

[5] Huang W, Tarakanova A, Dinjaski N, Wang Q, Xia X, Chen Y, et al. Design of Multistimuli Responsive Hydrogels Using Integrated Modeling and Genetically Engineered Silk-Elastin-Like Proteins. Advanced Functional Materials. 2016;26(23):4113-23.

[6] Costa AMS, Mano JF. Extremely strong and tough hydrogels as prospective candidates for tissue repair – A review. European Polymer Journal. 2015;72:344-64.

[7] Lv S, Dudek DM, Cao Y, Balamurali MM, Gosline J, Li H. Designed biomaterials to mimic the mechanical properties of muscles. Nature. 2010;465(7294):69-73.

[8] Chung DDL. Materials for vibration damping. Journal of Materials Science. 2001;36(24):5733-7.

[9] Gao G, Du G, Sun Y, Fu J. Self-healable, tough, and ultrastretchable nanocomposite hydrogels based on reversible polyacrylamide/montmorillonite adsorption. ACS applied materials & interfaces. 2015;7(8):5029-37.

[10] Liu S, Li L. Recoverable and Self-Healing Double Network Hydrogel Based on kappa-Carrageenan. ACS applied materials & interfaces. 2016;8(43):29749-58.

[11] Peak CW, Wilker JJ, Schmidt G. A review on tough and sticky hydrogels. Colloid and Polymer Science. 2013;291(9):2031-47.

[12] Sun TL, Kurokawa T, Kuroda S, Ihsan AB, Akasaki T, Sato K, et al. Physical hydrogels composed of polyampholytes demonstrate high toughness and viscoelasticity. Nature materials. 2013;12(10):932-7.

[13] Lin P, Ma S, Wang X, Zhou F. Molecularly engineered dual-crosslinked hydrogel with ultrahigh mechanical strength, toughness, and good self-recovery. Advanced materials. 2015;27(12):2054-9.

[14] Yang Y, Wang X, Yang F, Shen H, Wu D. A Universal Soaking Strategy to Convert Composite Hydrogels into Extremely Tough and Rapidly Recoverable Double-Network Hydrogels. Advanced materials. 2016;28(33):7178-84.

[15] Zhu L, Qiu J, Sakai E, Zang L, Yu Y, Ito K, et al. Design of a Rubbery Carboxymethyl Cellulose/Polyacrylic Acid Hydrogel via Visible-Light-Triggered Polymerization. Macromolecular Materials and Engineering. 2017:1600509.

[16] Zhu L, Qiu J, Sakai E, Ito K. Rapid Recovery Double Cross-Linking Hydrogel with Stable Mechanical Properties and High Resilience Triggered by Visible Light. ACS applied materials & interfaces. 2017;9(15):13593-601.

[17] Treat NJ, Fors BP, Kramer JW, Christianson M, Chiu C-Y, Read de Alaniz J, et al. Controlled Radical Polymerization of Acrylates Regulated by Visible Light. ACS Macro Letters. 2014;3(6):580-4.

[18] Dai X, Zhang Y, Gao L, Bai T, Wang W, Cui Y, et al. A Mechanically Strong, Highly Stable, Thermoplastic, and Self-Healable Supramolecular Polymer Hydrogel. Advanced materials. 2015;27(23):3566-71.

[19] Fakhru L, Razi A, Qudsieh IY, Yunus WMZW, Ahmad MB, Rahman MZA. Graft copolymerization of methyl methacrylate onto sago starch using ceric ammonium nitrate and potassium persulfate as redox initiator systems. Journal of applied polymer science. 2001;82(6):1375-81.

[20] Kamata H, Akagi Y, Kayasuga-Kariya Y, Chung UI, Sakai T. "Nonswellable" hydrogel without mechanical hysteresis. Science. 2014;343(6173):873-5.

[21] Luo F, Sun TL, Nakajima T, Kurokawa T, Zhao Y, Sato K, et al. Oppositely charged polyelectrolytes form tough, self-healing, and rebuildable hydrogels. Advanced materials. 2015;27(17):2722-7.

118

[22] Guo M, Pitet LM, Wyss HM, Vos M, Dankers PY, Meijer EW. Tough stimuli-responsive supramolecular hydrogels with hydrogen-bonding network junctions. Journal of the American Chemical Society. 2014;136(19):6969-77.

[23] Zheng WJ, An N, Yang JH, Zhou J, Chen YM. Tough Al-alginate/poly(N-isopropylacrylamide) hydrogel with tunable LCST for soft robotics. ACS applied materials & interfaces. 2015;7(3):1758-64.

[24] Yang CH, Wang MX, Haider H, Yang JH, Sun JY, Chen YM, et al. Strengthening alginate/polyacrylamide hydrogels using various multivalent cations. ACS applied materials & interfaces. 2013;5(21):10418-22.

[25] Sun JY, Zhao X, Illeperuma WR, Chaudhuri O, Oh KH, Mooney DJ, et al. Highly stretchable and tough hydrogels. Nature. 2012;489(7414):133-6.

[26] Chen Q, Zhu L, Zhao C, Wang Q, Zheng J. A robust, one-pot synthesis of highly mechanical and recoverable double network hydrogels using thermoreversible sol-gel polysaccharide. Advanced materials. 2013;25(30):4171-6.

[27] Fitzgerald MM, Bootsma K, Berberich JA, Sparks JL. Tunable stress relaxation behavior of an alginate-polyacrylamide hydrogel: comparison with muscle tissue. Biomacromolecules. 2015;16(5):1497-505.

[28] You J, Xie S, Cao J, Ge H, Xu M, Zhang L, et al. Quaternized Chitosan/Poly(acrylic acid) Polyelectrolyte Complex Hydrogels with Tough, Self-Recovery, and Tunable Mechanical Properties. Macromolecules. 2016;49(3):1049-59.

[29] Pal S. Mechanical Properties of Biological Materials. 2014:23-40.

[30] Wang Z, Tao F, Pan Q. A self-healable polyvinyl alcohol-based hydrogel electrolyte for smart electrochemical capacitors. J Mater Chem A. 2016;4(45):17732-9.

[31] Du G, Nie L, Gao G, Sun Y, Hou R, Zhang H, et al. Tough and biocompatible hydrogels based on in situ interpenetrating networks of dithiol-connected graphene oxide and poly(vinyl alcohol). ACS applied materials & interfaces. 2015;7(5):3003-8.

[32] Duan J, Liang X, Cao Y, Wang S, Zhang L. High Strength Chitosan Hydrogels with Biocompatibility via New Avenue Based on Constructing Nanofibrous Architecture. Macromolecules. 2015;48(8):2706-14.

[33] Fang J, Mehlich A, Koga N, Huang J, Koga R, Gao X, et al. Forced protein unfolding leads to highly elastic and tough protein hydrogels. Nature communications. 2013;4:2974.

[34] Moon RJ, Martini A, Nairn J, Simonsen J, Youngblood J. Cellulose nanomaterials review: structure, properties and nanocomposites. Chemical Society reviews. 2011;40(7):3941-94.

[35] Yang J, Han CR, Duan JF, Xu F, Sun RC. Mechanical and viscoelastic properties of cellulose nanocrystals reinforced poly(ethylene glycol) nanocomposite hydrogels. ACS applied materials & interfaces. 2013;5(8):3199-207.

[36] Pina S, Oliveira JM, Reis RL. Natural-based nanocomposites for bone tissue engineering and regenerative medicine: a review. Advanced materials. 2015;27(7):1143-69.

[37] Kim J, Conway A, Chauhan A. Extended delivery of ophthalmic drugs by silicone hydrogel contact lenses. Biomaterials. 2008;29(14):2259-69.

[38] Cai Z, Kwak DH, Punihaole D, Hong Z, Velankar SS, Liu X, et al. A Photonic Crystal Protein Hydrogel Sensor for Candida albicans. Angewandte Chemie. 2015;54(44):13036-40.

[39] Shanmugam D, Thiruchitrambalam M. Static and dynamic mechanical properties of alkali treated unidirectional continuous Palmyra Palm Leaf Stalk Fiber/jute fiber reinforced hybrid polyester composites. Materials & Design. 2013;50:533-42.

[40] Lillie M, Chalmers G, Gosline J. The effects of heating on the mechanical properties of arterial elastin. Connective tissue research. 1994;31(1):23-35.

[41] Zhong M, Liu XY, Shi FK, Zhang LQ, Wang XP, Cheetham AG, et al. Self-healable, tough and highly stretchable ionic nanocomposite physical hydrogels. Soft Matter. 2015;11(21):4235-41.

[42] Lakes R. High damping composite materials: effect of structural hierarchy. Journal of composite materials. 2002;36(3):287-97.

Chapter 6 Thermal Stability Cellulose Nanofiber/Polyvinyl Alcohol Hydrogel Synthesized via Aldolization Using Aldehyde Cellulose Nanofiber as Cross-linker

6.1 Introduction

Soft and wet hydrogels usually composed of three-dimensional polymer network structure and a large amount of water (50 ~ 99%) inside the network structure [1, 2]. Hydrogels can usually be divided into natural polymer hydrogels, synthetic polymer hydrogels, and natural-synthetic polymer hydrogels. It is widely used in biomedical application due to its physical properties similar to natural tissue and excellent biocompatibility [3-5].

Polyvinyl alcohol (PVA) is a linear synthetic polymer obtained from partial or full hydrolysis of polyvinyl acetate. The resulting PVA exhibits a high degree of water solubility, but resistant to most organic solvents [6]. Due to its water solubility, it is usually necessary to introduce a cross-linking network in the PVA polymer solution to form a hydrogel for use in several applications. The strategies of preparation PVA hydrogel usually including irradiation [7], cyclic freezing-thawing [8, 9] and chemical reaction [10, 11]. PVA hydrogel is widely used as a commercial product in the field of biomedical, such as contact lenses [12, 13], wound dressing [14, 15], and implantable medical materials [16], due to its nontoxic, biocompatibility, bio-adhesive and high chemical resistance [17].

Freeze-thaw technology is the most common cross-linking method for the preparation of PVA hydrogel [9]. The molecular motion of the aqueous solution can be fixed by van der waals forces and/or hydrogen bonds, and some molecular segments in

a certain region can form an ordered structure. When re-frozen, more new ordered micro-domain is generated. These closely bound ordered domains are no longer separated. The hydrogel prepared by this method can have good mechanical strength at higher water content. However, the PVA hydrogel formed by hydrogen bonding has thermal instability. Hydrogel as a biomedical material (e.g. wound dressing) require severe sterilization before use. In our previous experiment, the PVA hydrogel prepared by freeze-thaw method was completely decomposed when using conventional autoclave sterilization. Since sterilization is an integral part of modern medical care, the thermal instability may be a defect of the synthesized PVA hydrogel with physical cross-linking. It is reported that chemical cross-linking of linear polymers may provide feasible routes for the improvement of the mechanical properties and thermal stability [18, 19]. Therefore, a thermally stable PVA hydrogel may be obtained by chemical cross-linking.

In this work, cellulose nanofiber (CNF) was used as cross-linker to prepare chemical cross-linking PVA hydrogel. First, to increase the reactivity of the CNF, dialdehyde cellulose nanofiber is prepared by using sodium periodate as the oxidant. Then, the modified cellulose reacted with PVA at 80 °C under acidic condition through aldolization to obtain the hydrogel. At last, the CNF/PVA hydrogel was reinforced through evaporation-swelling method according to our previous study [20]. The oxidation degree of CNF has a significant effect on the activity of the acetal reaction, resulting in the mechanical properties and water content of the hydrogel are significantly different. The hydrogel shows excellent thermal stability, which enhanced its application in the field of biomedical, especially wound dressing.

6.2 Materials and methods

6.2.1 Materials

Cellulose nanofiber (CNF) purchased from Mori Machinery Corporation, Japan. Sodium periodate ($NaIO_4$) was obtained by Wako Pure Chemical Industries, Ltd.

Polyvinyl alcohol (PVA) and Nitric acid (HNO_3) provided by Nacalai Tesque, Inc. All of the chemical reagents were used as-received. Distilled water was used in all experiments.

6.2.2 Oxidation of cellulose nanofibers

40 g starchiness cellulose nanofiber (CNF, 5 wt% solid content) and 60 mL distilled water were added to 250 mL conical flask. The mixture was magnetically stirred for 10 minutes to disperse the CNF. Then a certain amount of $NaIO_4$ (12.5, 25, 37.5 and 50 wt%, $NaIO_4$ to CNF) was added into the conical flask, the mixture was magnetically stirred for 48 h under a dark environment. The oxidation products were separated by centrifugation and washing with distilled water for three times to remove the excess raw materials and reduced impurity ions. The number of the product is shown in Table 6.1.

Table 6.1 The oxidation condition of CNF

	CNF[a] (g)	$NaIO_4$ (g)	H_2O (mL)
CNF-1	2	0.25	60
CNF-2	2	0.50	60
CNF-3	2	0.75	60
CNF-4	2	1.00	60

[a]The weight of CNF is the solid content.

6.2.3 Synthesis of the hydrogel

0.60 g of the oxide-CNF (CNF-1, CNF-2, CNF-3, and CNF-4) and 2 g PVA were dispersed into 30 mL water. The mixture was magnetically stirred for 1 h at 95 °C to ensure that the PVA dissolved completely and the CNF homogeneous dispersed. 5 drops of 0.5 M HNO_3 were added as a catalyst to the mixture after it was cooled to 60 °C. The hydrogel precursor was transferred into a sealed transparent mold after it was stirred for 10 min. Finally, the mold was placed in an oven at 80 °C for 24 h. As a

comparison, CNF/PVA having the same components with CNF-3/PVA also be prepared.

The evaporation-swelling method was used to reinforce the mechanical performance of the hydrogel. In brief, the hydrogel was evaporation at 40 °C in electrical blast drying oven for 24 h. After that, the CNF/PVA hydrogel was obtained after the dried hydrogel was swollen in distilled water for 60 h.

6.2.4 Characterizations

A Thermo Scientific Nicolet iN 10 infrared spectrometer was used for the analysis of FT-IR. The sample was measured in the range of $650 - 4000$ cm^{-1} with a resolution of 4 cm^{-1}. Both KBr pellet and ATR technique were adopted in the test. A total of 32 scans were accumulated.

The crystallographic structure of samples was obtained by X-ray diffraction system with a diffractometer (XRD 6000, Shimadzu Corporation, Japan) in range of 5~90° by step scanning. Nickel-filter Cu Kα radiation (λ=0.15417 nm) was used with a generator voltage of 40 kV and a current of 30 mA.

Thermal gravimetric analyzer (TGA) and Differential Thermal Analysis (DTA) of the samples were performed with TG instrument (DTG-60, Shimadzu Co., Ltd., Kyoto, Japan) at a scan rate of 10 °C min^{-1} from room temperature to 600 °C in N$_2$ atmosphere (flow rate of 50 mL/min). Sample (4-6 mg) were placed in aluminum crucibles by using an empty aluminum crucible as a reference. All of the samples were obtained from freeze-drying.

The morphologies of samples were characterized by SEM (S-4300, Hitachi Co., Ltd., Tokyo, Japan). Both CNF and CNF/PVA hydrogel samples were prepared through freeze-drying method. The sample was sputter-coated by gold with Ion sputter (E-1030, Hitachi Co., Ltd., Tokyo, Japan) for 3 or 5 min to provide enhanced conductivity before the test. The test voltage was 3 or 5 kV, and electric current was 10 μA.

The uniaxial elongation properties were carried out on a universal testing machine (Instron 3350 series, 50 N load cell, Instron Co., Ltd., Canton, America) and the measurement conditions were as follows: hydrogels were cut into the rectangle with the

size of length 50 mm (l), gauge length 30 mm (l_o), width 10 mm (w) and height 0.5-1 mm (h), and tests were conducted at a cross-head speed of 500 mm/min. The cyclic compressive properties were measured using the same universal testing machine at a cross-head speed of 1 mm/min. Hydrogels were cut into disc shapes with a diameter 9 mm and height of 2.5 mm.

6.3 Results and discussions

6.3.1 Oxidation of CNF

Scheme 6.1 (a) Cellulose nanofiber oxidation. (b) Gelation process of PVA and aldehyde cellulose by aldolization.

Sodium periodate has a high selectivity for the oxidation of cellulose. This reaction breaks the C2-C3 bond of the glucopyranoside ring and produces two aldehyde groups at the C2 and C3 positions (Scheme 6.1a) [21]. The oxidation of CNF was carried out in a dark surrounding to prevent the degradation of $NaIO_4$, and the oxidation time was chosen for 48 h to achieve a higher degree of oxidation. FT-IR spectra show that the peak intensity at 1060 cm^{-1} and 1130 cm^{-1} gradually decreases, indicating that the amount of hydroxyl groups in CNF decreases with increasing the $NaIO_4$ content. In addition, the peak at 1160 cm^{-1} is the stretching vibration of C2-C3, the peak intensity decreases gradually, indicating that more C2-C3 bonds are oxidized with the number of

oxidant increases (Fig. 6.1a) [22]. The increase of NaIO$_4$ during the oxidation process of CNF resulted in a corresponding increase in carbonyl content. As shown in Fig. 6.1b, the stretching vibration peak at 1730 cm^{-1} confirms the aldehyde is formed on the cellulose surface. The C–OH group convert into –CHO on the surface of oxidized CNF, which obviously decrease the hydrophilic property of CNF. As shown in Fig. 6.2, the stability of the oxidized CNF in water decreases as the NaIO$_4$ content increases.
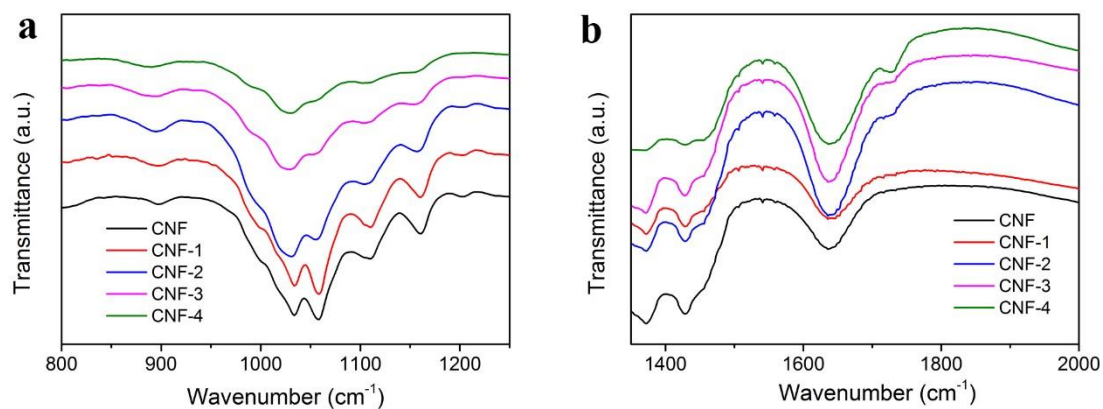
Fig. 6.1 FT-IR spectra of CNF and oxidized CNF. (a) Characterized by ATR. (b) Characterized by KBr pellet.
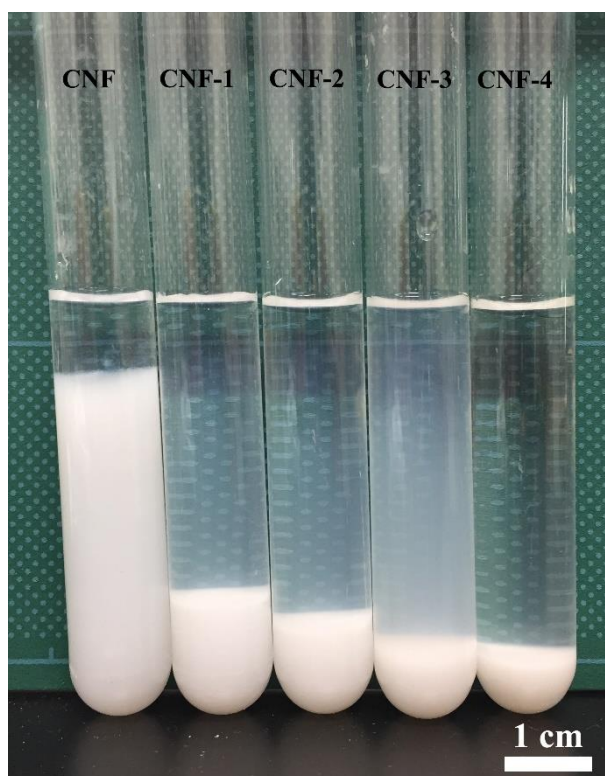
Fig. 6.2 Digital image of 0.15 wt.% CNF and oxidized CNF suspension after settlement for 7 days.
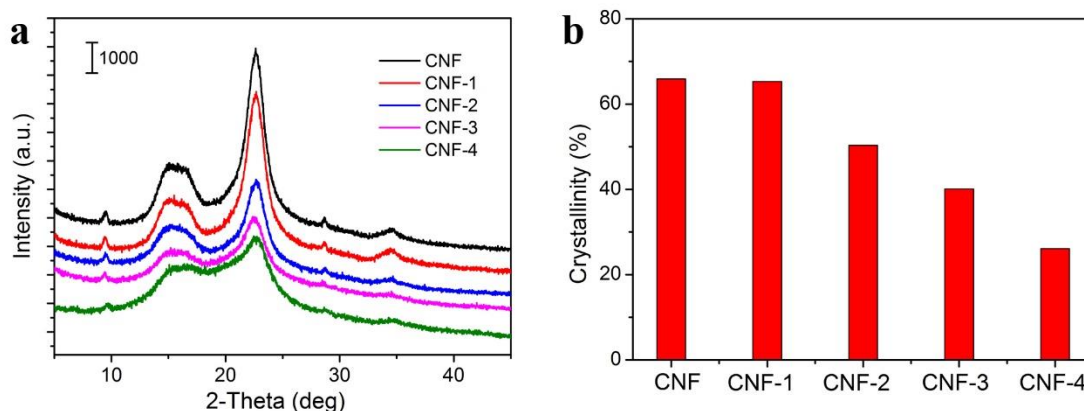
Fig. 6.3 (a) XRD of CNF and oxidation CNF. (b) The crystallinity of CNF and oxidation CNF.

As illustrated in Fig. 6.3a, the crystallographic diffraction peaks of CNF at about 2θ = 22.7° for the (002) plane, 34.5° for the (040) plane gradually weakened with the increase of $NaIO_4$ content [23]. The crystallinity of the oxidized CNF is calculated according to Segal method [24], the equation as follows:

$$x_{CR}\% = \frac{I_{200} - I_{AM}}{I_{200}} \times 100\% \quad (6\text{-}1)$$

Where I_{200} represents the crystalline and amorphous region, I_{AM} is the minimum between the 200 and 110 peak, and only represents the amorphous region. As shown in Fig. 6.3b, the crystallinity of CNF has only a slight change in the case of lower $NaIO_4$ content (from 65.9% to 65.3%). However, with more $NaIO_4$ added the crystallinity sharply decreased from 65.3% to 26.1%. The decrease in crystallinity of the oxidized CNF is due to the fact that the newly formed aldehyde groups reduce the hydrogen bonds interaction between cellulose molecules.

6.3.2 Thermal properties of oxidation CNF

The thermal stability of CNF and oxidized CNF were evaluated by TGA (Fig. 6.4). An obvious weight loss was observed at about 90-120 °C in CNF and oxidized CNF which due to evaporation of absorbed and intermolecular H-bonded water [18]. The degradation temperature of oxidized CNF was reduced when compared with CNF. The T_{20} (weight loss of 20%) of CNF is 323.2°C, which is higher than T_{20} of CNF-1, CNF-

2, CNF-3 and CNF-4 (310.9°C, 291.6°C, 259.1°C and 248.0°C, respectively). The thermal performance decreasing is due to the reduction of hydrogen bond after the oxidation of CNF [23].
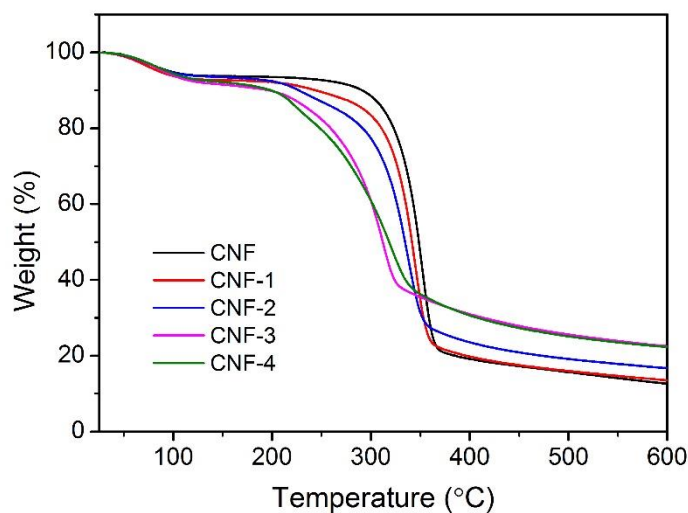

Fig. 6.4 TGA curves of CNF and oxidized CNF.
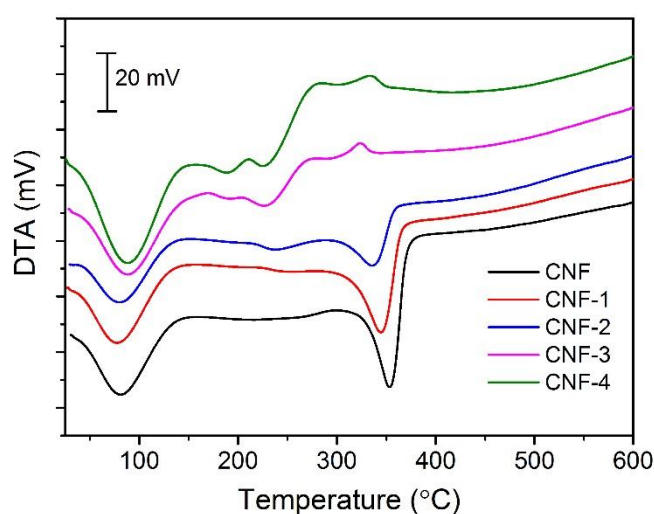
Fig. 6.5 DTA curves of CNF and oxidized CNF.

The crystallinity of cellulose after oxidation has undergone tremendous changes. The DTA result also indicates that the crystalline structure of CNF has changed. However, it finds that the cellulose crystalline endothermic peaks slightly shift from 80 to 88 °C with increasing the NaIO$_4$ content. Moreover, it also found that the decomposition endothermic peak intensity and the temperature of CNF, CNF-1, CNF-2 slowly decreased with increasing the oxidant content. While CNF-3 and CNF-4 only have the

weak decomposition endothermic peak at 227.2 and 188.5 °C, the decomposition process is basically a continuous exothermic state. This result is due to the high oxidation degree of CNF in the decomposition does not require additional heat to break the hydrogen bonds between the cellulose chains. Therefore, the effect of oxidation degree of CNF on thermal properties of cellulose in the high temperature is greater than that of in the low temperature.

6.3.3 Morphology of oxidation CNF
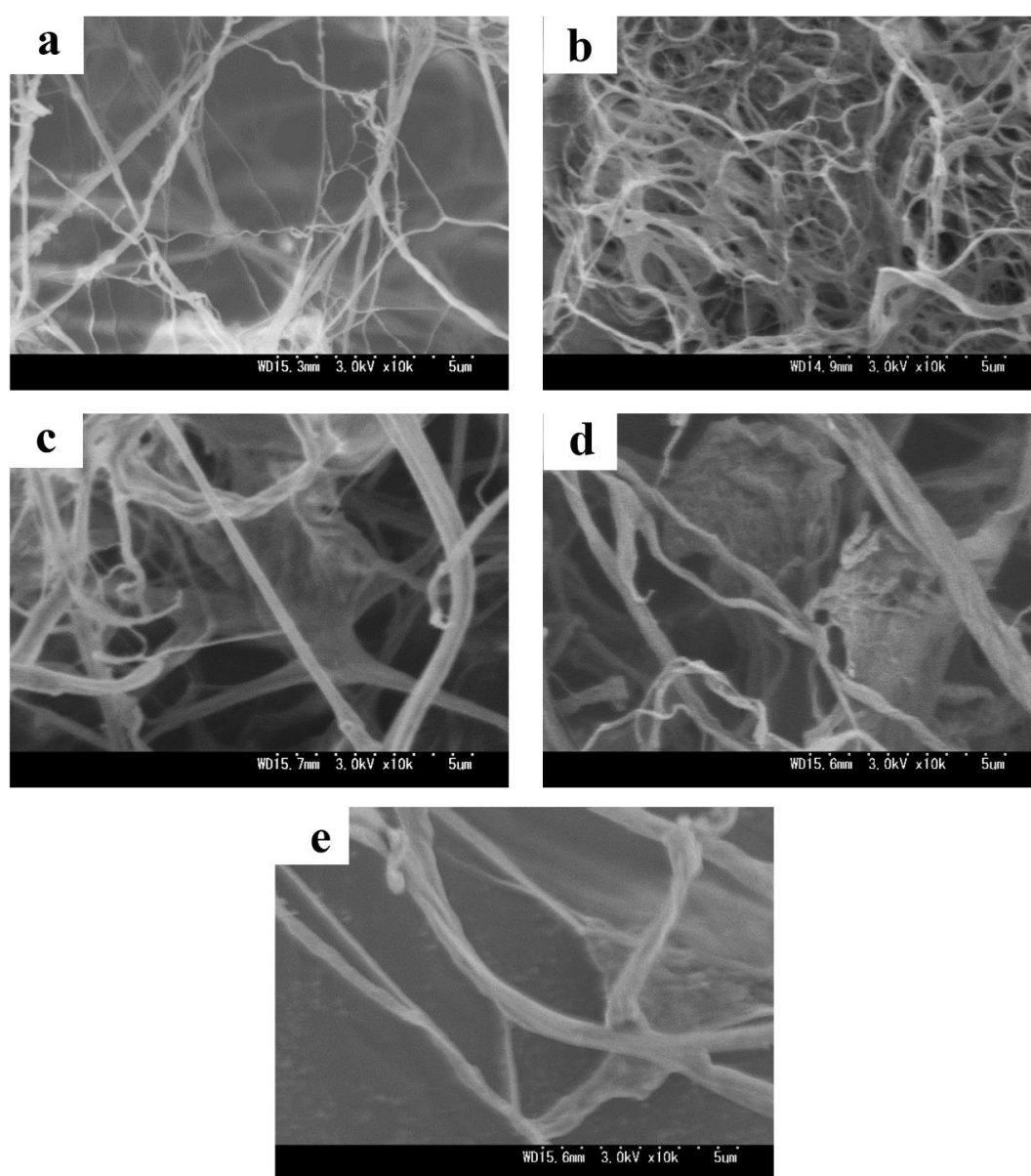
Fig. 6.6 SEM images of CNF and oxidized CNF. (a) CNF, (b) CNF-1, (c) CNF-2, (d) CNF-3, (e) CNF-4.

SEM was used to examine the morphology of CNF and oxidized CNF. As shown in Fig. 6.6a, the purchased commercial CNF shows that the diameter of cellulose nanofibers in the range of 50-500 nm. The diameter of CNF greatly changed when a certain amount of $NaIO_4$ was added to the CNF suspension. It is observed that the diameter of oxidized CNF is increased to 100-500 nm by adding 0.25g $NaIO_4$ (Fig. 6.6b). When more oxidants are added, the oxidized CNF with a diameter of less than 200 nm is essentially disappeared (Fig. 6.6c-e). The results show that as the oxidant content increases, a lot of hydrogen bonds between the cellulose molecules are ruptured, resulting in more dialdehyde CNF macromolecules dissolved in aqueous solution. The low-diameter CNF is more susceptible to oxidation and dissolves, thus, the remaining dialdehyde CNF shows large diameter after centrifugation.
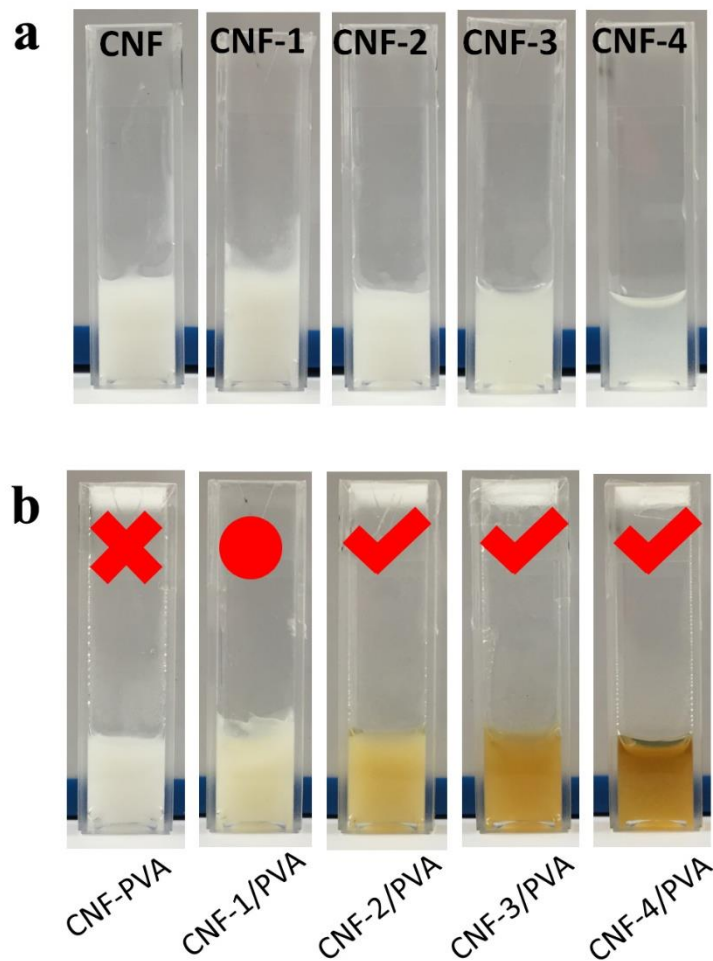
Fig. 6.7 Digital images of CNF and PVA mixture (a) before and (b) after aldolization.

6.3.4 Preparation of hydrogel

The reactivity of the CNF is greatly improved after the introduction of the aldehyde group on the surface of CNF. This CNF with multiple aldehydes can be used as a nature macromolecule crosslinker. For example, Ragauskas et al. reported a biocompatible gelatin hydrogel with oxidized cellulose nanowhiskers as cross-linker [22]. Although the preparation of the hydrogel is very gentle, the degree of chemical cross-linking between gelatin and nanowhiskers can reach to as high as 0.14-17%. In the present experiment, CNF/PVA hydrogels were prepared by aldolization with CNF and PVA under acid catalysis at 80 °C. The color of obtained hydrogels (CNF-1/PVA to CNF-4/PVA) turned from light yellow to deep yellow. As a comparison, the CNF and PVA mixture has no chemical reaction (Fig. 6.7). It should be noticed that although the CNF-1 and PVA mixture have aldolization, the resulting product is only more viscous and does not form a hydrogel. This may be due to the number of aldehydes on the surface of CNF-1 is little, which limits the formation of the large cross-linking network.
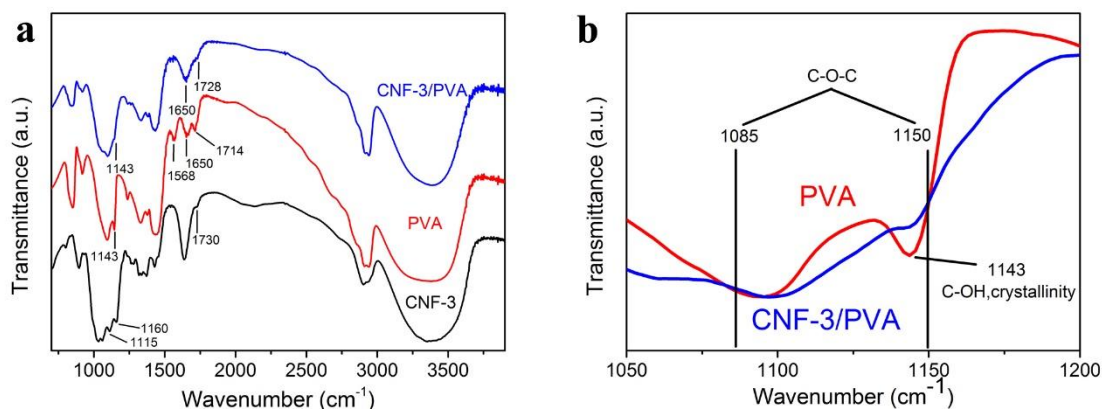

Fig. 6.8 (a) FT-IR spectra of CNF-3, PVA, and CNF-3/PVA. (b) Amplification image of (a).

In the spectrum of CNF-3, the peaks around 3370 cm^{-1} and 2900 cm^{-1} are attributed to the stretching vibration of O-H and C-H, respectively. The peak at 1115 cm^{-1} and 1160 cm^{-1} are the absorption peak of C-OH and C-C, respectively. CNF or PVA will adsorb a small amount of water during the FT-IR samples preparation due to their high hydrophilic. Thus, the peak at 1635 cm^{-1} or 1650 cm^{-1} is the absorption peak of water

[25]. Since PVA contains incompletely hydrolyzed ester groups, there are significant absorption peaks at 1714, 1568 and 1143 cm^{-1}. During the gelation reaction, the ester groups in the PVA were hydrolyzed due to the presence of the acid catalyst, and the absorption peaks at 1714 and 1568 cm^{-1} disappeared. After the aldolization, the absorption peak of CNF-3/PVA at 1143 cm^{-1} decrease compare the spectra of PVA and CNF-3/PVA, which result from the crystallization of C-OH in PVA decrease [26]. Moreover, the absorption peak of C-O-C at 1085-1150 cm^{-1} [11]. From Fig. 6.8b, the absorption intensity of CNF-3/PVA is higher than that of PVA at 1085-1150 cm^{-1}, indicating that C-O-C is formed in the hydrogel by aldolization.

6.3.5 Mechanical properties of hydrogel

At present, the widely used method of preparing PVA based hydrogel is cyclic freeze-thawing. The method is to use the hydrogen bonds of PVA to construct a physical cross-linking network during the cyclic freeze-thawing process, resulting in the PVA solution into a hydrogel. Although the preparation process is simple, the several times cyclic freeze-thawing process is very cumbersome and takes a long time. In addition, in the previous work, it found that the evaporation-swelling (E-S) method is also an efficient way to enhance the hydrogel mechanical properties [20]. This convenient method also uses the hydrogen bond reconstruction to reinforce the mechanical properties of the hydrogel.

The CNF-PVA, CNF-1/PVA and synthesized hydrogel (CNF-2/PVA, CNF-3/PVA, and CNF-4/PVA) were reinforced through E-S method. This convenient method enables the non-cross-linked mixture to become a hydrogel. The tensile property of produced hydrogel is shown in Fig. 6.9. The CNF and PVA mixture formed a hydrogel with the tensile strength of 1.49 MPa, the fracture elongation of 180% and the elastic modulus of 1.54 MPa after treating with E-S method. Similarly, CNF-1 and PVA also formed a tough hydrogel with the tensile strength, fracture elongation and elastic modulus are 3.13 MPa, 170%, and 2.10 MPa, respectively. The three samples (CNF-2/PVA, CNF-3/PVA, and CNF-4/PVA) that have been gelled possess lower mechanical

properties than the hydrogel (CNF-1/PVA) without gelation. The tensile strength and elastic modulus of CNF-2/PVA, CNF-3/PVA and CNF-4/PVA range from 0.25-0.96 MPa and 0.14-0.42 MPa, respectively. This phenomenon may be due to the abundant chemical cross-linking sites limit the formation of hydrogen bonds of the hydrogel during the evaporation-swelling process.
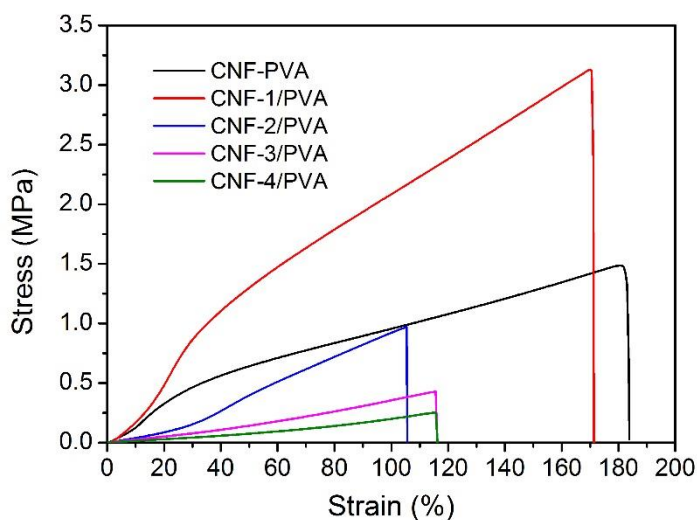

Fig. 6.9 Stress-strain curves of reinforced CNF/PVA hydrogel.

6.3.5 Water content of hydrogel

The water content of the hydrogel is inversely proportional to the cross-linking density [27, 28]. Thus, the water content of the CNF/PVA hydrogel after swelling
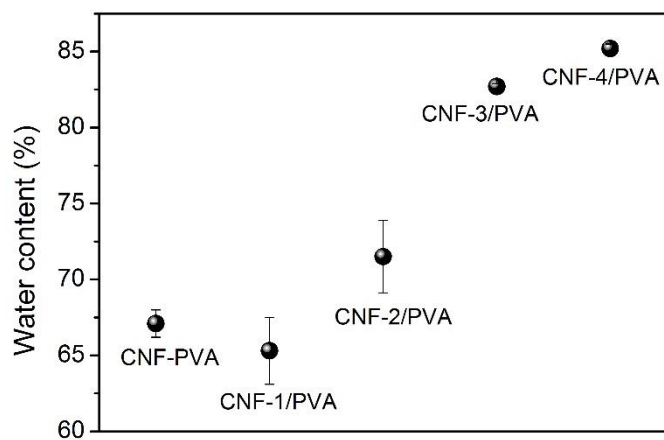
Fig. 6.10 Water content of reinforced CNF/PVA hydrogel.
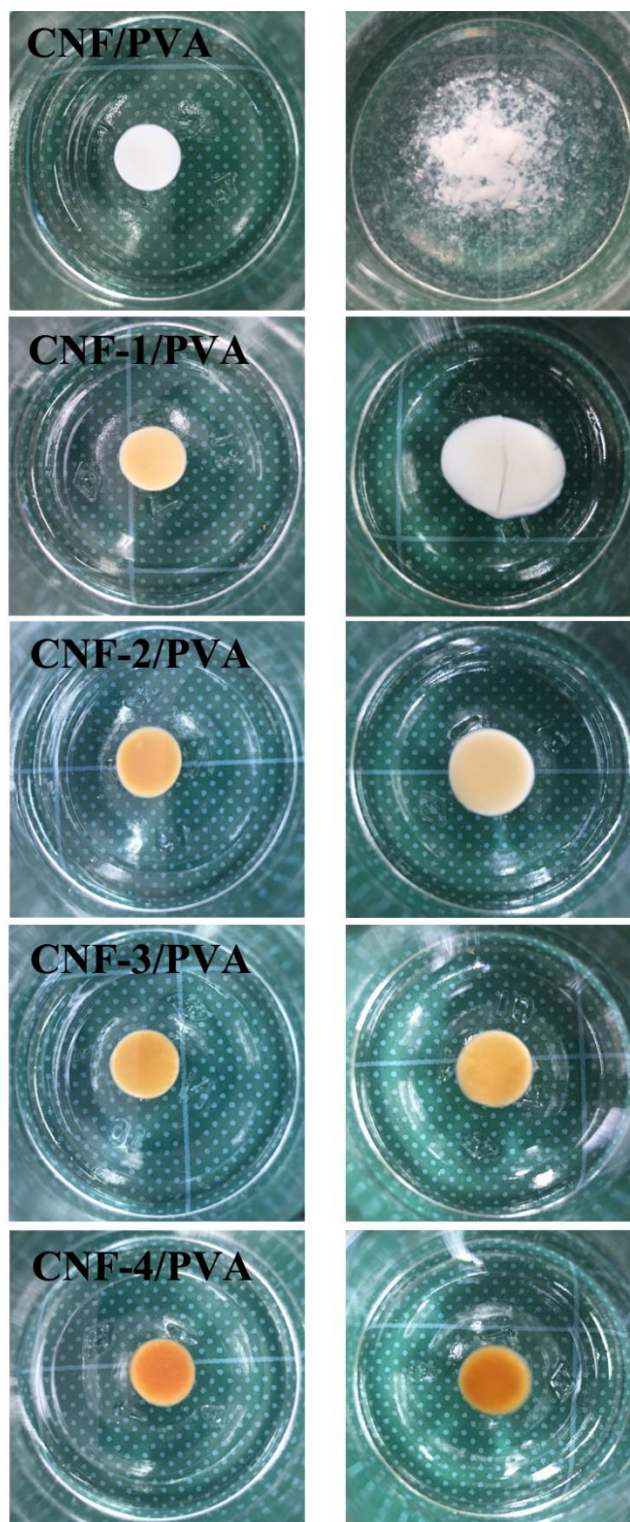
Fig. 6.11 Thermal property of CNF/PVA hydrogel before and after high temperature treatment.

equilibrium can reflect the state of the cross-linking network. As shown in Fig. 6.10, the water content increased from CNF-1/PVA to CNF-4/PVA, and it is interesting to find that the water content of hydrogel consistent with the tensile strength. The newly

formed physical cross-linking site by hydrogen bond increases the network cross-linking density resulting in a decrease in water content of the hydrogel.

Although the experimental data show that when the un-cross-linked mixture is enhanced by the E-S method, it can obtain better mechanical properties than the cross-linked hydrogel, its water content is obviously lower than that of the soft tissue in the organism. As a tissue engineering material, the mechanical properties of CNF-2/PVA, CNF-3/PVA, and CNF-4/PVA are closer to the properties of the soft tissue of the organism. In addition, the hydrogel crosslinked only through hydrogen bonds is directly decomposed during the use of conventional high temperature autoclaving process (Fig. 6.11). Thus, the CNF-3/PVA (tensile strength, fracture elongation and elastic modulus are 0.43 MPa, 115.6%, and 0.254 MPa, respectively) was selected as further research.

6.3.6 Morphology of CNF/PVA hydrogel

The prepared hydrogels generally show porous network structure after freeze-drying process [29]. To investigate the microstructure of CNF/PVA hydrogel, SEM was used to observe the structure. The reinforced CNF-3/PVA hydrogel exhibits an interconnected porous network structure with the size of the porous is about 1 um (Fig. 6.12a, b). No separate CNF is found in the SEM image, indicating that the CNF and PVA are completely fused together.
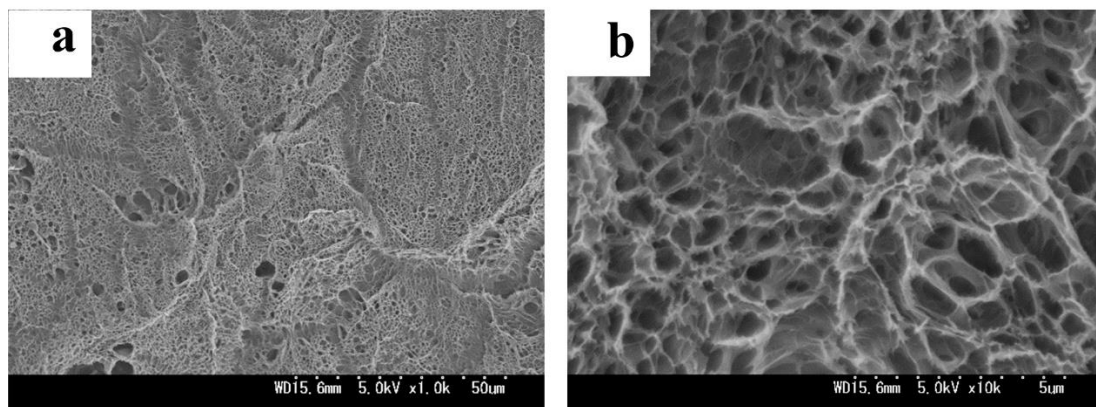

Fig. 6.12 (a) SEM images of CNF-3/PVA hydrogel. (b) Amplification image of (a).

6.3.7 Softening effect of reinforced CNF/PVA hydrogel

The reinforced CNF-3/PVA hydrogel can undergo large compressive strain without damage. However, most hydrogels with hydrogen bonds or/and ionic cross-linking sites generally show softening effect under cyclic large deformation [30]. The softening effect also found in natural living tissue which possesses a similar composition with hydrogel. Figure 6.13a shows that the initial compressive strength of CNF-3/PVA hydrogel can reach 1.7 MPa at a strain of 70%.
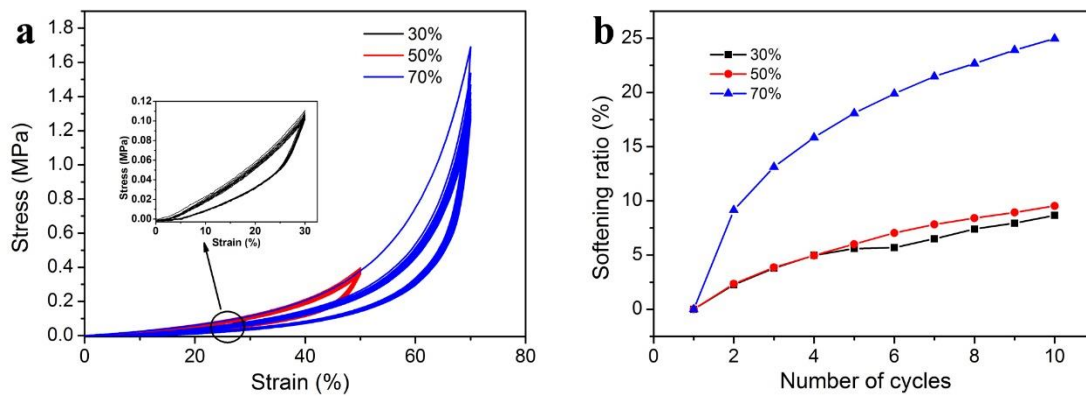

Fig. 6.13 (a) Cyclic compressive curves of CNF-3/PVA hydrogel obtained after 10 tests at various strains. (b) Softening ratio of CNF-3/PVA hydrogel at various strains.

With increasing the cyclic times the compressive stress was gradually decreased, indicating the softening effect occurred. The softening ratio was calculated according to the equation [31]:

$$SR\% = \frac{\sigma_n - \sigma_1}{\sigma_1} \times 100\% \quad (6\text{-}2)$$

Where σ_1 represents the maximum stress at the first cycle; σ_n represents the maximum stress at the current cycle. At compressive strains of 30% and 50%, the softening ratio of the hydrogel is less than 10% and gradually tends to be a plateau. However, the softening rate of the hydrogel reached 25% after 10 times of cyclic compression at 70% of the compressive strain (Fig. 6.13b). It indicated that when the compression strain is less than 50%, the internal network structure of the hydrogel is only a slight change. On the contrary, the softening effect may be caused by sliding and

disentanglement of polymer chains, and the rupture of hydrogen bonds and chemical bonds under large deformation.

6.4 Conclusion

In this study, CNF was first oxidized to the multi-aldehyde CNF by $NaIO_4$. Secondly, the CNF/PVA hydrogels were prepared with multi-dialdehyde CNF as chemical cross-linker. At last, the obtained hydrogels were reinforced through evaporation-swelling method. The crystallinity of oxidized CNF was reduced from 65.9% to 26.1% with an increase in the amount of $NaIO_4$. Moreover, the decomposition temperature of oxidized CNF also showed a decrease from 323.2 to 248.0°C with increasing the degree of oxidation. The tensile strength and elastic modulus of reinforced hydrogels are in the range of 0.25-3.13 MPa and 0.14-2.10 MPa, respectively, depending on various oxidized CNF. The chemical cross-linked hydrogels (CNF-2/PVA, CNF-3/PVA, and CNF-4/PVA) exhibit mechanical properties and water content closer to the natural soft tissue and show thermal stability during the use of the conventional high temperature autoclaving process.

References

[1] Chen Q, Chen H, Zhu L, Zheng J. Fundamentals of double network hydrogels. J Mater Chem B. 2015;3(18):3654-76.

[2] Gong JP. Why are double network hydrogels so tough? Soft Matter. 2010;6(12):2583.

[3] Hoffman AS. Hydrogels for biomedical applications. Advanced Drug Delivery Reviews. 2012;64:18-23.

[4] Slaughter BV, Khurshid SS, Fisher OZ, Khademhosseini A, Peppas NA. Hydrogels in regenerative medicine. Advanced materials. 2009;21(32-33):3307-29.

[5] Ekaputra AK, Prestwich GD, Cool SM, Hutmacher DW. The three-dimensional vascularization of growth factor-releasing hybrid scaffold of poly (epsilon-caprolactone)/collagen fibers and hyaluronic acid hydrogel. Biomaterials. 2011;32(32):8108-17.

[6] Tubbs RK. Sequence distribution of partially hydrolyzed poly (vinyl acetate). Journal of Polymer Science Part A: Polymer Chemistry. 1966;4(3):623-9.

[7] Peppas NA, Merrill EW. Differential scanning calorimetry of crystallized PVA hydrogels. Journal of Applied Polymer Science. 1976;20(6):1457-65.

[8] Shi Y, Xiong D. Microstructure and friction properties of PVA/PVP hydrogels for articular cartilage repair as function of polymerization degree and polymer concentration. Wear. 2013;305(1-2):280-5.

[9] Abitbol T, Johnstone T, Quinn TM, Gray DG. Reinforcement with cellulose nanocrystals of poly(vinyl alcohol) hydrogels prepared by cyclic freezing and thawing. Soft Matter. 2011;7(6):2373.

[10] Krumova M, López D, Benavente R, Mijangos C, Pereña JM. Effect of crosslinking on the mechanical and thermal properties of poly(vinyl alcohol). Polymer. 2000;41(26):9265-72.

[11] Mansur HS, Sadahira CM, Souza AN, Mansur AAP. FTIR spectroscopy characterization of poly (vinyl alcohol) hydrogel with different hydrolysis degree and

chemically crosslinked with glutaraldehyde. Materials Science and Engineering: C. 2008;28(4):539-48.

[12] Karlgard C, Wong N, Jones L, Moresoli C. In vitro uptake and release studies of ocular pharmaceutical agents by silicon-containing and p-HEMA hydrogel contact lens materials. International journal of pharmaceutics. 2003;257(1):141-51.

[13] Kim J, Conway A, Chauhan A. Extended delivery of ophthalmic drugs by silicone hydrogel contact lenses. Biomaterials. 2008;29(14):2259-69.

[14] Kamoun EA, Kenawy ES, Chen X. A review on polymeric hydrogel membranes for wound dressing applications: PVA-based hydrogel dressings. Journal of advanced research. 2017;8(3):217-33.

[15] Elsner JJ, Berdicevsky I, Zilberman M. In vitro microbial inhibition and cellular response to novel biodegradable composite wound dressings with controlled release of antibiotics. Acta biomaterialia. 2011;7(1):325-36.

[16] Chin SY, Poh YC, Kohler A-C, Compton JT, Hsu LL, Lau KM, et al. Additive manufacturing of hydrogel-based materials for next-generation implantable medical devices. Science Robotics. 2017;2(2):eaah6451.

[17] Baker MI, Walsh SP, Schwartz Z, Boyan BD. A review of polyvinyl alcohol and its uses in cartilage and orthopedic applications. Journal of biomedical materials research Part B, Applied biomaterials. 2012;100(5):1451-7.

[18] Mu C, Guo J, Li X, Lin W, Li D. Preparation and properties of dialdehyde carboxymethyl cellulose crosslinked gelatin edible films. Food Hydrocolloids. 2012;27(1):22-9.

[19] Ramaraj B. Crosslinked poly(vinyl alcohol) and starch composite films. II. Physicomechanical, thermal properties and swelling studies. Journal of Applied Polymer Science. 2007;103(2):909-16.

[20] Zhu L, Qiu J, Sakai E. A high modulus hydrogel obtained from hydrogen bond reconstruction and its application in vibration damper. RSC Adv. 2017;7(69):43755-63.

[21] Kim U-J, Wada M, Kuga S. Solubilization of dialdehyde cellulose by hot water. Carbohydrate Polymers. 2004;56(1):7-10.

[22] Dash R, Foston M, Ragauskas AJ. Improving the mechanical and thermal properties of gelatin hydrogels cross-linked by cellulose nanowhiskers. Carbohydr Polym. 2013;91(2):638-45.

[23] Cui Q, Zheng Y, Lin Q, Song W, Qiao K, Liu S. Selective oxidation of bacterial cellulose by NO2–HNO3. RSC Adv. 2014;4(4):1630-9.

[24] Thygesen A, Oddershede J, Lilholt H, Thomsen AB, Ståhl K. On the determination of crystallinity and cellulose content in plant fibres. Cellulose. 2005;12(6):563-76.

[25] Peresin MS, Habibi Y, Zoppe JO, Pawlak JJ, Rojas OJ. Nanofiber composites of polyvinyl alcohol and cellulose nanocrystals: manufacture and characterization. Biomacromolecules. 2010;11(3):674-81.

[26] Mallapragada SK, Peppas NA. Dissolution mechanism of semicrystalline poly (vinyl alcohol) in water. Journal of Polymer Science-B-Polymer Physics Edition. 1996;34(7):1339-46.

[27] Zhu L, Qiu J, Sakai E, Ito K. Rapid Recovery Double Cross-Linking Hydrogel with Stable Mechanical Properties and High Resilience Triggered by Visible Light. ACS applied materials & interfaces. 2017;9(15):13593-601.

[28] Akar E, Altinisik A, Seki Y. Preparation of pH- and ionic-strength responsive biodegradable fumaric acid crosslinked carboxymethyl cellulose. Carbohydr Polym. 2012;90(4):1634-41.

[29] Fang J, Mehlich A, Koga N, Huang J, Koga R, Gao X, et al. Forced protein unfolding leads to highly elastic and tough protein hydrogels. Nature communications. 2013;4:2974.

[30] Webber RE, Creton C, Brown HR, Gong JP. Large strain hysteresis and mullins effect of tough double-network hydrogels. Macromolecules. 2007;40(8):2919-27.

[31] Chen G, Zhang Y, Xu DK, Lin YC, Chen X. Low cycle fatigue and creep-fatigue interaction behavior of nickel-base superalloy GH4169 at elevated temperature of 650°C. Materials Science and Engineering: A. 2016;655:175-82.

Chapter 7 Conclusion

The high-performance hydrogel with fast recovery, high resilience, high modulus and thermal stability has been successful design, preparation, and testing. In this thesis, cellulose derivatives (CMC, CNF) were used as macromolecular cross-linker.

In chapter 3, we have successfully designed a new strategy to fabricate a rubbery hydrogel with mesoscopic movable inhomogeneous structure using curling CMC as cross-linker and initiator. This facile, one-pot, visible-light-triggered polymerization method provides a fast, convenient, and high efficiency strategy to synthesis rubbery hydrogel with instantaneous recovery and anti-fatigue properties. The hydrogel possesses some special properties such as negligible residual strain, instantaneous recovery, fatigue resistance and as high as 92% resilience after structure stabilizing, making the hydrogel an ideal candidate for further application in biomaterials.

In chapter 4, a novel design strategy was developed to fabricate a double cross-linking PAA hydrogel based on chapter 3. The tensile strength and the swelling ratio were reduced with increasing the MBA contents, while the elastic modulus showed an increased trend in the same conditions. The hydrogel exhibited a softening effect similar to conventional rubber materials, and further studies showed that the disentanglement and sliding of polymer chains as well as the rupture of the network led to this effect. The hydrogel exhibited remarkable recovery properties (resilience over 93% and 95% for successive and intermittent cyclic tensile tests, respectively, and residual strain less than 3%). It was noted that the recovery properties were almost constant under various conditions and independent of time. In addition, the hydrogel presented a higher resilience and lower residual strain after the hydrogel reached the swelling equilibrium. The hydrogel has potential applications in soft machines and biomaterials.

In chapter 5, to increase the modulus of the hydrogel, we leveraged the hydrogen bonds in the hydrogel to induce a CMC crystallization to alter the network structure within the hydrogel via the E-S method. The obtained optimal HM-Gel possessed excellent mechanical properties with tensile strength and elastic modulus of 1.55 MPa

and 1.02 MPa, respectively. Furthermore, different evaporation temperatures and the added various aluminum ion concentration have an extremely important effect on the tensile strength, modulus, and swelling ratio of the hydrogel. In addition, HM-Gel-0.5 exhibited stable mechanical properties in both the cyclic tensile and compression tests. The preliminary application experiment shows that the high-modulus hydrogel has a better vibration absorption effect than the low-modulus hydrogel. This design concept can enhance the modulus of more hydrogels containing hydrogen bonds, such that these hydrogels can be used not only as machinery vibration absorbers but also as biological vibration absorbers (for example articular cartilage).

In chapter 6, multi-aldehyde CNF was used as chemical cross-linker to fabricate the CNF/PVA hydrogel. Both crystallinity and decomposition temperature of oxidized CNF were reduced with an increase in the amount of $NaIO_4$. The tensile strength and elastic modulus of reinforced hydrogels are in the range of 0.25-3.13 MPa and 0.14-2.10 MPa, respectively, depending on various oxidized CNF. The chemical cross-linked hydrogels (CNF-2/PVA, CNF-3/PVA, and CNF-4/PVA) exhibit mechanical properties and water content closer to the natural soft tissue and show thermal stability during the use of the conventional high temperature autoclaving process.

Furthermore, hydrogels, as functional materials, have some potential applications in the field of temperature control, self-degradation, and fire-proof material. For example, we can add phase change energy storage reagent in hydrogel during the hydrogel preparation process to prepare the automatic temperature control material.

In conclusion, with the deep study of hydrogel properties, we believe that hydrogel is not only as an excellent biological material but also play an important role in the fields of automobile, aerospace etc.

Publications

Ⅰ. 審査付投稿論文

(1) **Longxiang Zhu**, Jianhui Qiu*, Eiichi Sakai, A High Modulus Hydrogel Obtained from Hydrogen Bond Reconstruction and Application in Vibration Damper. *RSC Advances*, 2017, 7 (69), 43755-43763. (IF=3.108)

(2) **Longxiang Zhu**, Jianhui Qiu*, Eiichi Sakai, Kazushi Ito, Rapid Recovery Double Cross-Linking Hydrogel with Stable Mechanical Properties and High Resilience Triggered by Visible Light. *ACS applied materials & interfaces*, 2017, 9(15), 13593-13601. (IF=7.504)

(3) **Longxiang Zhu**, Jianhui Qiu*, Eiichi Sakai, Limin Zang, Yanling Yu, Kazushi Ito, Peng Liu, Feiyu Kang, Design of a Rubbery Carboxymethyl Cellulose/Polyacrylic Acid Hydrogel via Visible-Light-Triggered Polymerization. *Macromolecular Materials and Engineering*, 2017, 302(6), 1600509. (IF=2.863)

(4) **Longxiang Zhu**, Jianhui Qiu*, Possible Application of Tough Hydrogel in Machinery, *Advances in Automobile Engineering*, 2017, 6, 170. (EI)

(5) **Longxiang Zhu**, Jingshan Guo, Peng Liu*, Effects of length and organic modification of attapulgite nanorods on attapulgite/polystyrene nanocomposite via in-situ radical bulk polymerization, *Applied Clay Science*, 2016, 119, 87-95. (IF=3.101)

(6) **Longxiang Zhu**, Jingshan Guo, Peng Liu*, Shibin Zhao, Novel strategy for palygorskite/poly(acrylic acid) nanocomposite hydrogels from bi-functionalized palygorskite nanorods as easily separable adsorbent for cationic basic dye, *Applied Clay Science*, 2016, 121-122, 29-35. (IF=3.101)

(7) Peng Liu*, Liping Jiang, **Longxiang Zhu**, Jinshan Guo, Aiqin Wang, Synthesis of covalently crosslinked attapulgite/poly(acrylic acid-co-acrylamide) nanocomposite hydrogels and their evaluation as adsorbent for heavy metal ions. *Journal of Industrial and Engineering Chemistry,* 2015, *23*, 188-193. (IF=4.421)

注：博士論文テーマ関連：**4 編（（1）～（4）），その他：3 編（（5）～（7））**

Ⅱ．　国際会議論文・発表

(1) **Longxiang Zhu**, Jianhui Qiu, Eiichi Sakai, Hydrogen Bond Reconstruction Reinforced Attapulgite/Poly (acrylic acid) Nanocomposite Hydrogel with Ultrahigh Mechanical Strength, Modulus, and pH Response, The 3RD China International Congress on Composite Materials (CCCM-3).

Ⅲ．　国内学会

(1) **朱 龍祥**、邱 建輝、境 英一、伊藤 一志. 水素結合の再構築による高強度 CMC/PAA ハイドロゲルの創製. 日本複合材料学会、第 42 回複合材料シンポジウム、2017、仙台市.

(2) **朱 龍祥**、邱 建輝、境 英一、伊藤 一志、工藤 素、野辺 理恵、小林 純一. 異なる無機ナノ粒子の添加による稲わら/ポリ乳酸複合材料の力学特性の向上. 日本プラスチック成形加工学会シンポジア '16、2016 年 10 月、仙台市.

(3) **朱 龍祥**、邱 建輝、境 英一、伊藤 一志. 稲わら/ポリ乳酸複合材料の機械的および熱的特性を強化するための新規戦略. 日本機械学会東北支部第 52 期秋季講演会、2016、秋田市.

(4) **朱 龍祥**、邱 建輝、境 英一. 水素結合による稲わら／ポリ乳酸複合材料の引張特性の向上. 日本機械学会東北支部第５１期秋季講演会、2015 年 9 月 26 日、福島市.

　　注：博士論文テーマ関連：**1 件　（4），その他：3 件　（（1）～（3））**

Acknowledgements